AN ABSTRACT OF THE DISSERTATION OF

Babak Mirzaei for the degree of Doctor of Philosophy in Wood Science and Materials Science presented on February 5, 2016.

Title: Durability Assessment of Wood Composites Using Fracture Mechanics.

Abstract approved:

John A. Nairn Arijit Sinha

The advent of synthetic adhesives has transformed the structural applications of wood. However, a persistent issue in adhesively-bonded wood products has been moisture durability. When designing wood based composites, moisture durability will depend on both the wood phase and the adhesive phase. A key question, therefore, is how does one rank adhesives for their ability to convey moisture durability in wood composites? Typical wood-based composite tests for moisture durability assessments do not consider the post-peak load regime of the material or are merely qualitative. This research explores the suitability of crack propagation fracture experiments to develop new methodologies for durability assessment of wood composites and adhesives.

Fracture resistance curves (*R* curves) were measured for solid wood Douglas-fir and laminated veneer lumber (LVL) made with Douglas-fir veneer and a variety wood adhesives, namely, polyvinyl acetate, phenol formaldehyde, emulsion polymer isocyanate and phenol resorcinol formaldehyde. The LVL and solid wood *R* curves were similar for initiation of fracture, but the LVL toughness rose much higher than solid wood. Because a rising *R* curve is caused by fiber bridging effects, these differences show that the LVL adhesive has a large effect on the fiber bridging process. This resin effect was exploited to develop a test method for characterizing the ability

of a resin to provide wood composites that are durable to moisture exposure. In characterizing toughness changes, it was important to focus on the magnitude and rate of the toughness increase attributed to fiber bridging. A new method was developed for ranking the role of adhesives in the durability of wood-based composites by observing changes in fracture toughness during crack propagation following cyclic exposure to moisture conditions. This new approach was compared to conventional mechanical performance test methods, such as observing strength and stiffness loss after exposure. Comparing changes in fracture toughness as a function of crack length after moisture cycling shows that fracture-mechanics based methods can distinguish different adhesive systems on the basis of their durability, while conventional test methods do not have similar capability. Using steady-state toughness alone, the most and least durable adhesives (phenol formaldehyde and polyvinyl acetate) could be distinguished, but the performance of two other adhesives (emulsion polymer isocyanate and phenol resorcinol formaldehyde) could not. Further analysis of experimental *R* curves based on kinetics of degradation was able to rank all adhesives confidently and therefore provided the preferred method. The likely cause for the inability of conventional tests to rank adhesives is that they are based on initiation of failure while the fracture tests show that comparisons that can rank adhesives require consideration of fracture properties after a significant amount of crack propagation has occurred.

Additionally, a new method was proposed for determining fiber-bridging cohesive laws in fiber-reinforced composites and in natural fibrous materials. In brief, the method requires direct measurement of the *R* curve, followed by a new approach to extracting a cohesive law. This new approach was applied to finding fiber bridging tractions in LVL made with four different adhesives. Moreover, observations of changes in the bridging cohesive laws were used to rank the adhesives for their durability. Finally, both analytical and numerical models for fiber bridging materials were developed. The numerical modeling developed using material point method (MPM) simulated crack propagation that included crack tip propagation, fiber bridging zone development, and steady state crack growth. The simulated *R* curves agreed with experimental results.

Durability Assessment of Wood Composites Using Fracture Mechanics

by
Babak Mirzaei

A DISSERTATION

submitted to

Oregon State University

in partial fulfillment of
the requirements for the
degree of

Doctor of Philosophy

Presented February 5, 2016
Commencement June 2016

Doctor of Philosophy dissertation of Babak Mirzaei presented on February 5, 2016

APPROVED:

Co-major Professor, representing Wood Science

Co-major Professor, representing Materials Science

Head of the Department of Wood Science and Engineering

Director of the Materials Science Graduate Program

Dean of the Graduate School

I understand that my dissertation will become part of the permanent collection of Oregon State University libraries. My signature below authorizes release of my dissertation to any reader upon request.

Babak Mirzaei, Author

ACKNOWLEDGEMENTS

I would like to expresses my sincere appreciation to the following individuals and organizations for their support of this project:

My major divisors, Dr. Arijit Sinha and Dr. John Nairn, for their invaluable support, guidance and patience throughout this project.

Wood Based Composites Center for funding this project and for providing technical advice and feedback throughout the project.

Hexion® and Georgia Pacific Chemicals® for donating materials to this project.

Dr. Fred Kamke, Dr. Jamie Kruzic and Dr. Ryan Contreras for their service and support on my graduate defense committee.

Dr. Lech Muszyński and Dr. Fred Kamke for allowing me to use their lab equipment.

Milo Clauson for his helpful experience and technical support.

Arezoo Rajabi for assistance in creating Matlab scripts.

My parents and family for their unending love and support.

TABLE OF CONTENTS

Page

TABLE OF CONTENTS (Continued)

Page

LIST OF FIGURES

Figure Page

LIST OF FIGURES (Continued)

Figure Page

LIST OF FIGURES (Continued)

Figure Page

LIST OF TABLES

Table Page

1 General Introduction

1.1 Background

The advent of synthetic adhesives has transformed the structural applications of wood. The process of breaking down solid wood into smaller components, and reforming them into integral laminate or composite products, through adhesive bonding, can extend the use of the wood resource, randomize natural variability, produce a variety of product sizes and geometries, and improve dimensional stability (Paris, 2014). However, a persistent issue in adhesively-bonded wood products is moisture durability. Due to the hydrophilic character of natural fibers, any structural composite material containing wood fibers should properly address durability in aggressive environments (Assarar, et al., 2011). When designing wood based composites, moisture durability will depend on both the wood phase and the adhesive phase. A key question, therefore, is how does one rank adhesives for their ability to convey moisture durability to wood composites? Typical wood-based composite tests for moisture durability operate by exposing products to wet and/or hot environments and then inspecting for signs of damage (*e.g.*, ASTM D2559 or D1037). Such tests are often qualitative (*e.g.*, pass/fail based on observation of damage). These tests can be made quantitative by coupling with suitable mechanical tests. For example, static bending and shear tests are common methods for evaluating the resistance of wood-based composites to aging. While the former supposedly addresses material durability as a whole; the latter aims to evaluate the quality of the bond-line after accelerated aging (ASTM D1037, 2012; NIST PS1, 2007). Unfortunately, these common tests look only at early stages of loading up to initiation of failure. These properties do not depend strongly on the adhesive and therefore, are poor tests for ranking adhesives (Stoeckel, et al., 2013). Some wood adhesives, studied in this dissertation, were previously used in studies that attempted to use conventional methods to differentiate them with regard to moisture durability (Follrich, et al., 2010; Raftery, et al., 2009). In contrast, it was recently shown that fracture analysis of

crack propagation within a single composite material may provide more information than conventional bond stiffness and strength testing (Sinha, et al., 2012).

The hypothesis of this project is that characterizing fracture properties of wood and wood composites for crack growth can provide accelerated results that will correlate better with actual durability properties than other mechanical or accelerated exposure methods currently in use. A similar approach was used for accelerated testing of aerospace composites by monitoring microcracking fracture toughness during hydrolytic degradation experiments on aerospace composites (Kim, et al., 1995; Han & Nairn, 2003). This approach was a great improvement over pass/fail methods that were previously used by Boeing. In this study, measuring and modeling experimental *R* curves provided useful data for characterizing the durability of wood composites.

The toughness or critical energy release rate for a material is the amount of energy released by unit increment in new crack area (Irwin, et al., 1958). For some materials, including wood, this critical energy changes as the crack propagates, which implies the importance of proper monitoring of crack propagation. An experimental measure of this change is known as the crack resistance curve, or *R* curve. Another aspect of this study was analyzing the little studied full *R* curves of wood and wood composites which were directly measured using an energy approach. Most prior studies on fracture of wood and wood composites merely reported total work of fracture, initiation toughness or relied on crack compliance methods which do not work for wood due to the presence of fiber bridging zone. Additionally, bridging stress profiles of all studied materials were analyzed and the proper approach for obtaining them from experimental *R* curves was discussed.

1.2 Objectives

Solid Douglas-fir wood and LVL made with the same wood species and a variety of adhesives, namely, polyvinyl acetate (PVA), phenol formaldehyde (PF), emulsion polymer isocyanate (EPI), and phenol resorcinol formaldehyde (PRF) were prepared in lab, and

their fracture properties including the entire *R* curve, initiation toughness (G_{init}), steady state toughness (G_{ss}), bridging toughness (G_b), bridging density (ρ_b), and cohesive stress ($\sigma(\delta)$), as well as conventional shear strength and bending modulus were investigated before and after subjecting specimens to various VPSD cycles to determine if the contribution of adhesive to the crack propagation fracture properties of LVL can be used as a proper moisture durability indicator as opposed to the conventional indicators that ignore the post-peak load regime of the material, and determine whether a protocol for ranking wood adhesives with regard to their durability can be proposed by experimental and numerical measurement of fracture properties.

1.3 Organization of Dissertation

This dissertation is written in manuscript format which means each chapter, except introduction and conclusion chapters, is an independent journal publication. This introduction chapter is a general introduction and goes over the thesis theme and identifies the overall objectives of this study. Chapter 2 titled “Using crack propagation fracture toughness to characterize the durability of wood and wood composites” deals with methodology establishment and statistical concerns of using fracture properties as a durability indicator. *R* curves of Laminated Veneer Lumber (LVL) and solid wood of the same species, exposed to various cycles of vacuum pressure soaking and drying (VPSD), were analyzed to find the loss of fracture properties due to aging and the contribution of adhesive to the fracture toughness of wood composite. This chapter focused on a single adhesive (PVA). Chapter 3 titled “Assessing the role of adhesives in durability of wood-based composites using fracture mechanics” analyzes the *R* curves of LVL made with various adhesives before and after various cycles of accelerated aging and proposes methodologies based on fracture properties for ranking wood adhesives with regard to their durability. The results of conventional test methods are also presented in this chapter. Chapter 4 which is titled as “Measuring and modeling fiber bridging: application to wood and wood composites exposed to moisture cycling” a new approach to experimental

determination of the cohesive law for fiber bridging in composites and reduction of those laws to a form suitable for use in modeling. Based on bridging stress results, durability attributes of different wood adhesives were evaluated and *R* curves were modeled to predict fracture properties in the presence of fiber bridging using Material Point Method (MPM). Chapter 5 is general conclusions and summary followed by an appendix which provides Matlab® scripts created for this project.

2 Using Crack Propagation Fracture Toughness to Characterize the Durability of Wood and Wood Composites

Babak Mirzaei, Arijit Sinha, and John A. Nairn

Materials and Design 87 (2015) 586–592

Abstract

We measured fracture resistance curves (or *R* curves) for laminated veneer lumber (LVL) made with Douglas-fir veneer and polyvinyl acetate adhesive and for solid wood Douglas-fir. The LVL and solid wood *R* curves were the same for initiation of fracture, but the LVL toughness rose much higher than solid wood. Because a rising *R* curve is caused by fiber bridging effects, these differences show that the LVL adhesive has a large effect on the fiber bridging process. We exploited this adhesive effect to develop a test method for characterizing the ability of an adhesive to provide wood composites that are durable to moisture exposure. The test method exposed LVL specimens to vacuum pressure soaking and drying (VPSD) cycles and then monitored the rising portion of the LVL *R* curves as a function of treatment cycles. Douglas-fir/polyvinyl acetate LVL lost about 30% of its toughness after 16 cycles. In characterizing toughness changes, it was important to focus on the magnitude and rate of the toughness increase attributed to fiber bridging. We suggest that these properties are much preferred over other fracture or mechanical properties of wood that might be used when characterizing durability.

Keywords: Wood based composites, Adhesives, Durability, Fracture

2.1 Introduction

A persistent issue in wood products is moisture durability. Due to the hydrophilic character of natural fibers, a structural composite material containing wood fibers should properly address durability in aggressive environments (Assarar, et al., 2011). When designing wood based composites, moisture durability will depend on both the wood phase and the adhesive phase. A key question, therefore, is how does one rank adhesives for their ability to convey moisture durability to wood composites? Most current tests are qualitative such as exposing composites to moisture conditions followed by checking for onset or extent of cracking (ASTM D2559, 2012). Other tests might monitor strength as a function of some moisture exposure. These tests may not be the best approach to evaluating the durability of

adhesives. Our hypothesis is that measuring certain fracture properties as a function of moisture exposure can provide new properties that will correlate better with adhesive quality for moisture durability. An analogous approach that monitored toughness as a function of exposure time was a great improvement over pass/fail methods that were previously used by the aerospace industry (Han & Nairn, 2003).

Unlike metals, ceramics, and polymers, the fracture properties of wood are more complex and more difficult to measure. The main complexity in wood fracture is that crack propagation leaves a fracture damage zone in the wake of the crack consisting of fibers that bridge the crack surfaces (Nairn, 2009). One consequence of damage zones is that wooden structures rarely experience sudden and catastrophic failures due to the consumption of energy in such zones (Anaraki & Fakoors, 2010). Two other consequences of fiber bridging are that the toughness of wood increases with crack growth and measuring that increase requires methods that account for the fiber bridging. The measurement issue has recently been solved for wood fracture (Matsumoto & Nairn, 2012) and the same methods work well for crack propagation in wood composites (Sinha, et al., 2012). These new experiments measure wood fracture toughness as a function of crack growth, which is known as the fracture resistance curve or the *R* curve. After measuring the fracture properties of laminated veneer lumber (LVL), it was noted that the *R* curve of LVL is much higher than the *R* curve of the solid wood for the species used in the LVL veneer (Sinha, et al., 2012). Clearly, this large increment in toughness is caused by adhesive and/or by wood/adhesive interactions. The goal of this work was to look for changes in wood composite *R* curves as a quantitative marker for the role of adhesive in moisture durability properties of that composite.

LVL is a unidirectional wood based composite manufactured from veneers bonded together with a variety of wood adhesive systems (Sulaiman, et al., 2009). We focused on LVL experiments because the role of the adhesive is large and we could make custom LVL billets with various adhesives. Although some works have looked at LVL

toughness, none have looked at toughness changes due to moisture exposure. Sinha et al. (2012) studied the effect of elevated temperature on the *R* curves of solid wood and some wood composites. They reported initiation and steady state toughness of 1050 J/m^2 for LVL with PF adhesive. Most other prior studies considered only initiation toughness (G_{init}) or total work of fracture (G_f) (Stanzl-Tchegg & Navi, 2009). Ardalany et al. (2012) reports an initiation toughness of 144 to 266 J/m^2 for pine LVL. They also investigated G_f of pine lumber and pine LVL.

Although important characteristics, G_{init} and G_f provide incomplete characterization of wood based composites. G_{init} is highly scattered and does not provide any information about rising *R* curves found for materials with fracture bridging, while G_f falls short in monitoring the behavior of the material throughout the fracture process. At best, G_f provides an average toughness value. For wood and wood composites, it is preferable to use the entire *R* curve when evaluating their fracture properties.

This work's objective was to use crack propagation fracture toughness as a method for characterizing the moisture durability of wood composites (LVL) and solid wood. In these experiments, the fracture toughness as a function of crack propagation was continuously monitored resulting in full *R* curves. A challenge in following crack propagation in wood products is accurately recording crack length. We solved this challenge by monitoring crack growth using digital image correlation (DIC) techniques (Bruck, et al., 1989). In control experiments, the fracture toughness of LVL was compared to solid wood of the same species. The fracture toughness at initiation was similar for LVL and solid wood, but as the crack propagated, the LVL toughness became much higher. This extra toughness increase was attributed to adhesive interactions with wood. We next measured changes in the rate and magnitude of the toughness increase after exposing LVL specimens to 4 to 16 vacuum pressure soaking and drying (VPSD) cycles. By careful analysis of key features of the *R* curves, we could monitor the moisture degradation processes. We suggest these

fracture methods can provide a new tool for ranking the contribution of adhesives to the durability of wood composites.

2.2 Materials and Methods

2.2.1 Materials

Laminated veneer lumber (LVL) billets were lab-made under controlled conditions using all B grade Douglas-fir veneers. Each billet consisted of 11 plies (each 3 mm thick), and polyvinyl acetate adhesive was used to bond veneers at room temperature. One-component PVA adhesive and the veneers were supplied by Momentive® Specialty Chemicals. The adhesive was spread on the veneers using a roll coater with coverage of 250–300 g/m^2. After stacking 11 layers, the billet was put in a hydraulic press at 2 MPa (300 psi) at room temperature for about 1 h. After pressing, the LVL billets were kept in a standard conditioning room (20 °C, 65% RH) for about one week before further testing. These samples are denoted DF/PVA LVL. Note that commercial LVL normally uses high-grade veneers on the surfaces and low-grade veneers in the middle. For this work, however, it was important to have uniform grade veneer throughout. Solid wood specimens (for comparison) were cut from No. 2 grade Douglas-fir dimension lumber.

Crack propagation experiments were done using double cantilever beam (DCB) specimens (see Fig. 2-1), which were cut from billets after they reached equilibrium and prior to moisture exposure. The initial cracks were cut with a band saw. To avoid possible weak adhesion zones near the edges, the edges of billets were marked before sawing and the initial specimen cracks were cut from the marked ends, such that all cracks propagated away from the edges. Hence, the quality of the inner zone adhesion was tested. Dimensions of all DCB samples were 35 ± 2 × 35 ± 2 × 300 ± 5 mm^3 and the initial, sawn pre-crack was 100 mm.

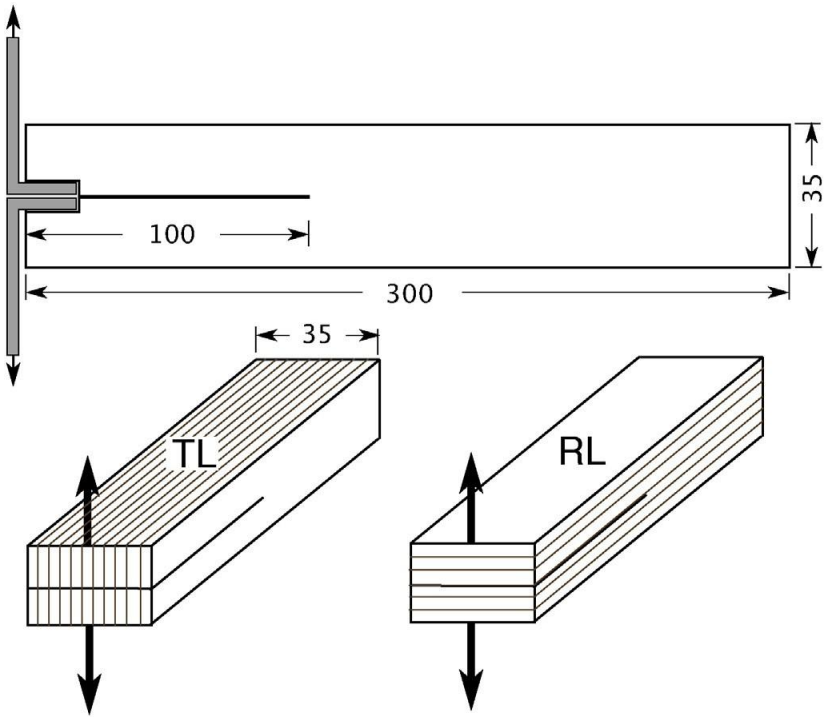

Figure 2-1. The top shows geometry of the DCB specimens, which were loaded by angle irons that fit into a slot on one edge. The bottom shows TL and RL orientations for LVL fraction. The thin lines are glue lines between veneer layers in the LVL.

Accelerated moisture exposure was carried out according to (ASTM D2559, 2012) but we excluded the steam exposure step. Each cycle started by exposing the sample to 85 kPa vacuum for 5 min followed by submersion in water in a pressure vessel at 517 kPa for 1 h. After removal from the pressure vessel, the samples were oven-dried at 65 ± 2 °C for 21–22 h (ASTM D2559, 2012). These steps represented 1 VPSD cycle. Samples were subjected to 4, 8, 12 and 16 VPSD cycles. After these selected cycle numbers, samples to be tested were thoroughly dried at 103 °C for 24 h and then stored in the standard conditioning room to reach equilibrium. Details of the studied materials and number of replicates are in Table 2-1.

Table 2-1. Test matrix with number of replicates for measuring R curves for DF/PVA LVL and for solid wood DF.

Treatment	DF/PVA LVL	Solid wood
Control (untreated)	8 ± 2	4 ± 1
4 Cycles	8 ± 2	4 ± 1
8 Cycles	8 ± 2	4 ± 1
12 Cycles	8 ± 2	4 ± 1
16 Cycles	8 ± 2	4 ± 1

2.2.2 Data Acquisition System

The load and displacement data during fracture tests were recorded using an Instron 5582 universal testing machine. DCB fracture tests were conducted in opening mode under displacement control at 2 mm/min. The crack plane at the edge of each specimen was widened (see Fig. 2-1) and loading was applied using angle irons inserted into the gap. Crack growth data were collected using the 3D Digital Image Correlation (DIC) technique. For DIC data acquisition, two 50 mm Pentax® lenses (stereo system), attached to high speed Correlated Solutions® cameras mounted on a tripod, were used to capture images during the tests. Images were acquired at 1 Hz. DIC is a technique to map strains by tracking a small subset of pixels in deformed images (Bruck, et al., 1989). To facilitate the DIC analysis, a speckle pattern was applied by painting the surface black and then spraying a random pattern of white dots. Applying a proper speckle pattern is essential for good DIC analysis. Also, using a proper external light source considerably improved test precision by reducing the subset size. Before conducting the test, the stereo camera system was calibrated. No further adjustments of light condition, camera focus or position were allowed after calibration. VIC 3D® software analyzed the acquired images and mapped strains. The tensile strain normal to the crack plane ahead of the crack tip was monitored throughout the loading. The strain profiles were high near the crack tip and decreased as a

function of distance away from the crack tip (Matsumoto & Nairn, 2009). Crack propagation was measured by observing shifts in the position to reach 1% vertical strains between subsequent images. All DIC strain-position data were exported to data sheets for further processing with Matlab®. A Matlab® script was written to populate crack propagation data from DIC output based on the 1% strain criterion. The DIC approach did not precisely measure the crack tip location, but it accurately measured each crack growth increment. Fortunately, the *R* curve analysis depends only on incremental crack growth and does not need the absolute crack length.

2.2.3 Fracture Test and R-curve Construction

In materials that develop fracture process zones, such as fiber bridging in bone (Nalla, et al., 2004), fiber reinforced epoxy composites (Shokrieh, et al., 2012), solid wood (Wilson, et al., 2013), and wood products (Matsumoto & Nairn, 2009), it is important to monitor fracture toughness as a function of crack growth, which is known as the *R* curve. For fiber-reinforced composites and by analogy for wood, energy methods are typically more useful than stress intensity methods (Sinha, et al., 2012). For example, the stress intensity assessment by (ASTM E399, 2013) assumes crack propagation is self-similar implying a straight crack with traction-free fracture surfaces — in other words, without an evolving fracture process zone as seen in wood. An alternative to stress intensity methods is to directly measure released energy by experiments (Matsumoto & Nairn, 2012). Since energy methods do not depend on any assumed crack process, they can be used for any material provided both energy and crack length are correctly measured and if the measured energy is correctly identified with fracture work and not some alternative mechanisms such as crack-plane interference effects (Matsumoto & Nairn, 2009). Crack-plane interference can be caused by bridging fibers in the wake of crack propagation. Because these fibers can be damaged by unloading phases commonly used in fracture testing, the *R* curve for wood and wood composites has to be measured by monotonically increasing loads with no

unloading phases (Matsumoto & Nairn, 2009). A revised energy method was recently developed for direct *R* curve measurement. This method includes four steps (Nairn, 2009):

1. Measure force and crack length as a function of displacement.

2. Find the cumulative released energy per unit thickness by integrating the force, F(d), up to some displacement point d and then assuming unloading from F(d), if it could be done without interference, would return to the origin. This energy (per unit thickness) is:

$$U(d) = \frac{1}{B}\left(\int_0^d F(x)dx - \frac{d}{2}F(d)\right) \qquad (2\text{-}1)$$

3. By treating U(d) and a(d) as parametric functions of displacement, the cumulative energy as a function of crack length, U(a) can be plotted.

4. By energy analysis, R is the slope of U(a) or:

$$R = \frac{dU(a)}{da} \qquad (2\text{-}2)$$

This slope calculation may benefit from smoothing by spline fits or running-regression methods.

2.2.4 Wood and Wood Composite Fracture

Wood can be considered an orthotropic material with three perpendicular growth directions, namely, longitudinal (L), tangential (T), and radial (R). Accounting for this anisotropy, six crack propagation systems can be defined, i.e., TL, RL, LR, TR, RT and LT (Smith & S. Vasic, 2003). The first letter stands for the normal to crack plane while the second indicates the propagation direction. In the present study, all fracture tests were either TL or RL crack propagation. For LVL specimens, T and L refer to tangential and radial direction of the veneer layers; hence a TL crack spans all adhesive bond lines while

an RL crack would be along one bond line in the middle of the specimen (see Fig. 2-1). Our first experiments looked at both RL and TL fracture. For solid wood, the TL *R* curve rises more than RL. In LVL the differences are dramatic with much greater rise in *R* curve for TL compared to RL fracture. The significantly higher TL *R* curves for LVL indicate more contribution of adhesive in this direction compared to RL direction. In RL crack growth, the crack is along a single bond line or may deviate into the veneer. Hence, it does not provide sensitive information on the adhesion quality. In contrast, TL cracks span all adhesive bond lines in the specimen. Such cracks will always break bond lines and veneers. For these reasons, all crack propagation experiments reported here, for both LVL and solid wood, were in the TL direction.

2.2.5 Statistical Analysis

Each moisture exposure condition was evaluated by replicate specimens. Each specimen gave an *R* curve. Several approaches can average multiple *R* curves. One approach is to divide the crack growth space into fixed-width boxes, collect all results that fall within each box, and then average those results (Wilson, et al., 2013). Another approach is to determine a common range for the average curve by performing interpolation/ extrapolation on each curve to get new datasets with a common set of crack length points, followed by averaging the corresponding interpolated toughness values. The latter approach was used for all averaged curves in this paper. Standard deviation and coefficient of variation of toughness were computed for each crack increment and plotted along with averaged *R* curves. For additional statistical analysis, two-way ANOVA tests were carried out to account for the effect of crack growth, accelerated aging, and their interaction on fracture toughness. Origin® software was used for the statistical analyses.

2.3 Results and Discussion

Individual specimen *R* curves in the TL direction for 10 control DF/PVA LVL samples made with Douglas fir veneer are shown in Fig. 2-2. Initiation toughness was highly

scattered and ranged from 40 to 400 J/m^2 with an average of about 200 J/m^2. The *R* curve for materials with fiber bridging is expected to increase as the fiber bridging zone develops. If that zone reaches a steady state, the toughness should level off at a constant value (Sinha, et al., 2012). Fig. 2-2 shows that all LVL *R* curves increased with crack propagation but the increase started to slow down and level off at about 100–120 mm of crack growth. While overall variation can be large, samples cut from a single billet (drawn with dashed, bold lines and triangles) showed much less difference in their *R* curves than samples from different billets. Because this study needed multiple billets to have enough specimens for all aging conditions, samples cut within each billet were randomly assigned to the various treatment conditions. Some specimens had a rapid rise in R near the end of the test (samples marked with "*"). These rises were attributed to edge effects. The R value is determined from R = dU/da where U is energy area and a is crack length. As the crack approaches the edge of the specimen, however, the crack slows down and da approaches zero, which can cause R to become large and unreliable (Matsumoto & Nairn, 2012).

Two specimens (samples marked with "#") decreased in toughness at long crack length, which could be due to material heterogeneity such that toughness in those specimens happened to vary with crack length; in other words the crack propagation in those specimens encountered a weaker region of the specimens.

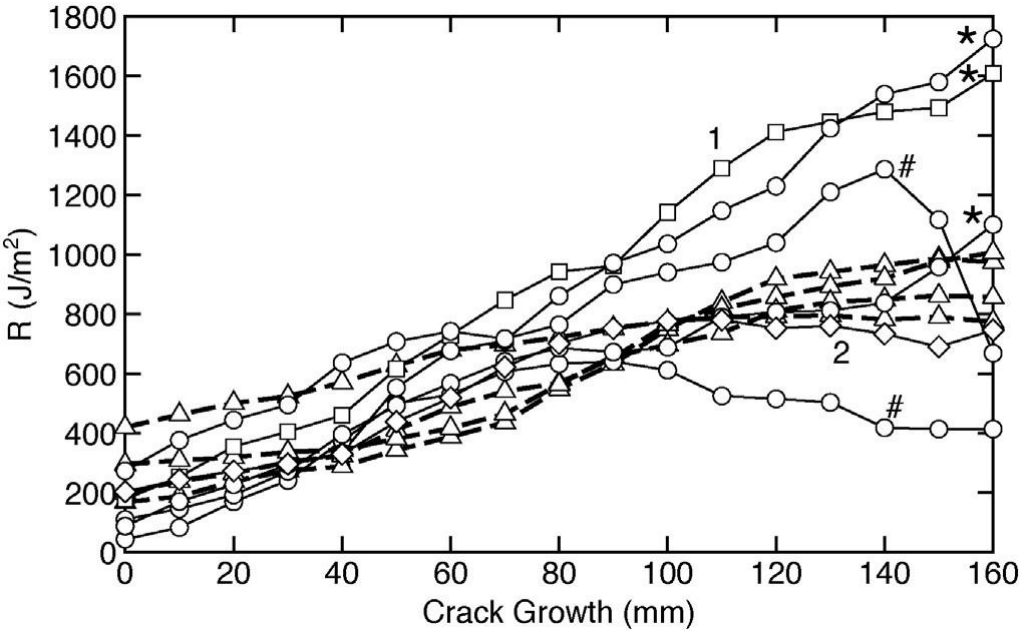

*Figure 2-2. Fracture resistance curves (*R *curves) of 10 individual control DF/PVA LVL specimens. The dashed, bold curves are four results for specimen taken from a single billet. The labels ("1", "2", "*", and "#") indicate specific result discussed in the text of the paper.*

We looked for several causes for variability in the *R* curves. Although density can be an important source of variation for solid wood, the density of all tested LVL samples were similar (approximately 0.62 g/cm^3). The variability seen here was more likely caused by material heterogeneity and perhaps sometimes by crack direction. In heterogeneous materials, the crack plane may deviate from the specimen's midplane causing mixed-mode fracture (mixed opening mode I and shear mode II). Because mode II toughness is generally higher than mode I toughness, when a crack deviates to include mode II character, the expectation is that the *R* curve will rise. The role of this phenomenon in the *R* curves of solid wood was studied by (Mohammadi & Nairn, 2014). We observed similar crack deviations in TL or RL LVL crack propagation. For example, Fig. 2-3 compares the crack paths of samples 1 and 2 (as labeled in Fig. 2-2). The crack in sample 2 propagated fairly straight and its *R* curve leveled off at steady state toughness of 750 J/m^2. In contrast, the crack in sample 1 deviated from the midplane. Fig. 2-2 shows that at 100 mm crack growth,

the *R* curve for this sample increased to over 1400 J/m^2. Part of this increase was likely caused by the crack deviation.

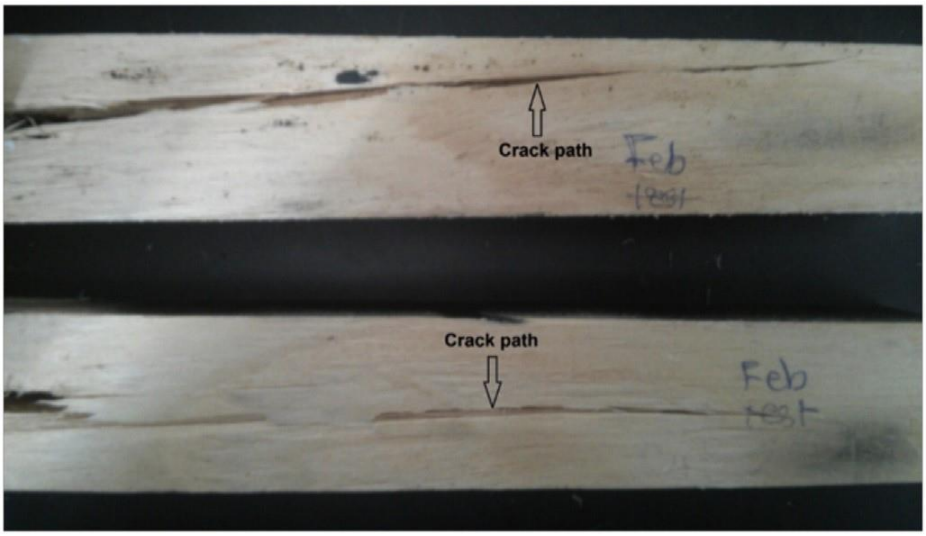

Figure 2-3. The crack propagation path for two control DF/PVA LVLpecimens when tested in TL direction. The top path is for specimen 1 and the bottom is for specimen 2; the R curves for these specimens are indicated in Fig. 2.

To get average *R* curves, results of several specimens (such as in Fig. 2-2) were averaged as explained in Materials and methods. The averaging included all specimens and therefore averaged over billet-to-billet variations and crack path deviation effects. Fig. 2-4 plots the average *R* curve for control DF/PVA LVL and compares it to average *R* curves for control solid wood and to both DF/PVA LVL and solid wood after 16 VPSD cycles. The error bars indicate standard deviations. All *R* curves show typical behavior where toughness increases as a function of crack length and the *R* curves approached a steady state toughness at high crack growth. The wood curves stop at shorter total crack length because some samples broke after about 100 mm of crack growth. Because our averaging did not extrapolate outside recorded data ranges, the averaging had to be limited to that lowest amount of crack growth. Comparing control to aged specimens, both DF/PVA LVL and solid wood showed significant decreases in toughness after 16 exposure cycles with the difference being larger than the standard deviations. Comparing DF/ PVA LVL to solid wood, the toughness

increment with crack growth in both control and aged solid wood is much smaller than the LVL results. For control specimen, both DF/PVA LVL and solid wood start at about 200 J/m^2 but DF/PVA LVL rises to about 1000 J/m^2 while solid wood rises only to 300 J/m^2 at 140 mm of crack growth without reaching a steady state toughness. This result corroborates a previous study on the *R* curve of Douglas-fir (Wilson, et al., 2013). Similarly for samples aged for 16 cycles, both DF/PVA LVL and solid wood start at about 100 J/m^2 but DF/PVA LVL rises to about 650 J/m^2 while solid wood rises only to 150 J/m^2 at 100 mm of crack growth without reaching a steady state toughness.

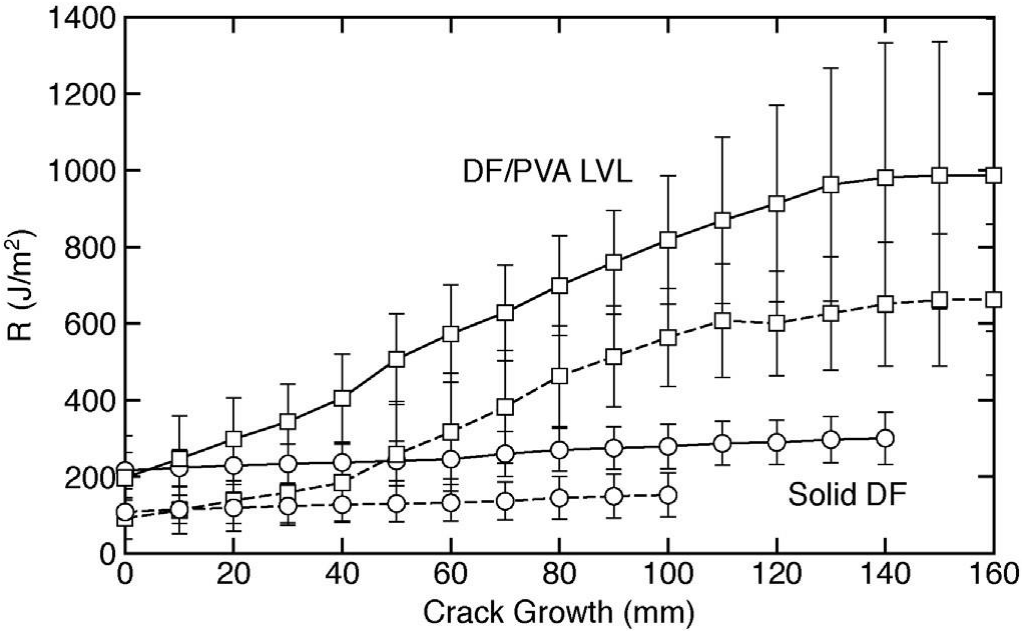

Figure 2-4. Fracture resistance curves (R curves) of DF/PVA LVL and solid wood (DF) for crack growth in the TL direction. The solid lines are control specimens and the dashed were exposed to 16 cycles. The error bars are standard deviations of the averaged curves.

Fig. 2-4 has important results for understanding the role of adhesive in LVL toughness and for understanding the best methods for using *R* curves to evaluate the role of the adhesive in moisture durability. Interestingly, the initiation toughness of solid wood is almost the same as the initiation toughness of LVL exposed to the same number of VPSD cycles. In other words, initiation of LVL cracking is mostly a property of the wood in the LVL and

not much affected by the adhesive. Any testing method to evaluate adhesives that relies on initiation properties (e.g., onset of cracking) will likely be a poor predictor of adhesive quality. Because the crack initiation was observed to correspond closely to the peak load in the force displacement curves, any testing method that relies on maximum stress (i.e., standard strength tests) will likely also be a poor predictor of adhesive quality. Instead, tests to evaluate adhesives should ignore the initiation phase and focus instead on the increment in toughness or on the rate of toughness increase. The importance of considering the post-peak regime will be investigated further in a future publication. Fig. 2-4 shows these properties to be vastly different in LVL compared to solid wood. Because a rising *R* curve in wood is associated with fiber bridging, these data show that the adhesive in LVL has a large impact on fiber bridging; Fig. 2-5 visually shows more fiber bridging in LVL than in solid wood. The magnitude of the rise is associated with the toughness of the bridging fibers while the rate of the rise is associated with cohesive stress that those bridging fibers can carry (Nairn, 2009). Both the toughness and cohesive stress of bridging fibers increased due to adhesive effects. Any test to evaluate adhesive quality based on fracture tests should be based on these properties from the rising phase of *R* curves.

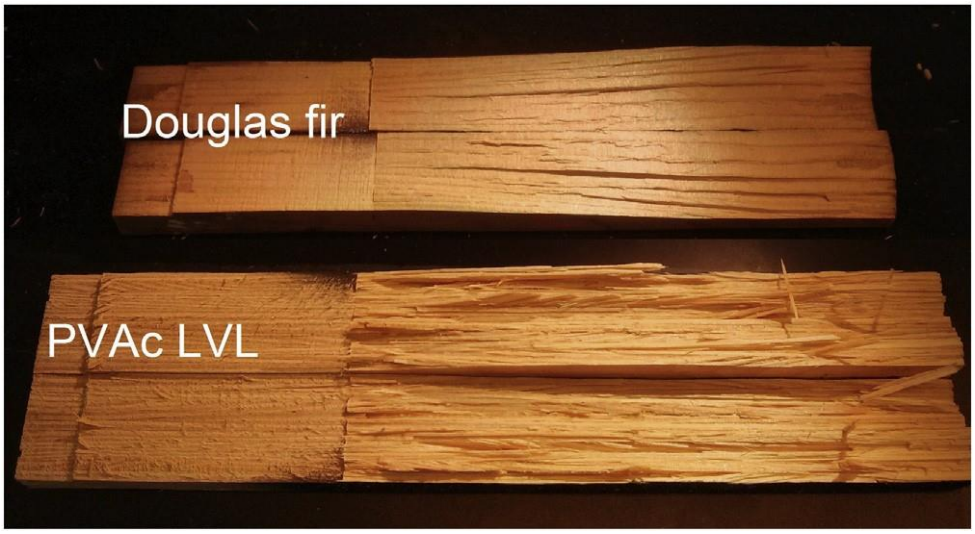

Figure 2-5. The fracture surface solid DF wood (top) and for DF/PVA LVL (bottom).

Fig. 2-6 shows the changes in fracture resistance of DF/PVA LVL as a function of the number of cycles of exposure from 0 to 16. Each curve was averaged as explained in Materials and methods using 8 ± 2 replicates. The error bars give the standard deviations of the interpolated points. All DF/PVA LVL *R* curves increased with crack growth and generally trended to lower toughness as the number of VPSD cycles increased. The toughness showed a significant drop between control and 4 cycles, but then remained nearly constant from 4 and 12 cycles. Continuing to 16 cycles, however, resulted in another significant drop in toughness.

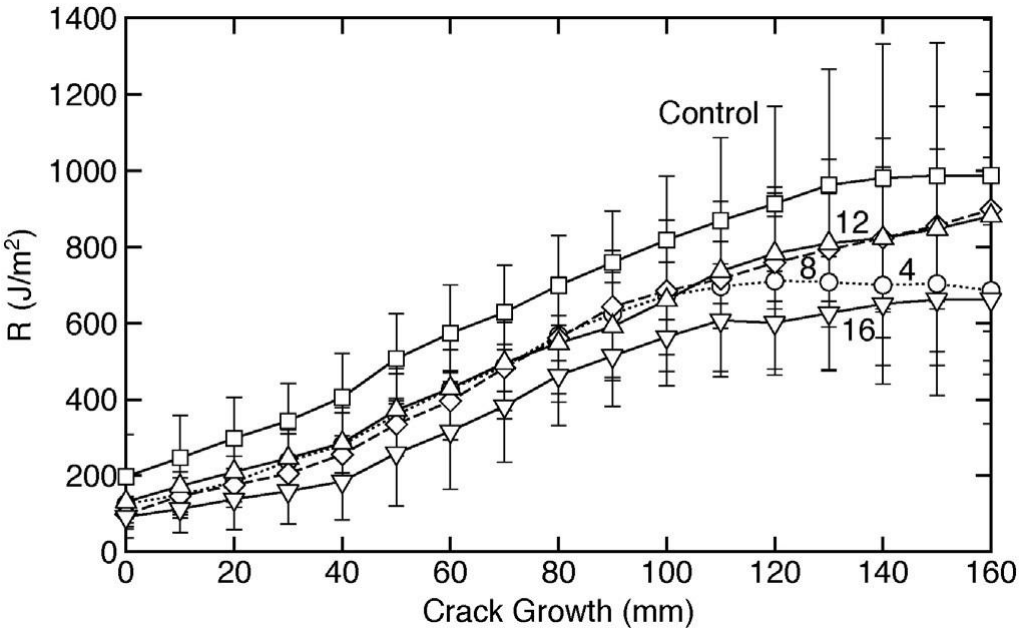

Figure 2-6. Degradation of fracture resistance (R curves) of DF/PVA LVL as a function of the number of cycles (Control, 12, and 16 are solid lines, 4 is a dotted line, and 8 is a dashed line). The error bars are standard deviations of the averaged curves.

The onset of a steady state toughness was most clearly observed in the *R* curves for control, 4 cycle, and 16 cycle samples. The other two *R* curves (8 cycle and 12 cycle samples) started to approach steady state at 120 mm of crack growth, but then started to increase again at 160 mm of crack growth. As mentioned above, this increase was likely an artifact due to edge effects. The fiber-bridging zone length can be determined from the amount of

crack propagation required for the rising toughness to start leveling off. These data indicate that the bridging zone for control specimen is about 130 mm and drops slightly with aging to close to 100 mm for 16 cycle samples. Besides bridging length, the steady state toughness for control and 16 cycle samples dropped from about 980 J/m^2 to 650 J/m^2, respectively. The bridging toughness (G_B), or the toughness associated with the fiber bridging mechanisms, is found by subtracting initiation toughness from the plateau toughness. Therefore, G_B of DF/PVA LVL for control samples was about 780 J/m^2 and G_B dropped to about 560 J/m^2 after 16 wetting and drying cycles. Similarly, one could determine in situ adhesive toughness (or the incremental toughness associated with the PVA adhesive) by subtracting the entire solid wood *R* curve from the LVL *R* curves. In this calculation, the in situ adhesive toughness for control specimens starts at zero and plateaus at about 680 J/m^2 while the in situ adhesive toughness after 16 cycles rises from zero to about 510 J/m^2. These results are clearly not equal to PVA toughness. First, they depend on crack length. Second, they differ from the reported toughness for PVA of about 200 J/m^2 (Khan, et al., 2013). In other words, the LVL toughness is not simply the summation of the toughness of its components. Rather, the rising *R* curve is caused by a complex interaction between wood and adhesive that leads to a significant change in fiber bridging occurring in LVL specimens compared to the fiber bridging of solid wood. Some interactions could be how the adhesive reinforces bridging fibers, how it affects their strength, or how it affects the way the fibers pull out of the fracture surfaces. Whatever the mechanism, the adhesive/wood interactions have a large effect on fiber bridging and therefore evaluation of adhesive quality should focus on the fiber bridging results that depend on the rising portion of *R* curves.

Fig. 2-7 shows the changes in fracture resistance of solid wood DF as a function of VPSD cycles from 0 to 16. Each curve is an average of 4 ± 1 replicates. The increased heterogeneity of solid wood (compared to LVL) can affect toughness. For example, toughness rises when a knot is located at the pre-cracked tip and then suddenly drops as

the crack propagates past the knot (not shown here). To avoid such effects, we selected clear regions of the lumber samples for the fracture tests. The aging trends are remarkably similar to the trends in LVL samples. Specifically, we observed a significant drop between control and 4 cycles, very little change between 4 and 12 cycles, and then perhaps a drop (albeit a smaller drop compared to LVL) between 12 and 16 cycles. The initiation toughness of solid wood as a function of VPSD cycles was very close to the corresponding toughness in LVL. Compared to LVL, the solid wood *R* curves had much lower slope in the rising portion of the *R* curves. Linear fits to the rising portion of solid wood *R* curves varied between 0.4 and 0.7 kPa, which is an order of magnitude smaller than the corresponding slopes for LVL. Note that the slope of an *R* curve has units of stress and is related (by a specimen-dependent conversion process) to the cohesive stress carried by the bridging fibers (Nairn, 2009). Hence, bridging zones in LVL samples carried about an order of magnitude higher stress than bridging zones in solid wood samples.

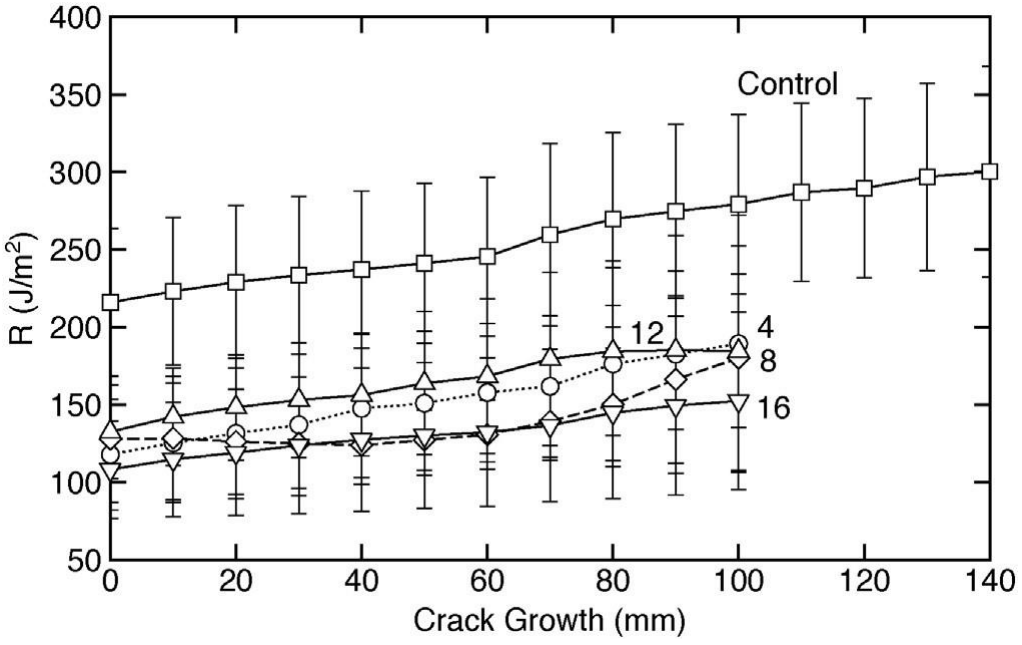

Figure 2-7. Degradation of fracture resistance (R curves) of solid wood DF as a function of the number of cycles (Control, 12, and 16 are solid lines, 4 is a dotted line, and 8 is a dashed line). The error bars are standard deviations of the averaged curves.

A two-way ANOVA test was carried out to consider the effects of crack propagation, number of cycles, and their interaction on the fracture toughness of LVL and solid wood. The effect of crack length on toughness was statistically significant ($p < 0.01$), and toughness increased as function of crack growth (as clearly displayed in all *R* curves). Hence, crack propagation should be considered when studying the fracture toughness of wood-based materials with fiber bridging zones. This result is true even for solid wood with relatively little fiber bridging capacity. The effect of number of cycles on toughness was also significant ($p < 0.01$), but there is no significant interaction between number of cycles and crack propagation.

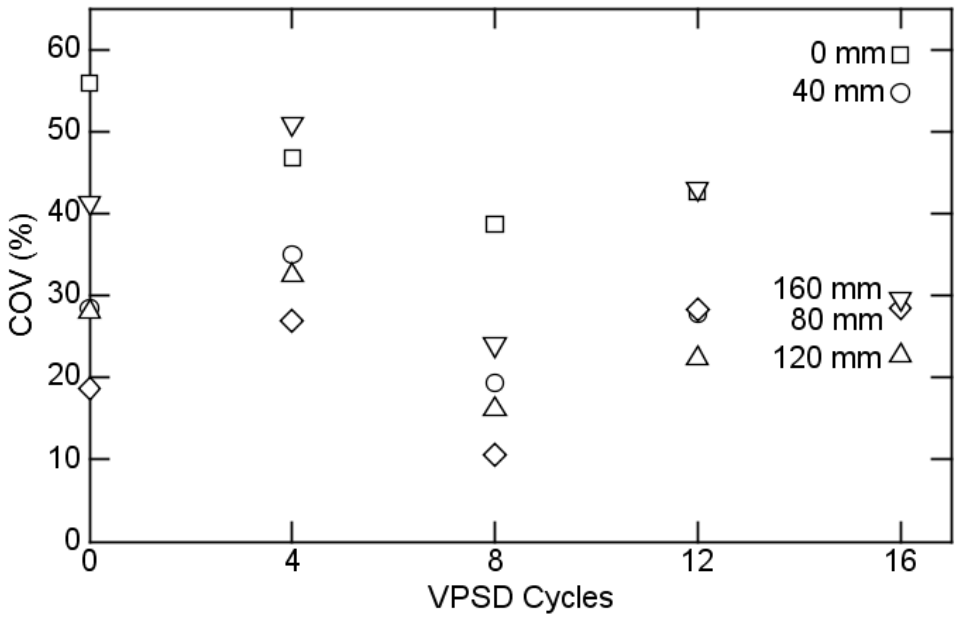

Figure 2-8. The coefficient of variation (COV) of DF/PVA LVL toughness as a function of the number of cycles at different amounts of crack growth.

The statistical analysis lumped all results together; perhaps more careful data selection would result in better comparisons. The coefficient of variation (COV) of the DF/PVA LVL toughness as a function of number of cycles for different extents of crack growth is shown in Fig. 2-8. The initiation toughness (0 mm) had the highest COV, again indicating that initiation toughness is a poor property for characterizing fracture properties. As the

amount of crack growth increased the COV dropped and reached a minimum for 80 mm of crack growth. This drop can be seen graphically in Fig. 2-6. The magnitudes of the standard deviation error bars were fairly constant for the first 100 mm of crack growth. Because the standard deviation remained constant while the mean increased, the COV decreased. For longer crack growths (120 and 160 mm), the COV increased again. This effect is also seen graphically in Fig. 2-6 by the increased standard deviations for high crack growth. The larger deviations at high crack growth were caused by a mixture of specimen heterogeneity (e.g., reaching steady state at different amounts of crack growth) and edge effects seen in some specimens.

With the goal of defining to a simpler quantity for analysis, we focused on results after some amount of crack propagation rather than attempt to use the entire *R* curve. According to our statistical analyses for both LVL and solid wood, toughness significantly increased as a function of crack growth and was significantly degraded by moisture cycling.

The observation of no significant interaction between crack growth and cycles implies that the effect of aging does not depend on crack length. In principle, therefore, the effect of aging on fracture toughness can be investigated at any amount of crack growth. One approach we tried was to focus on the results at the crack length that had the smallest COV. Based on results in Fig. 2-8, the preferred crack length for characterization of DF/PVA LVL is 80 mm of crack growth. This crack growth level had the minimum COV. It also had the maximum amount of crack growth prior to the onset of higher statistical variations at higher crack growth. It is thus sensitive to the increases in the *R* curve while being minimally affected by edge effects. In other words, initiation toughness is not the best criterion to study the fracture toughness of wood based materials and artifacts such as edge effects make *R* curves near the end of the sample unreliable. In contrast, evaluating toughness in the middle of the rising *R* curve has potential.

A similar analysis of solid wood *R* curves suggested that 50 mm of crack growth was the optimal amount of crack growth for characterization. Compared to LVL, the solid wood COV's were less sensitive to the amount of crack growth except at very high crack growth where they increased analogously with LVL results. We chose 50 mm of crack growth because it had low COV and also included some amount of the rising *R* curve. Comparing the toughness COV of LVL and solid wood revealed that the toughness COV of untreated solid wood was about 20% throughout the fracture process, which is generally smaller than that of the LVL. In some properties, such as strength and modulus, solid wood generally has a higher COV than the LVL of the same species (Erdil, et al., 2009), which is due to homogenization of defects in LVL compared to solid wood. This higher COV, however, may not be true for toughness. Ardalany et al. (2012) report a larger COV for the G_{init} of LVL than for solid wood. Fruhmann et al. (2002) report a high COV of 25–70% for G_{init} of LVL in mode I testing. The overall average COV of either LVL or solid wood for all extents of crack growth and all treatments was about 30%, which is comparable to the reported solid wood toughness without considering crack propagation of 34% (Liswell, 2004). The high variation is perhaps due to the prominent contribution of grain direction to crack propagation and therefore, toughness. Note that we used low grade (B grade) veneer in our homemade LVL billets. Using a higher grade veneer may reduce the scatter. Also, the high COV of LVL can be, to some degree, attributed to variation between billets. The overall average COV of LVL when samples all taken from a single billet was 23% with the smallest COV of 13% at 100 mm crack propagation. Hence, our variations in LVL toughness may be partly attributed to manufacturing process variations. Nevertheless, monitoring crack propagation enables us to detect crack length at which the associated scatter is a minimum.

Using the amounts of crack growth identified above, Fig. 2-9 plots toughness retention for both DF/PVA LVL and solid wood as a function of number of exposure cycles. The retention percent is defined as: (property after treatment / property for control samples) $*$

100. For both DF/PVA LVA and solid wood, the toughness at 80 mm crack growth (for LVL) or 50 mm crack growth (for solid wood) indicates a near continuous decrease. As shown in Figs. 6 and 7, both materials dropped from 0 to 4 cycles, remained relatively constant between 4 and 12 cycles, and then dropped again between 12 and 16 cycles. Although solid wood dropped faster than LVL, the toughness in LVL is higher and includes drops in fiber bridging toughness as well as in the solid wood component. In other words, the LVL retention plot is characterizing adhesive effects in the moisture durability of DF/PVA LVL. Such experiments, if applied to composites made with other adhesives, can be used to compare and rank those adhesives for their ability to make durable wood composite materials.

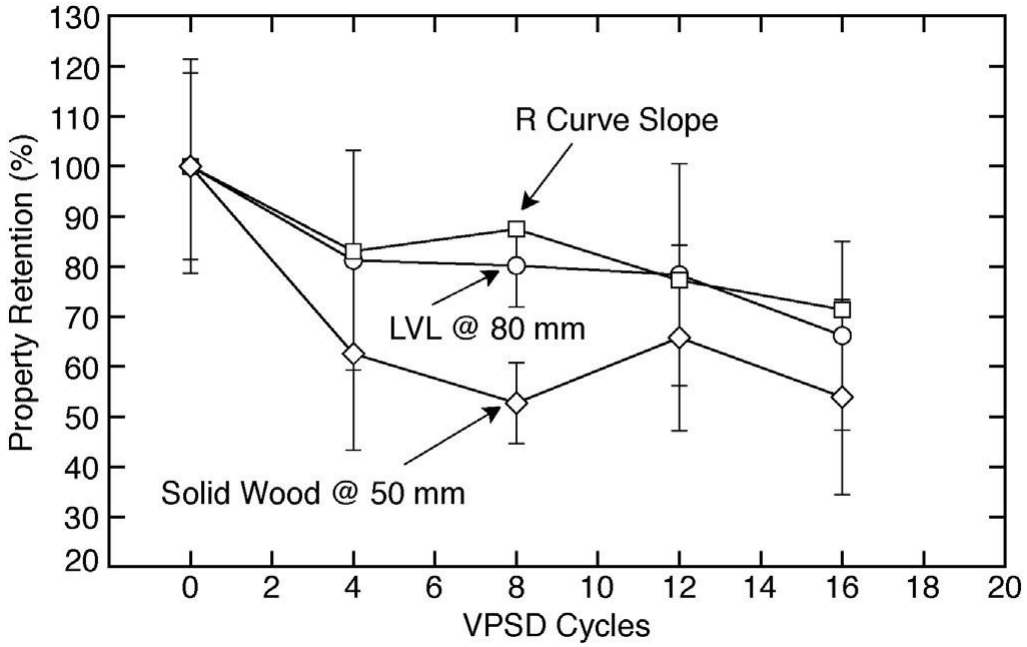

Figure 2-9. The fracture toughness of DF/PVA LVL and solid wood as percent of control value and as determined at a specific amount of crack growth (at 80 mm for LVL and at 50 mm for solid wood). The "R curve slope" is the slope of the R curve over the first 100 mm

Besides toughness associated with fiber bridging, fiber-bridging effects can also be characterized by the rate of rise of the *R* curve. Fig. 2-9 also plots the slope of the DF/PVA LVL *R* curves as determined by linear fits over the first 100 mm of crack growth and plotted

as percent of the slope in the control specimen. This slope is a function of the critical cohesive stress in the bridging fibers (Nairn & Matsumoto, 2009). The retention plot indicates a loss in the strength of those fibers with moisture conditioning. The slope retention parallels the toughness retention. In other words, both the slope of *R* curves and the magnitude of the increment over initiation toughness are good candidates for characterizing the role of adhesive on the moisture durability of wood composites.

2.4 Conclusions

The fracture resistance, or *R* curve, of LVL can be measured and the results are significantly different from the *R* curves for solid wood made out of the same species as the veneer in the LVL. Furthermore, the differences are only apparent during crack propagation. The initiation toughness for LVL and solid wood are very close, but the *R* curves rise much more for LVL than for solid wood. Because a rising *R* curve can be attributed to fiber bridging, the conclusion is that adhesive and adhesive/wood interaction play a significant role in the strength and toughness of the fibers that bridge the crack surface.

The research highlights can be summarized as follows:

1. Toughness augmentation as a function of crack propagation was directly measured and shown to be statistically significant in solid wood and laminated veneer lumber. Therefore, any work dealing with this subject should properly address the *R* curve behavior of the material.

2. Although the initiation toughness of solid wood and laminated veneer lumber are very close, toughness rises much more in the latter after some crack propagation. This difference can be attributed to the contribution of adhesive to fiber bridging, and emphasizes the importance of monitoring crack propagation.

3. Contingent upon the source variation from which samples are collected, scatter in toughness can be small or large. Nevertheless, monitoring crack propagation enables us to detect crack length at which the associated scatter is a minimum.

4. Toughness characteristics, excluding initiation toughness, properly reflect the moisture durability of solid wood and laminated veneer lumber.

Here we proposed to use the large adhesive effect on *R* curves to quantify the role of adhesive in the moisture durability of LVL. The method works, but it was essential to focus on either the increment in toughness over initiation toughness or the rate of rise of the *R* curves. The observation that initiation toughness for LVL and for solid wood are nearly the same suggests that any test protocol based on the onset of cracking or peak force in strength tests should be expected to be a very poor test for quantifying adhesive effects in wood composite durability. The experiments here were for a single PVA adhesive. Future work will compare the moisture durability for LVL made from various adhesives. The importance of fiber bridging effects on the toughness of wood composites recommends future work aimed at modeling crack growth with bridging fibers. Applying such modeling to crack growth in wood composites may help quantify adhesive effects further.

Acknowledgments

Financial support was provided by the National Science Foundation Industry/University Cooperative Research Center for Wood-Based Composites, Award No. IIP-1034975. We thank Momentive® Specialty Chemicals for supplying all adhesives and veneer materials.

3 Assessing the Role of Adhesives in Durability of Wood-based Composites Using Fracture Mechanics

Babak Mirzaei, Arijit Sinha, and John A. Nairn

Holzforschung DOI: 10.1515/hf-2015-0193

Abstract

This study explored the use of fracture toughness properties for durability assessment of wood composite panels. The main objective was to develop a new method for ranking the role of adhesives in the durability of wood-based composites by observing changes in fracture toughness during crack propagation following cyclic exposure to moisture conditions. We compared this new approach to conventional mechanical performance test methods, such as observing strength and stiffness loss after exposure. Comparing changes in fracture toughness as a function of crack length after moisture cycling shows that fracture-mechanics based methods can distinguish different adhesive systems on the basis of their durability, while conventional test methods do not have similar capability. Using steady-state toughness alone, the most and least durable adhesives (phenol formaldehyde and polyvinyl acetate) could be distinguished, but the performance of two other adhesives (emulsion polymer isocyanate and phenol resorcinol formaldehyde) could not. Further analysis of experimental *R* curves (toughness as a function of crack length) based on kinetics of degradation was able to rank all adhesives confidently and therefore provided the preferred method. The likely cause for the inability of conventional tests to rank adhesives is that they are based on initiation of failure while the fracture tests show that comparisons that can rank adhesives require consideration of fracture properties after a significant amount of crack propagation has occurred.

Keywords: crack propagation, durability assessment, *R* curve, wood adhesive

3.1 Introduction

The ideal experiment for assessing durability of a product is to fabricate actual-sized specimens, subject them to actual service loads (either loads or moisture), and then periodically monitor their residual properties. This "ideal" approach is impractical for several reasons. First, the experiments are too time consuming; it may take a long time for

specimens to show effects under actual service loads. Second, most durability experiments are highly variable making it difficult to gain any statistical confidence in the results (Sinha, et al., 2012). The solution is to develop accelerated methods that can give useful information about durability in shorter term tests.

Typical wood-based composite tests for moisture durability operate by exposing products to wet and/or hot environments and then inspecting for signs of damage (*e.g.*, ASTM D2559 or D1037). Such tests are often qualitative (*e.g.*, pass/fail based on observation of damage). These tests can be made quantitative by coupling with suitable mechanical tests. For example, static bending and shear tests are common methods for evaluating the resistance of wood-based composites to aging. While the former supposedly addresses material durability as a whole, the latter aims to evaluate the quality of the bond-line after accelerated aging (ASTM D1037, 2012; NIST PS1, 2007). Unfortunately, these common tests look only at early stages of loading up to initiation of failure. These properties do not depend strongly on the adhesive and therefore are poor tests for ranking adhesives (Stoeckel, et al., 2013). In contrast, it was recently shown that fracture analysis of crack propagation within a single composite material (OSB, plywood, LVL, *etc*.) provides more information than conventional bond stiffness and strength testing (Sinha, et al., 2012). For example, the increase in toughness for LVL specimens during crack growth contains a large contribution from the adhesive (Mirzaei, et al., 2015).

Our goal was to develop a methodology for quantitative assessment of wood adhesives that can predict which ones provide advantages for moisture durability. Our hypothesis was that a good approach would be to combine exposure experiments with fracture property characterization. Furthermore, the fracture property experiments should include fracture toughness changes during crack propagation to include information beyond the initiation stage. In other words, we explored expanded use of fracture toughness as a design tool for durable wood composite panels. The key experiment was to look for correlations between fracture toughness and durability by parallel fracture and durability experiments. If

successful, fracture tests could be proposed as an accelerated method for ranking adhesives and designing durable composite panels. The same approach was used for accelerated testing of aerospace composites by monitoring microcracking fracture toughness during hydrolytic degradation experiments on aerospace composites (Kim, et al., 1995; Han & Nairn, 2003). This approach was a great improvement over pass/fail methods that were previously used by Boeing. A similar approach was also used to assess high-temperature performance of wood-based composites (Sinha, et al., 2012). The fracture properties helped identify which composites were most susceptible to thermal damage.

The new aspects of this study were to compare different adhesives and to focus on moisture durability. We assessed the durability of four conventional adhesive systems used for Laminated Veneer Lumber (LVL). The main task was to develop methods for analyzing observed changes in fracture toughness during crack propagation following cyclic exposure to moisture conditions in order to rank adhesives for durability. We compared these new methods to conventional mechanical performance test methods such as observation of strength and stiffness loss after exposure. An advantage of the new methods is that they extend into the post-peak regime while conventional methods focus on pre-peak response (for stiffness loss) or peak load only (for strength loss). The additional information in the post-peak regime can help compare adhesives. Finally, several data analysis methods were examined in order to determine which method provides the best information for adhesive comparisons.

3.2 Materials and Methods

3.2.1 Materials

LVL billets were manufactured in the laboratory under controlled conditions using all B grade Douglas-fir veneers. Each LVL billet had dimensions 61cm X 91cm (2ft X 3ft), consisted of 11 plies (each 3 mm thick), and one of the following four adhesives: Wonderbond® EL-35 Emulsion Polymer Isocyanate (EPI), GP® 421G83 RESI-MIX®

Phenol Formaldehyde (PF), CASCOPHEN® LT-5210J/CASCOSET® FM-6210 adhesive system Phenol Resorcinol Formaldehyde (PRF), and a one-component Polyvinyl Acetate (PVA). Glue spread rate (coverage of 250-300 g/m^2) and press conditions were adjusted according to the guidelines of the relevant adhesive manufacturer. PVA billets were pressed at 2.07 MPa (300 psi) at room temperature for about 1 hour. PF billets were pressed at 0.69 MPa (100 psi) for 5 minutes at room temperature and then hot-pressed at 2.07 MPa (300 psi) for 20 minutes at 180°C. EPI and PRF billets were pressed at room temperature at 0.83 MPa (120 psi) for 20 minutes and 8 hours, respectively.

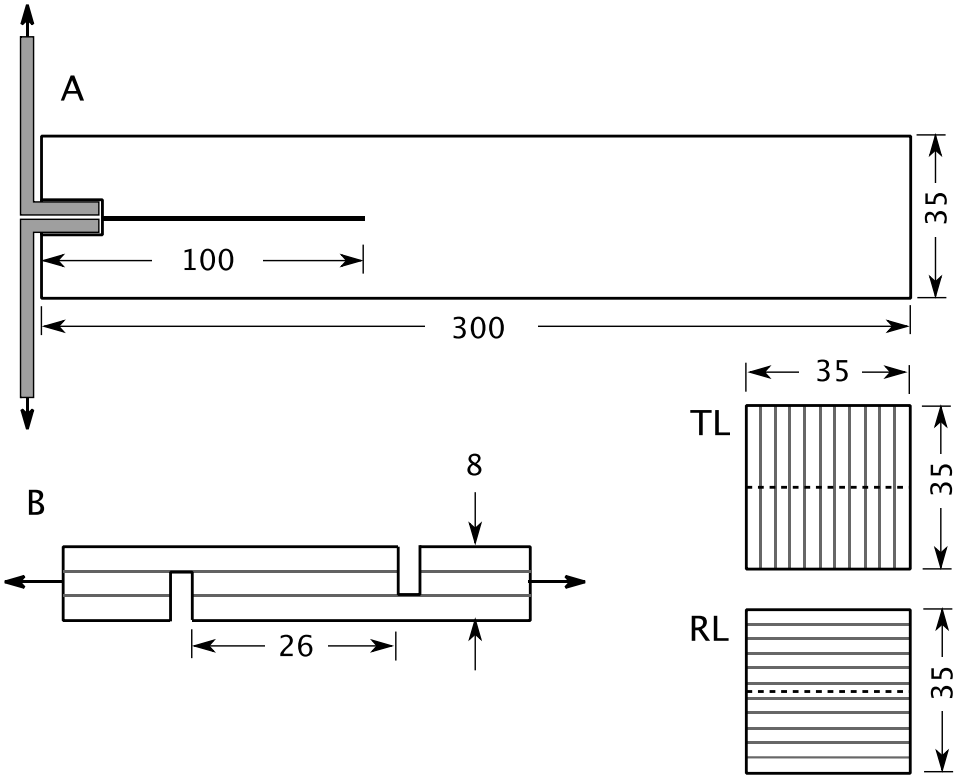

Figure 3-1. A. The double cantilever beam specimen (DCB) used for crack propagation experiments. The TL and RL diagrams on the lower right show end view of those specimens with gray lines indicating bond lines between veneers and the dashed line indicating the crack propagation plane. B. The 3-ply, lap shear specimen used for conventional shear strength tests by loading in tension. All dimensions are in mm.

After pressing, the LVL billets were conditioned in a standard room maintained at 20°C, 65% RH for one week before further testing. Note that commercial LVL normally uses high-grade veneers on the surfaces and low-grade veneers in the middle (Wang & Dai, 2005). For this work, however, it was important to have uniform grade veneer throughout.

3.2.2 Moisture Treatment

Accelerated moisture exposure was carried out according to ASTM Standard D2559, but we excluded the steam exposure step. Each cycle started by exposing the samples to 85 kPa vacuum for 5 minutes followed by submersion in water in a pressure vessel at 517 kPa for 1 hour. After removal from the pressure vessel, the samples were oven-dried at 65 ± 2° C for 21-22 hours (ASTM D2559, 2012). These steps represented one moisture cycle or vacuum pressure soaking drying (VPSD) cycle. Samples were subjected to 0 (for controls), 8, 16 and 24 cycles. After these selected numbers of cycles, samples to be tested were thoroughly dried at 103° C for 24 hours and then stored in the standard conditioning room until they reached equilibrium. After reaching equilibrium, the samples were tested for fracture properties and for stiffness and strength properties.

3.2.3 Crack Propagation Experiments

The toughness or critical energy release rate for a material is the amount of energy released by unit increment in new crack area (Irwin, et al., 1958). For some materials, including wood, this critical energy changes as the crack propagates. An experimental measure of this change is known as the crack resistance curve, or *R* curve. *R* curves can be measured from experimental data for load, displacement, and crack length by integrating load-displacement data up to some point for which crack propagation data is available and then dividing the incremental released energy by newly created fracture surface area (Nairn, 2009).

Wood can be considered as an orthotropic material with three perpendicular material directions, namely, longitudinal (L), tangential (T), and radial (R). For LVL specimens, T

and R refer to tangential and radial direction of wood in the veneer layers, which correspond to in-plane and thickness direction of the rotary-peeled veneers, respectively. Accounting for this anisotropy, six crack propagation systems can be defined, *i.e.*, TL, RL, LR, TR, RT and LT (Smith, et al., 2003). The first letter stands for the normal to crack plane while the second indicates the propagation direction. In the present study, all fracture tests were either TL or RL crack propagation.

A TL crack in LVL spans all adhesive bond lines while an RL crack plane would be parallel to the bond lines (see Fig. 3-1). Our first experiments looked at both RL and TL fracture. For solid wood, the TL *R* curve rises more than the RL. In LVL the differences are dramatic with much greater rise in *R* curve for TL compared to RL fracture and with much higher toughness than solid wood (Mirzaei, et al., 2015). The significantly higher TL *R* curves for LVL indicate more contribution of adhesive to TL fracture compared to RL fracture. In RL crack growth, the crack may propagate along a single bond line or may deviate into the wood within a single veneer layer. Hence, RL fracture may not provide sensitive information on adhesion quality. In contrast, TL cracks span all adhesive bond lines in the specimen. Such cracks will always break bond lines and veneers. Because of this greater role of adhesive in TL fracture, all crack propagation experiments reported here for LVL were in the TL direction.

Crack propagation fracture toughness tests were carried out using an energy method developed for direct *R* curve measurement (Nairn, 2009). More specifically, crack propagation experiments were conducted using double cantilever beam (DCB) specimens that were cut from equilibrated LVL billets (see Fig. 3-1). The initial cracks were cut with a band saw for TL fracture tests. To avoid possible weak adhesion zones near the edges, the edges of the LVL billets were marked before sawing and the initial specimen cracks were cut from the marked ends, such that all cracks propagated away from the edges. Hence, the quality of the inner zone adhesion was tested. Dimensions of all DCB samples were $35 \pm 2 \times 35 \pm 2 \times 300 \pm 5$ mm^3 and the initial, sawn pre-crack was 100 mm.

The samples were tested in an Instron 5582 universal testing machine. Load and displacement data were continuously recorded during tests. The DCB fracture tests were conducted in opening mode under displacement control at 2 mm/min. The crack plane at the edge of each specimen was widened and loading was applied using angle irons inserted into the gap. Crack growth data were collected using the 3D Digital Image Correlation (DIC) technique. Mirzaei et al. (2015) has successfully demonstrated the use of DIC techniques for crack propagation in wood. Similar techniques were used in this study. A brief description is provided here, but a detailed description on DIC implementation for crack data population can be found in a previous paper (Mirzaei, et al., 2015). DIC is a technique to map strains by tracking a small subset of pixels in deformed images. It is especially useful for materials whose surface cannot be polished, such as wood. The tensile strain normal to the crack plane ahead of the crack tip was monitored throughout the loading. Crack propagation was measured by observing shifts in the position to reach 1% vertical strains between subsequent images.

Replicate specimens (8±2 for PVA LVL and 6±2 for the rest) were used to evaluate each moisture exposure condition. Each specimen gave an R curve. To average multiple R curves, we determined a common range for the average curve by performing interpolation/extrapolation on each curve to get new datasets with a common set of crack length points, followed by averaging the corresponding interpolated toughness values. Standard deviations of toughness were computed for each crack increment and plotted along with averaged R curves. For additional statistical analysis, two-way Analysis of Variance (ANOVA) tests were carried out to account for the effect of crack growth, accelerated aging, and their interaction on fracture toughness.

3.2.4 Conventional Strength and Stiffness Testing

Parallel stiffness and strength tests were carried out for comparison to toughness results. Modulus of elasticity E can be computed from DCB arm bending using the following beam equation:

$$E = \frac{8Pa^3}{\delta b h^3} \qquad (3\text{-}1)$$

where, P/δ is slope of the load *vs*. crack opening displacement curve before the proportional limit, a is initial crack length, b is beam breadth and h is height of the beam arm. This modulus, however, needs correction due to shear and crack tip arm rotation, especially because the length to depth ratio of the arms (a/h ~ 6) was rather small. The correction can be done by replacing crack length, a, with an effective crack length a+χh, where χ is a correction factor. A correction factor developed for uniaxial fiber-polymer composite can be applied to wood-based composite using the following equation (Hashemi, et al., 1990):

$$\chi = \sqrt{\left(\frac{E_L}{11G_{LT}}\right)\left(3 - 2\left(\frac{\Gamma}{1+\Gamma}\right)^2\right)} \qquad (3\text{-}2)$$

where, $\Gamma = 1.18\sqrt{(E_L E_T)}/G_{LT}$. E and G are the elastic moduli in the appropriate directions approximated using solid Douglas-fir elastic properties provided by US Forest Products Laboratory (2010) as E_L = 13 GPa, E_T = 0.65 GPa and G_{LT} = 1.01 GPa. The moduli were found for each DCB specimen and therefore had the same number of replicates as the fracture tests.

For a strength-based test, notched 3-ply shear specimens were cut from the arms of the DCB samples after fracture tests to test the same material that was exposed to the same weathering conditions as the fracture specimens. Because the arms do not sustain damage during fracture tests the material in those arms can provide suitable comparison specimens. A shear test (NIST PS1, 2007) was conducted using an Instron 5582 universal testing machine. The shear area needed to find the shear stress was measured for each specimen using calipers. The test configuration and nominal dimensions are shown in Fig. 3-1. Shear test results consisted of 6±2 replicates for each condition.

3.3 Results and Discussion

LVL samples made using EPI, PVA, PRF and PF adhesives and B grade Douglas fir veneers were tested for fracture toughness during crack propagation. The resulting *R* curves for control specimens and specimens exposed to 8, 16, and 24 VPSD cycles are in Fig. 3-2. Each curve is the average of several replicates. With the error bars indicating standard deviations. All *R* curves show typical behavior with initiation toughness (G_{init}), which was a relative low toughness and comparable to the initiation toughness of solid wood (100 to 300 J/m^2), followed by an increase in toughness as a function of crack length. Most curves approached a steady-state toughness, G_{ss}, at high crack growth. After reaching steady state toughness, deviations from the resulting plateau are likely due to either edge effects or to material inhomogeneity. The *R* value is determined from $R = (1/t)dU/da$ were *U* is total energy released up to crack length *a* and *t* is thickness. As the crack approaches the edge of the specimen, however, the crack slows down and *da* approaches zero, which can cause *R* to become large and unreliable (Matsumoto & Nairn, 2012). As a result, the rises at long crack length were attributed to edge effects. After reaching steady state, the fracture toughness does not normally drop in homogeneous materials, however, in wood or wood composites, a crack may enter a weak zone affecting material's toughness. It is important to recognize that the B grade veneer used for LVL fabrication in this study may have some weak zones.

The plot scales in Fig. 3-2 were adjusted to be the same for all materials for ease of comparison (the extra crack length data for PVA was compensated by stretching the plot). The PF, PRF, and EPI adhesives seem to equally contribute to the fracture energy of the materials in the control condition, hence, creating roughly equal *R* curves. In contrast, the control *R* curve for PVA was higher and reached higher G_{ss} at longer critical crack length. The one-component PVA used in this study was the only adhesive without any considerable crosslinking capability. The high fracture toughness maintained by PVA can be attributed to additional flexibility of linear molecular chain segments, as compared with

the more brittle behavior of the other adhesives with cross-linked molecular structures (Suzuki & Schniewind, 1987). That being said, we did not observe as much contrast among the adhesives in terms of their fracture toughness when bonded to wood as some other studies have reported, but those studies did not carry out a full *R* curve analysis. Most prior work did fracture tests on the bond-line, which corresponds to RL fracture instead of the TL fracture used here. Additionally, they reported only initiation toughness or total work of fracture. Pizzi and Mittal (2003) have collected these results.

The crack length at which toughness becomes constant is a measure of the size of the fiber bridging zone that develops in the wake of the crack propagation. Once the bridging zone is fully developed, additional crack growth will be at constant bridging zone length and constant G_{ss} (Nairn, 2009). According to Fig. 3-3, the fiber bridging zone is roughly 130 mm for PVA-made LVL while it is about 90 mm for LVL made with other adhesives. Fracture toughness at these crack lengths were considered to be G_{ss} for that material. Exposure to accelerated aging (VPSD cycles) caused G_{ss} to decrease and also affected other toughness attributes such as the G_{init} and the *R* curve shape. *R* curve shape can be translated into bridging stress distribution (Gallops, 2011) as a measure of the ability of those fibers in combination with adhesive to increase toughness. Quantitative interpretation of *R* curve shape requires numerical modeling and will be covered in a future publication. This work looked at various changes in experimental features of the *R* curves to find the preferred assessment criterion for ranking the ability of adhesives to provide durable wood composites.

According to Fig. 3-2, *R* curves clearly showed degradation as a function of accelerated aging cycles. According to the results of a two way ANOVA, fracture toughness significantly increases as a function of crack propagation ($p < 0.05$). It also significantly deteriorates due to aging ($p < 0.05$). However, the interaction of aging and crack growth on toughness was not statistically significant.

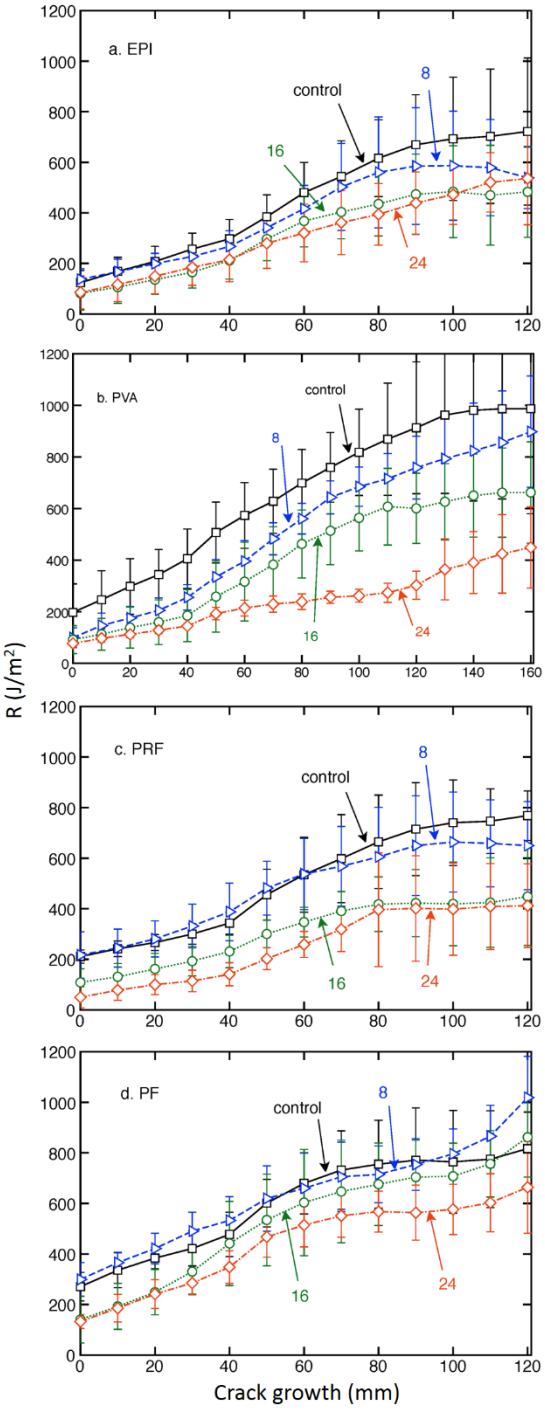

Figure 3-2. Average fracture R curves of LVL made using a. EPI, b. PVA, c. PRF and d. PF adhesives exposed to 0 (control), 8, 16, and 24 VPSD cycle treatments (as indicated on each plot). Note that x-axis scale on b. PVA differs from the other three plots.

For each durability indicator studied, our comparisons used percentage property retention defined as the property after aging normalized to the control property (and expressed as a percentage). This approach gives emphasis to degradation trends due to aging. Additionally, the comparison can be carried out among various properties to choose the most suitable durability indicator. We also compared the degradation trends of toughness properties to degradation trends measured using conventional strength and stiffness properties. These conventional properties are based on initial slope (stiffness) or on load at initiation of failure (strength) and therefore, do not take into account any experimental results after crack propagation.

The first toughness property to consider was the initiation toughness or G_{init}. For materials with fiber bridging zones, such as wood and LVL, G_{init} is less than G_{ss} and may be significantly less as determined by material's toughening capacity. It has been observed that G_{init} of solid wood and PVA LVL made out of the same species are similar, but their G_{ss} levels are considerably different (Mirzaei, et al., 2015). Even after aging, the decreases in solid wood and LVL G_{init} values are similar indicating minimal contribution of adhesive to the initiation of fracture (Mirzaei, et al., 2015). Besides PVA LVL, the results here showed inconsistent decreases in G_{init} as a function of aging for EPI, PRF, and PF made LVL (see Fig. 3-2). In brief, it is likely that the G_{init} of LVL is determined predominantly by solid wood properties, which implies that G_{init} is not a proper indicator for assessing the role of adhesive in durability.

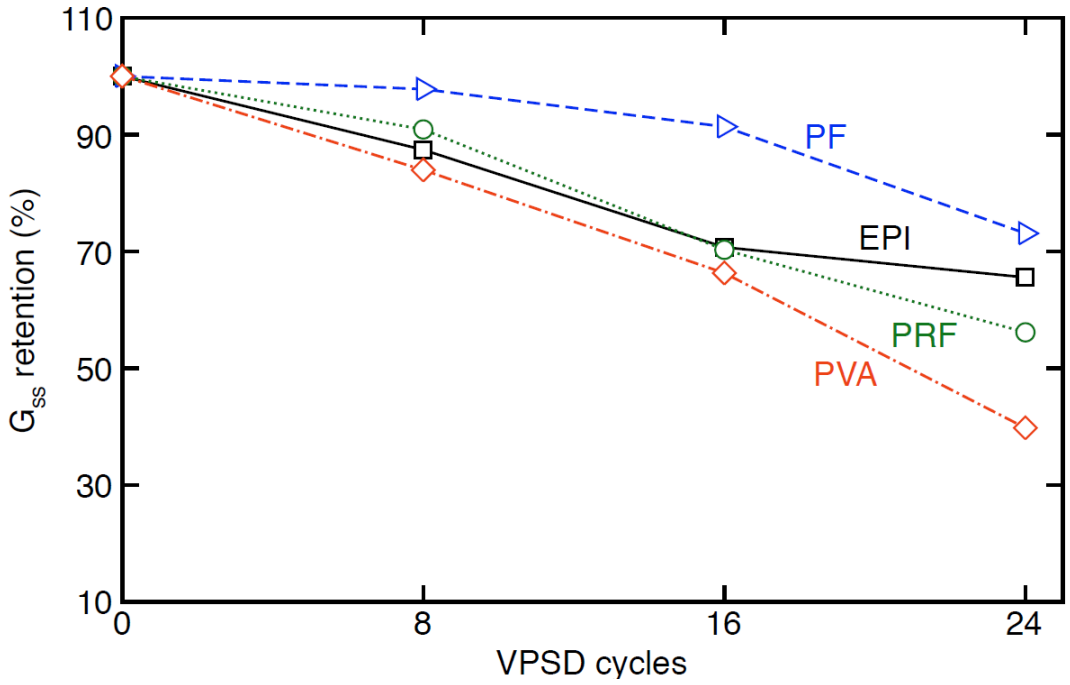

Figure 3-3. Steady state toughness (Gss) retention of various adhesives as a function of the number of VPSD cycles.

In contrast to G_{init}, G_{ss} is the toughness of the material after the full development of bridging zones. In the steady-state regime, the size of the bridging zone is constant (it propagates along with crack growth) and therefore, toughness become constant as well. As suggested by the larger increase in toughness of LVL compared to solid wood, adhesives considerably promote the contribution of fiber bridging to LVL toughness (Mirzaei, et al., 2015). As a result, G_{ss} should relate to adhesive quality. The retention of G_{ss} for the various adhesives as a function of aging is shown in Fig. 3-3. The materials clearly varied in terms of durability performance. G_{ss} constantly declined due to aging for all adhesives. The PVA-made LVL relatively lost the most toughness, while PF-made LVL lost the least (or maintained toughness the most). For both PF and PVA, the degradation observed due to exposure from 16 to 24 VPSD cycles was the sharpest, hence, the deterioration effect in the final cycles was the most severe. The average retention after the final cycle is approximately 73% and 40% for PF and PVA, respectively. Based on this plot, the most

and least durable adhesives, *i.e.*, PF and PVA, can be detected, but no judgment can be made regarding the durability of EPI *vs*. PRF.

3.3.1 Kinetics of Toughness Degradation

To distinguish adhesives further, we looked at the rate of degradation at different crack lengths. First, we assumed a simple first-order kinetics analysis based on an assumption of water causing some sort of hydrolysis degradation:

$$\frac{dR(\Delta a)}{dt} = -K(\Delta a, T)[H_2O](t) \qquad (3\text{-}3)$$

where $R(\Delta a)$ is toughness at crack length Δa, $K(\Delta a,T)$ is a rate constant that may depend on crack length (*i.e.*, the extent of adhesive involvement) and temperature (*i.e.*, though an activation energy) and $[H_2O](t)$ is the time-dependent concentration of water. Integrating this equation gives:

$$R(\Delta a) = R_0(\Delta a) - K(\Delta a, T)\int_0^t [H_2O](t)dt = R_0(\Delta a) - k(\Delta a, T)t \qquad (3\text{-}4)$$

where $R_0(\Delta a)$ is the toughness before aging. Because the integrated moisture concentration should be the similar for wood samples exposed to identical moisture conditions, that term can be rolled into an effective rate constant, $k(\Delta a,T)$, which can be found from the slope of $R(\Delta a)$ *vs*. cycle number at constant crack growth (Δa). Sample fracture toughness degradation plots for PVA LVL at 50 to 110 mm crack propagation along with linear degradation rate fits are presented in Fig. 3-4. In brief, this 3D figure shows scatter plot of individual experimental results for different crack growth and different numbers of cycles. To calculate degradation rates, we considered all combinations of points for a given Δa, found $k(\Delta a,T)$ for each set, and normalized by intercept to get relative toughness degradation rates. For error analysis results, we found average and standard deviations of those normalized rates. The lines in Fig. 3-4 are plots using the averaged slopes. Finally degradation rates for all adhesives at 50 to 110 mm of crack propagation and normalized to initial toughness are plotted in Fig. 3-5 together with error bars determined from the

above error analysis. Because of the unsuitability of G_{init}, all these results are for after some crack propagation. Additionally, after some crack growth the degradation trends tend to become flat making ranking of the adhesives easier. Welch's t-tests were done to statistically compare all adhesives one by one at each crack size. According to the results, the durability differences shown in Fig. 3-5 are significantly different at most crack sizes ($p < 0.05$). The smallest degradation rate, indicating the highest durability, is associated with PF while the largest degradation rate is associated with PVA. This result is in agreement with Fig. 3-3 based on G_{ss}. Kinetics analysis helps distinguish adhesives further. According to the results of this study, LVL composites made using PF, EPI, PRF and PVA adhesives and the same wood species, are ranked in terms of durability in that order with PF being the most durable. Using G_{ss} alone the boundaries (PVA and PF) could be established, but EPI and PRF could not be distinguished. Kinetics analysis allows for differences to be observed in the durability performances of EPI and PRF, making this a preferred method to rank adhesive performance in a composite panel.

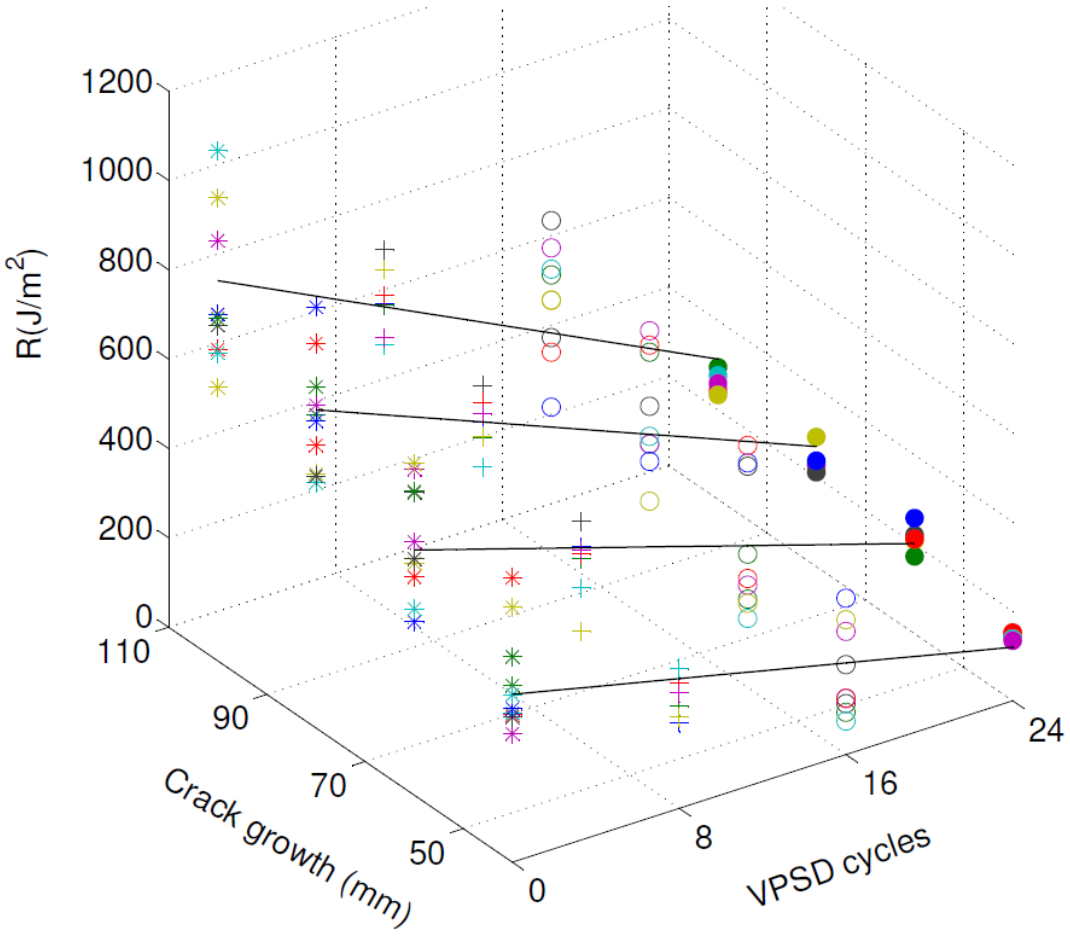

Figure 3-4. Fracture toughness degradation rates of PVA LVL at 50-110 mm of crack propagation. The symbols are individual experiments. The lines are fits using our error analysis procedure.

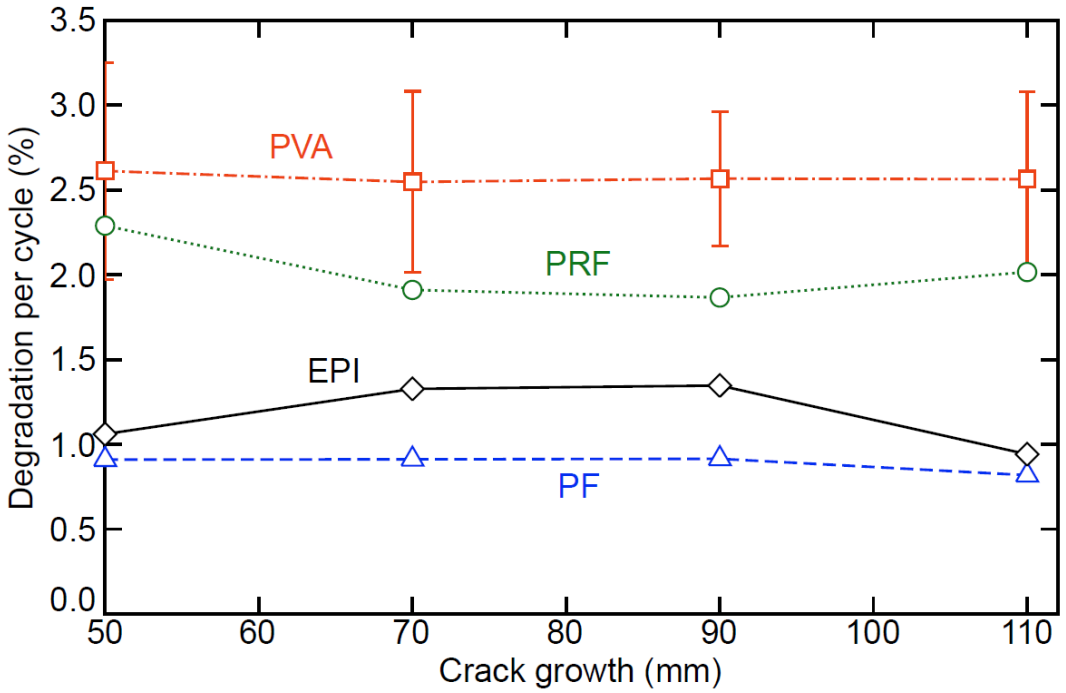

Figure 3-5. The rate of degradation of toughness (due to hydrolysis) for each adhesive calculated at different amounts of crack growth. The typical error bars are standard deviations to the rates as estimated by our error analysis procedure. Some error bars are hidden for clarity.

3.3.2 Conventional Durability Indicators

Strength and stiffness tests were carried out in parallel and the outcomes were compared to the fracture toughness results. Based on shear strength retention results (Fig. 3-6a), the adhesives are indistinguishable within the scatter of the results. Although a general shear strength decline due to aging can be observed, the scatter in the results renders any statistical comparison inconclusive. While parallel to grain shear strength tests have relatively small COV (14%) in clear wood (Liswell, 2004), our shear strength tests had higher COV (up to 42%). Because both wood and adhesive failures can occur in bond strength tests of wood composites, the scatter of such tests is usually higher, which complicates interpretation of the results. Overall, adhesive performance cannot be differentiated based on shear strength results. Follrich et al. (2010) compared the moisture

durability of PRF and EPI wood bonds using internal bond strength tests before and after 24 cycles of accelerated aging and reported a marginally better performance for PRF. They reported, however, that the wood failure area considerably decreased in PRF-bonded specimens after accelerated aging while in EPI-bonded specimens the trend was reverse. These observations indicate better performance for EPI. The inconsistency in their results between strength tests and wood failure area observation corroborates the shortcomings of conventional bond durability tests.

The modulus retention, as calculated from corrected DCB stiffness, is plotted in Fig. 3-6b. The DCB modulus correction factor, χ, was found to be relatively large, about 1.45, for the studied materials indicating the necessity of modulus correction. The corrected DCB modulus method was randomly verified by comparison to standalone 3 point bending modulus tests that were also corrected for shear. For example, the ratio of corrected moduli in 3 point bending to corrected DCB modulus was found to be 1.03 for untreated PVA LVL and 1.1 for PVA LVL after 8 VPSD cycles. In brief, the modulus determined from initial DCB stiffness gave good results for actual LVL modulus. Except for EPI, other adhesives exhibited constant degradation in modulus as a function of aging, however, there is no clear distinction among the adhesives. Similar to shear strength, stiffness merely demonstrates general degradation due to aging. Modulus had smaller error bars compared to toughness and shear strength experiments, but the change in modulus was too similar among the tested adhesives to help distinguishing durability of those adhesives. Similar modulus and strength effects were reported for plywood, another laminated composite (MacLean, 1953; Kojima & Suzuki, 2011; Sinha, et al., 2011). In particulate composites, however, such as particleboard, stiffness seems to be affected by aggressive environments more than strength (MacLean, 1953; Kojima & Suzuki, 2011; Sinha, et al., 2011).

The likely cause for the inability of shear and stiffness tests to rank adhesives is that they are based on initiation of failure or, in the case of stiffness, on pre-failure properties. Our

fracture tests in the post-failure regime show that much better comparisons comes only after a significant amount of crack propagation.

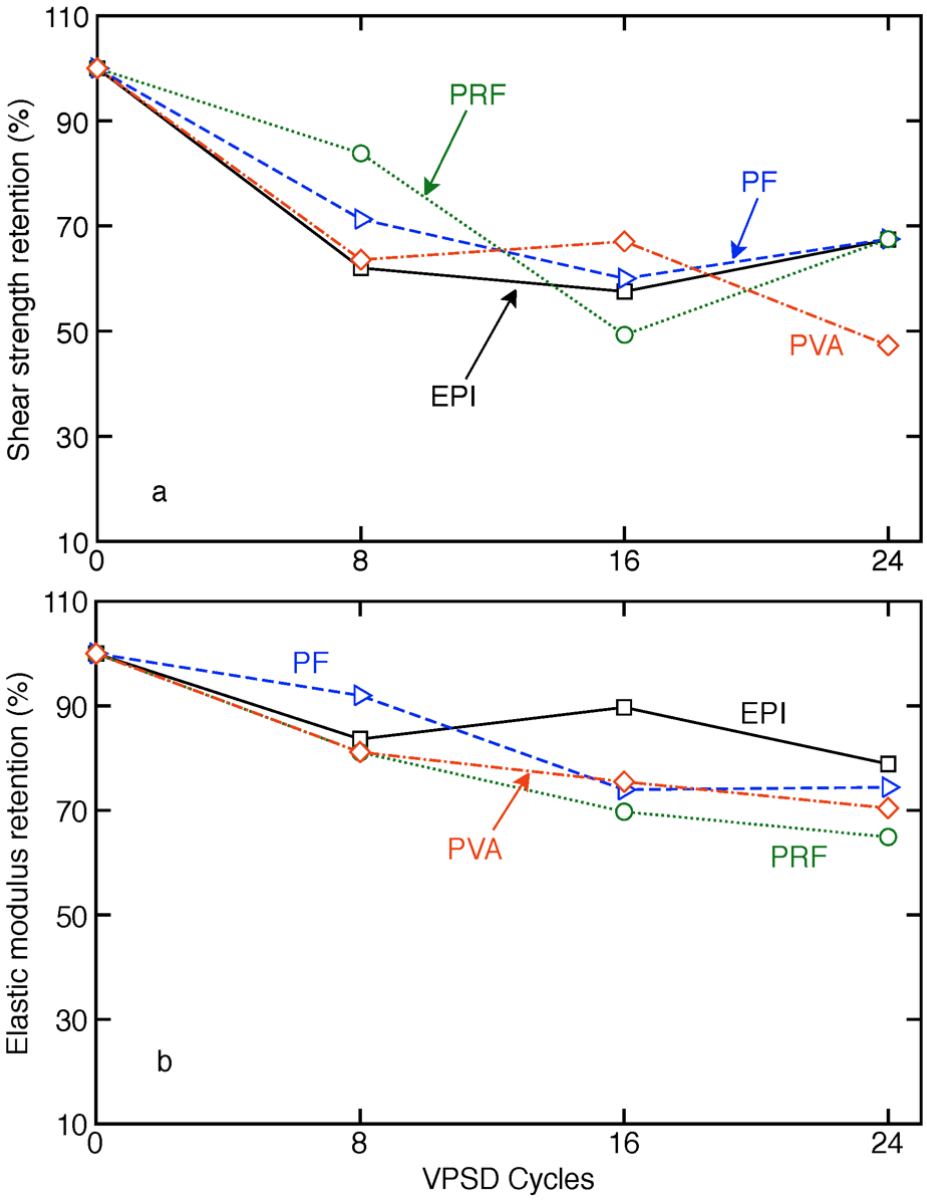

Figure 3-6. a. The retention in shear strength from lap shear tests for each adhesive as a function of the number of VPSD cycles. b. The retention in modulus measured from initial stiffness of DCB specimens as a function of the number of VPSD cycles.

3.3.3 Adhesive Bond Microscopy

To examine the studied adhesives further, we looked at bond line characteristics through bright field and Ultra Violet (UV) microscopy. Micrographs are presented in Fig. 3-7. While PF shows a considerable interphase region where adhesive penetrates the wood cells, PVA shows almost no penetration into the substrate. This result agrees with the X-ray analyses of wood adhesive bond lines (Kamke, et al., 2014). According to the durability assessment results of wood adhesives obtained by crack propagation fracture experiments, PF and PVA are respectively the most and least durable adhesives studied here. PF was the only adhesive requiring high temperature for curing which may have helped to increase adhesive penetration. PRF seems to have slightly larger wood interphase than EPI and has been reported to penetrate into wood only about 20% more than PVA (Adamopoulos, et al., 2012). In addition to micrographs, macrographs representing sample cross sections were helpful for clarifying the results. Fig. 3-8 compares cross sections of EPI and PRF-made LVL after exposure to 24 VPSD cycles where we observed cracks across this thickness direction of the veneers. These swelling cracks are likely caused by drying cycles, promoted by greater swelling in the tangential direction, and form along weak ray cells with crack normal in the tangential direction (Vasic & Stanzl-Tschegg, 2007). They are across the thickness of the veneers because in rotary peeled veneers, the tangential direction of the wood is in the plane of the veneer. Because the crack normal of the drying cracks is the same as the crack normal in TL fracture tests, it is expected that formation of drying cracks will show up as degradation in TL fracture toughness. As a consequence, an adhesive's ability to distribute shrinkage and swelling stresses during aging could considerably affect swelling crack formation and that effect would be reflected in TL toughness.

Because these experiment were intended to characterize overall durability, rather than focus on bond lines alone, our fracture tests were mostly in the TL direction Experimental results show that TL fracture was affected more by the adhesive then RL fracture and

therefore is the preferred mode for characterizing the role of the adhesive (Mirzaei, et al., 2015). Possible interactions between TL and swelling-induced cracks with normal in the tangential direction provide additional support for using TL fracture. In contrast, RL crack growth (when used) often deviates into wood and would interact less with tangential swelling cracks. RL fracture would interact with swelling cracks with their normal in the radial direction, but our microscopy indicates that such swelling cracks are absent or at least much less common than tangential swelling cracks. In other words, RL fracture tests, like shear strength tests, are not expected to be informative about adhesive quality.

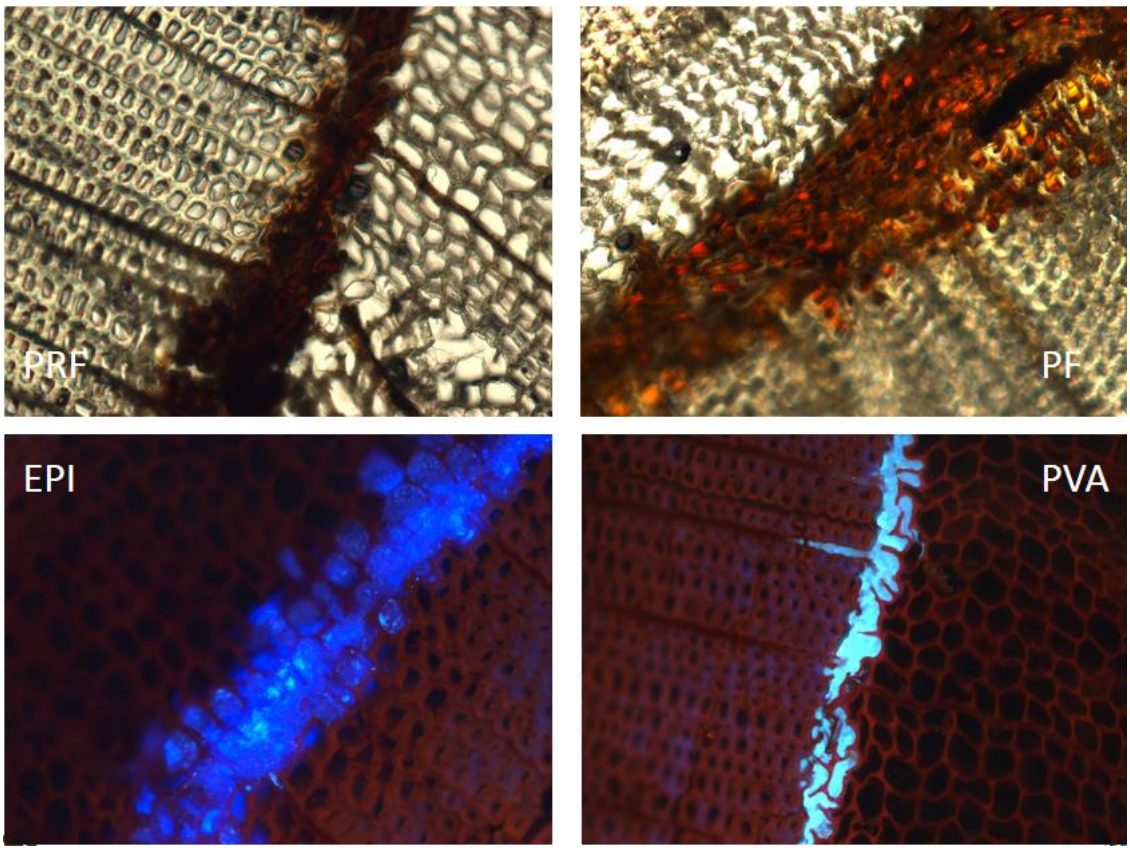

Figure 3-7. Micrographs of bond lines of various adhesives and Douglas fir substrate obtained with bright filed microscopy for PRF and PF (top) and UV microscopy after Safranin staining for EPI and PVA (bottom). 10X magnification.

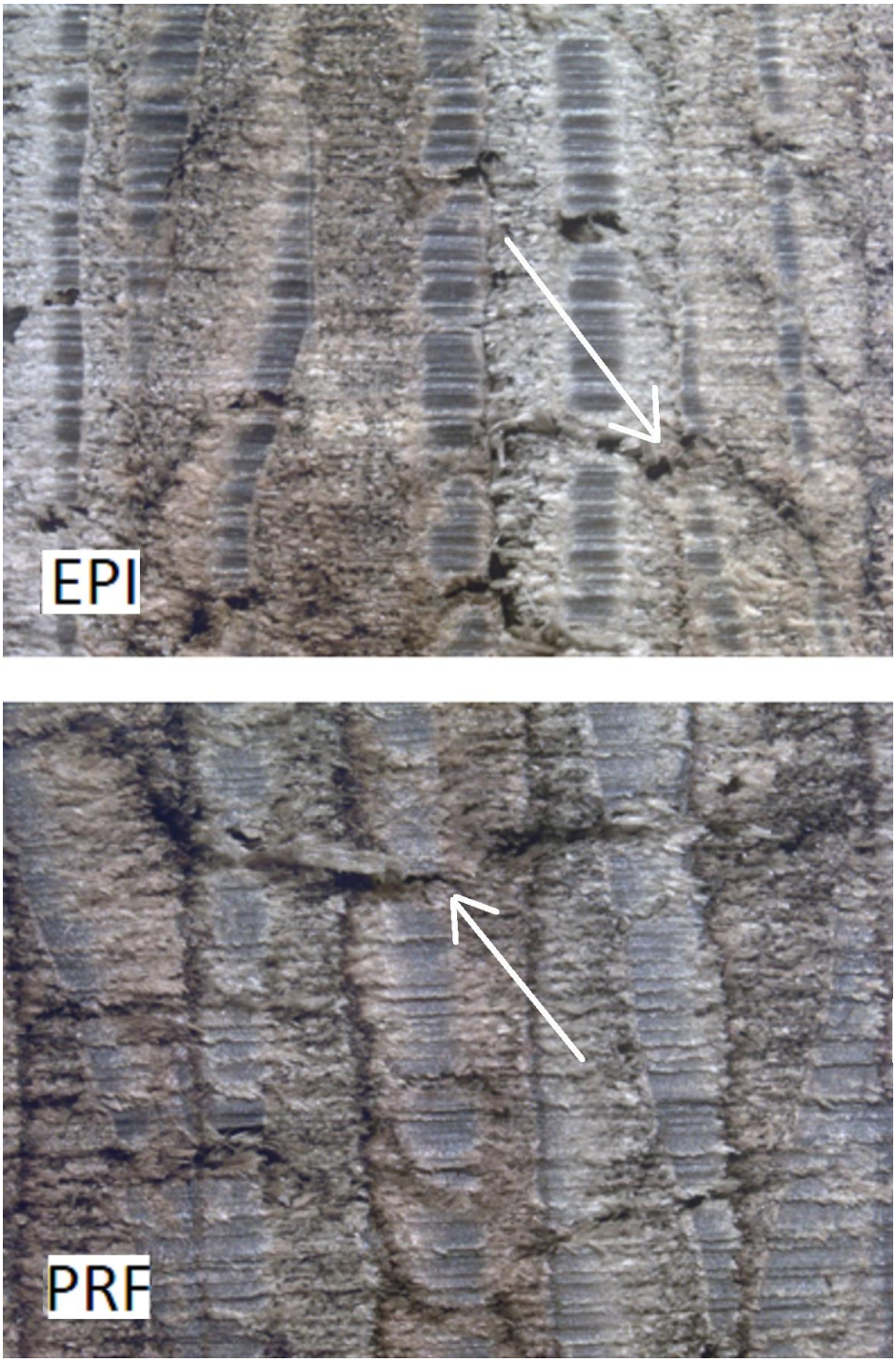

Figure 3-8. Crack formation in TR direction of EPI (top) and PRF (bottom) LVL due to aging.

3.4 Conclusions

R curves of LVL samples made out of Douglas-fir and various wood adhesives were constructed with data from DCB fracture tests before and after exposure to cyclic accelerated aging, and the contribution of adhesives to the material durability was investigated. Comparing average G_{ss} of LVL samples reflects the capability of crack propagation fracture toughness to distinguish different adhesive systems in terms of their durability, while the results of conventional test methods do not reveal such capability. Kinetics analysis of *R* curves was carried out to further investigate the correlation of durability and adhesives. The results demonstrate quantitative comparison of degradation rates of different adhesives after some crack propagation. Contrary to test methods that do not consider post-peak load regimes, crack propagation fracture toughness seems to be a promising tool for ranking and differentiating wood adhesives for their ability to make durable wood composites.

Acknowledgements

Financial support was provided by the National Science Foundation Industry/University Cooperative Research Center for Wood-Based Composites, Award No. IIP-1034975. We thank Momentive® Specialty Chemicals and Georgia Pacific Chemicals® for supplying all adhesives and veneer materials.

4 Measuring and Modeling Fiber Bridging: Application to Wood and Wood Composites Exposed to Moisture Cycling

Babak Mirzaei, Arijit Sinha, and John A. Nairn

Submitted to Composites Science and Technology

Abstract

We propose a new method for determining fiber-bridging, cohesive laws in fiber-reinforced composites and in natural fibrous materials. In brief, the method requires direct measurement of energy released during crack growth, known as the *R* curve, followed by a new approach to extracting a cohesive law. We claim that many previous attempts at determining cohesive laws have used inappropriate, and potentially inaccurate, methods. This new approach was applied to finding fiber bridging tractions in laminated veneer lumber (LVL) made from Douglas-fir veneer and four different adhesives. In addition, the LVL specimens were subjected to moisture exposure cycles and observations of changes in the bridging cohesive laws were used to rank the adhesives for their durability. Finally, we developed both analytical and numerical models for fiber bridging materials. The numerical modeling was a material point method (MPM) simulation of crack propagation that includes crack tip propagation, fiber bridging zone development, and steady state crack growth. The simulated *R* curves agreed with experimental results.

Keywords: wood, durability, fracture toughness, computational mechanics, fiber bridging

4.1 Introduction

Many materials develop process zones in the wake of crack tip propagation including both synthetic composites (Hashemi, et al., 1990; Lindhagen & Berglund, 2000) and natural materials such as bone (Nalla, et al., 2004), wood (Mohammadi & Nairn, 2014; Smith, et al., 2003; Wilson, et al., 2013), or wood composites (Matsumoto & Nairn, 2012; Matsumoto & Nairn, 2009; Sinha, et al., 2012). For both fiber-reinforced composites and fiber-based natural materials such as wood, a common type of processing zone is a fiber bridging zone. Such zones can be a significant component of a material's toughness because the zone size can be comparable to, or larger than, the specimen size (Matsumoto & Nairn, 2009). One way to guide interpretation of experiments or to design structures that

use fiber bridging materials is to model the process zone with a cohesive law that gives crack surface tractions as a function of crack opening displacement. The practical use of such laws, however, requires methods to measure them. This paper describes a new approach to measuring cohesive laws with application to wood and wood composites. The measured laws are also implemented in a numerical model to validate their role in modeling crack propagation.

The analysis of crack propagation in the presence of a process zone necessitates consideration of two crack tips — the actual crack tip at the leading edge of the process zone and the notch root at its trailing edge (see Fig. 4-1b). When a crack propagation experiment begins, the crack tip and notch root coincide at the "initial" crack tip. When loading causes energy release rate for crack tip growth to exceed the initiation toughness, the crack tip propagates, but the notch root does not. Instead, a "developing" process zone is left in the wake of the crack tip that grows as the crack tip propagates.

During this phase, the crack resistance, R, increases, which is known as the material's R curve. Eventually the crack opening displacement (COD) at the notch root, δ_{root}, exceeds the critical COD for the process zone, δ_c. After δ_c is reached, the crack tip and the notch root propagate together in a regime termed "steady state" crack growth. In steady state crack growth, R is constant at a plateau called the steady state toughness, G_{ss}.

Figure 4-1a shows a contour Γ from the bottom crack surface to the top surface that completely encloses the process zone. The J integral along this contour, called here the farfield J integral, is (Bao & Suo, 1992):

$$J_{ff}(\delta_{root}) = J_{tip,c} + \int_0^{\delta_{root}} \sigma(\delta) d\delta \qquad (4\text{-}1)$$

where $\sigma(\delta)$ is a traction law associated with the process zone. But, as is known in J-integral analysis, this J is only equal to the energy release rate when the crack growth is "self-similar" (Rice, 1968). When a process zone is involved, self-similarity implies that the

process zone length is constant during crack growth and this condition only occurs during steady state crack growth. Prior to steady state, the energy required to propagate the crack needs to account for energy required both to propagate the crack tip and to enlarge the process zone. Therefore, the increasing R curve in the developing phase should be found not from $J_{ff}(\delta_{root})$, but rather from:

$$R(\delta_{root}) = J_{ff}(\delta_{root}) - W_B^{(r)}(\delta_{root}) = J_{tip,c} + \int_0^{\delta_{root}} \sigma(\delta) d\delta - W_B^{(r)}(\delta_{root}) \qquad (4\text{-}2)$$

where $W_B^{(r)}(\delta_{root})$ is recoverable energy in the process zone, which is non-zero when $\delta_{root} < \delta_c$ (Nairn, 2009). The amount of recoverable energy will depend on the mechanics of the process zone. A reasonable approximation for fiber bridging is that the process zone is an elastic zone undergoing damage such that recoverable energy is found by unloading back to the origin or $W_B^{(r)}(\delta_{root}) = \delta_{root}\sigma(\delta_{root})/2$ (see Fig. 4-1b). Stated differently, $J_{ff}(\delta_{root})$ is always the correct J integral, but that single quantity cannot simultaneously give energy release rate both for process zone development (where crack tip propagates but notch root does not) and for steady-state crack growth (where crack tip and notch root propagate together as self-similar propagation). The solution is to use Eq. (4-2) to find the R curve. This calculation of R will differ from $J_{ff}(\delta_{root})$ during process zone development, but will equal it during steady-state crack growth.

Based on the preceding comments, we describe three valid methods for determining $\sigma(\delta)$. The first is to measure $J_{ff}(\delta_{root})$ during process zone development and then differentiate to get:

$$\sigma(\delta) = \frac{dJ_{ff}(\delta_{root})}{d\delta_{root}} \qquad (4\text{-}3)$$

Unfortunately, in general it is not possible to measure $J_{ff}(\delta_{root})$ from typical fracture specimens because the calculated result depends on the cohesive law. One exception, as

pointed out by Rice (1968), is a pure moment-loaded, double cantilever beam specimen. Lindhagen and Berglund (2000) used such a specimen to measure cohesive laws in several glass mat composites with random in plane fiber orientation and observed monotonic softening behavior. They incorrectly labeled $J_{ff}(\delta_{root})$ as the material's toughness (or R curve), when the actual toughness is given by $R(\delta_{root})$, which is not equal to $J_{ff}(\delta_{root})$ prior to steady state. This mislabeling was fortunate, however, because their measurement of $J_{ff}(\delta_{root})$ is what made use of Eq. (4-3) acceptable. The drawbacks of this approach are that it requires special fixturing to apply a pure moment and only works for one specimen geometry. This approach could never, for example, be used to probe important questions about potential changes in cohesive laws depending on specimen loading method.

A second, valid approach is to avoid measurement of $J_{ff}(\delta_{root})$ or $R(\delta_{root})$ by directly measuring displacements in the arms of a double cantilever beam specimen and then numerically solving the inverse problem to find the traction law required such that the calculated and measured displacements agree. This approach was used by Botsis and coworkers (Manshadi, et al., 2013; Sorensen, et al., 2008; Stutz, et al., 2011; Stutz, et al., 2011); they measured arm displacements using an embedded Fiber Bragg Grating (FBG) sensor and used finite element analysis to extract a cohesive law. The drawbacks of this approach are that specimens with FBGs are expensive and the technique is limited to synthetic composites where FBGs can be embedded during fabrication. The approach could not be used for studying fiber bridging in natural materials, such as solid wood.

A third option is to directly measure $R(\delta_{root})$ using energy tracking methods. Differentiating this result using Eq. (4-2) and using an elastic approximation to $W_B(\delta_{root})$ (which is appropriate for fiber bridging), gives:

$$\frac{dR(\delta_{root})}{d\delta_{root}} = \frac{1}{2}\left(\sigma(\delta_{root}) - \delta_{root}\frac{d\sigma(\delta_{root})}{d\delta_{root}}\right) \qquad (4\text{-}4)$$

This differential equation can be solved for $\sigma(\delta_{root})$ to give a new approach for finding cohesive law from $R(\delta_{root})$ (Nairn, 2009):

$$\sigma(\delta_{root}) = 2\delta_{root}\int_{\delta_{root}}^{\infty}\frac{R\prime(\delta)}{\delta^2}d\delta \qquad (4\text{-}5)$$

Once a material reaches a critical crack opening displacement, δ_c, the R curve will reach steady state toughness, which implies $R'(\delta) = 0$ for $\delta > \delta_c$. Using this result, the upper limit in Eq. (4-5) can be replaced by δ_c. This method requires direct energy tracking to measure the amount of energy released during crack propagation (actual R curve) along with measurement of notch root opening displacement.

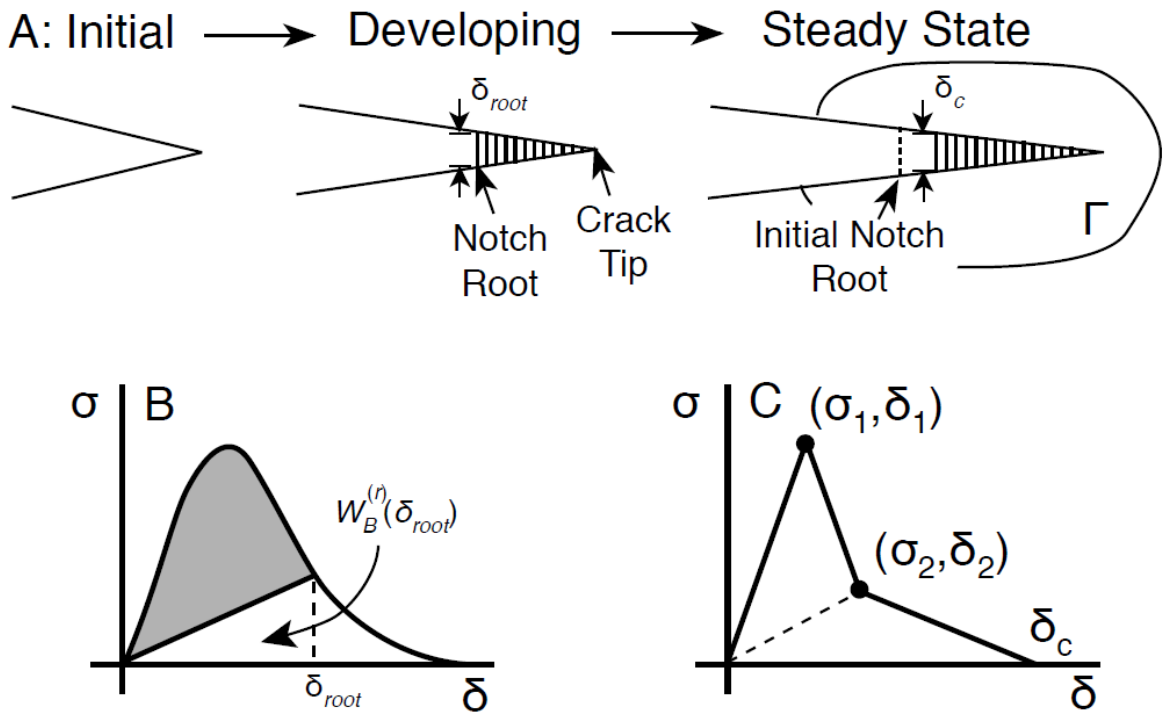

Figure 4-1. A. Stages of crack propagation in the presence of a process zone, which is defined by two crack tips — the actual crack tip and the notch root. B. Schematic drawing for a cohesive law. The shaded region is the energy dissipated in the zone and $W_B^{(r)}(\delta_{root})$ is the recoverable energy in the zone (shown here as elastic recovery, but other types of recovery could be modeled). C. A representation of fiber bridging tractions as a trilinear traction law derived for modeling purposes.

This paper used the third option to find cohesive laws for fiber bridging in laminated veneer lumber (LVL) made from Douglas-fir (*Pseudotsuga menziesii*) veneers and various adhesives. The results were derived from prior experiments that included direct energy tracking methods to find R as a function of crack length and to observe changes in R caused by exposure of the specimens to moisture cycling (Mirzaei, et al., 2015; Mirzaei, et al., 2016). The new results here were to measure crack opening displacement at the notch root and then to use the resulting $R'(\delta)$ to find cohesive laws using Eq. (4-5). The experimentally measured cohesive laws were fit to a trilinear traction law form (see Fig. 4-1c). The trilinear law fitting parameters were examined to add insights into degradation due to moisture exposure. The trilinear fits also provided a convenient and realistic traction law for use in numerical modeling to predict the crack propagation properties of LVL. Finally, an analytical model for fiber bridging up to the peak cohesive stress was derived and used to further interpret traction law parameters.

4.2 Materials and Methods

4.2.1 Wood Composite Materials

LVL billets were manufactured in the laboratory under controlled conditions using all B grade Douglas-fir veneers. Each LVL billet had dimensions 61 × 91 cm (2 × 3 ft), consisted of 11 plies (each 3 mm thick), and used one of the following four adhesives: Wonderbond®EL-35 Emulsion Polymer Isocyanate (EPI), GP ® 421G83 RESI-MIX ® Phenol Formaldehyde (PF), CASCOPHEN® LT-5210J/CASCOSET ® FM-6210 adhesive system Phenol Resorcinol Formaldehyde (PRF), and a one-component Polyvinyl Acetate (PVA). For comparison, experiments were also done on solid Douglas-fir specimens. Detailed descriptions can be found in Refs. (Mirzaei, et al., 2015; Mirzaei, et al., 2016).

Accelerated moisture exposure of LVL and solid wood was carried out according to ASTM standards (ASTM D2559, 2012), but we excluded the steam exposure step. Fracture experiments were done after selected number of cycles each of which consisted of vacuum,

pressure, soaking, and drying and denoted here as VPSD cycles. All mechanical tests were done on specimens after drying and after re-equilibrating in a conditioning room (maintained at 21° C and 65% RH) to standard moisture conditions (about 12% moisture content). Details on the VPSD cycles for aging are given elsewhere (Mirzaei, et al., 2015; Mirzaei, et al., 2016).

4.2.2 Fracture Experiments

The fracture experiments used double cantilever beam (DCB) specimens in opening mode under displacement control at 2 mm/min. Dimensions of all DCB specimens were $35\pm2\times35\pm2\times300\pm5$ mm^3 and the initial, sawn pre-crack was 100 mm. The crack plane at the edge of each specimen was widened and loading was applied using angle irons inserted into the gap. The long direction of the DCB specimen was the wood grain or longitudinal direction of the wood. The crack plane may be cut either parallel to adhesive bond planes in the LVL or cut to cross all adhesive bond lines. The former is known as an RL fracture (because the normal to the crack plane is in the thickness direction of the veneer, which is the radial direction of solid wood for rotary peeled veneer), while the latter is called TL fracture (because normal to the crack plane is in the tangential direction of the wood in the veneers). The L in each fracture mode is for crack growth in the longitudinal direction. Because TL cracks break all bond lines, it has been observed that the adhesive plays a much greater role in TL fracture than in RL fracture (Mirzaei, et al., 2015). Because of this greater role of adhesive, all crack propagation experiments reported here for LVL were in the TL direction. For comparison, the solid wood specimens were also studied using TL fracture. In solid wood, a TL crack plane spans multiple growth rings in the specimen.

The load and displacement data during fracture tests were recorded using an Instron 5582 universal testing machine. Crack growth data were collected using the 3D Digital Image Correlation (DIC) technique (Sutton, et al., 1983). For DIC data acquisition, two 50 mm Pentax® lenses (stereo system), attached to high speed Correlated Solutions® cameras mounted on a tripod, were used to capture images during the tests. Images were acquired

at 1 Hz. DIC is a technique to map strains by tracking a small subset of pixels in deformed images. To facilitate the DIC analysis, a speckle pattern was applied by painting the surface black and then spraying a random pattern of white dots. VIC 3D ® software analyzed the acquired images and calculated strains. The tensile strain normal to the crack plane ahead of the crack tip was monitored throughout the loading. This strain was high near the crack tip and decreased as a function of distance away from the crack tip. Figure 4-2 shows sample strain profiles for a solid wood specimen. Crack propagation was measured by observing shifts in the position to reach 1% vertical strains between subsequent images. All DIC strain-position data were exported to data sheets for further processing. A Matlab® script was written to populate crack propagation data from DIC output based on the 1% strain criterion. (Mirzaei, et al., 2016).

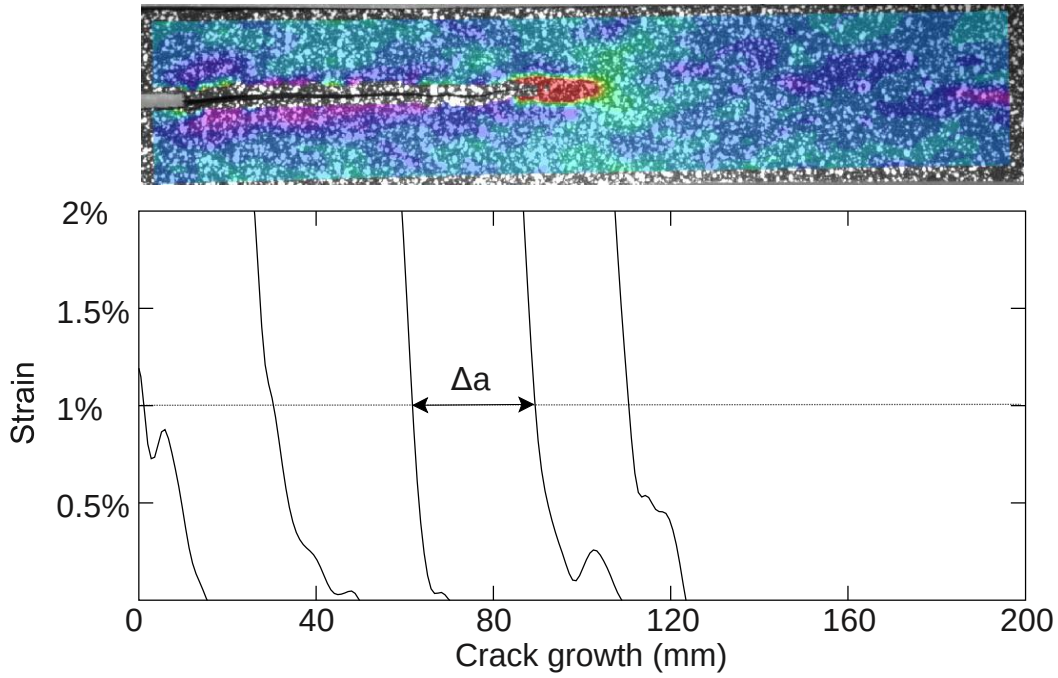

*Figure 4-2. DIC analysis of a solid wood DCB specimen to monitor crack propagation and determine δ_{root}. The colors in the specimen image indicate strain normal to the crack (with red as maximum strain). The plot shows that strain and several time stages along a line though the crack plane. As the crack propagates the strain plot shifts. The shifts between curves (*e.g.*, shift of position to reach 1% strain) indicate the amount of crack growth between the times corresponding to the two curves. Accumulating such crack growths allows accurate tracking of crack growth and was more accurate that attempting visual tracking of crack growth.*

The fracture experiments consisted of multiple replicates each for control (0 VPSD cycles) and after 8, 12, and 24 VPSD cycles. The number of specimens used per treatment were 4±1 for solid wood, 8±2 for PVA, and 6±2 for all other adhesives. Each experiment measured load and crack length as a function displacement. These data were reduced for direct energy calculation of R curves as a function of crack length by methods described elsewhere (Matsumoto & Nairn, 2009; Nairn, 2009; Mirzaei, et al., 2015). An important detail is that these experiments directly measured energy released without any need to impose assumptions about beam or process zone mechanics. The results for all replicates were averaged to get average R curves.

For evaluation of cohesive laws, it is necessary to determine R as a function of δ_{root} instead of the more commonly measured R as a function of crack growth. To measure δ_{root}, the same DIC data used to measure crack length were used to place a virtual extensometer at the notch root of the specimen. In brief, two locations above and below the initial notch root were selected and the net displacement difference between these locations was determined to find δ_{root}. This method is identical to the method used by Lindhagen and Berglund (2000) except that it used DIC data and VIC software to measure δ_{root} rather than a physical crack opening displacement gage. These results were used to convert $R(a)$ curves to $R(\delta_{root})$ curves. Formally, $R(\delta_{root})$ found by this method is only valid up to δ_c because after reaching δ_c, the process zone edge moves and measuring zone δ_{root} would require moving the DIC detection locations along with the process zone. Instead, our experiments always measured δ at the *initial* notch root. After reaching δ_c, however, the material enters steady state propagation with constant toughness G_{ss}. In other words, a true $R(\delta_{root})$ curve would increase until δ_c and then remain at a fixed point with $(\delta_c) = G_{ss}$ and δ_{root} constant and equal to δ_c. Our experimental $R(\delta_{root})$ curves are identical to true curves up to δ_c but then $R(\delta_{root})$ remains constant at G_{ss} while δ at the original notch root location gets larger than δ_c. Fortunately, determination of cohesive law from $R(\delta_{root})$ only requires information up to the onset of steady state crack growth or up to $\delta_{root} = \delta_c$.

4.2.3 Experimental Determination of Cohesive Laws

We determined cohesive laws for fiber bridging in LVL wood composites and in solid wood from the directly measured $R(\delta_{root})$ curves described above by using Eq. (4-5). This approach was proposed by Nairn (2009), but has not previously been used on real experiments. The first step is to locate the steady state regime, which then determines δ_c. Given $R(\delta_{root})$ up to δ_c, the cohesive laws were then found with a Matlab® script using the following algorithm:

1. Divide up experimental data from $\delta_{root} = 0$ to $\delta_{root} = \delta_c$ into n intervals such that $\delta_i = i\delta_c/n$.

2. For each δ_i, pick a smoothing interval size, k, and do a linear fit to all data from $R(\delta_i - k)$ to $R(\delta_i + k)$ and assign the slope of that fit to be $R'(\delta_i)$ denoted here as S_i.

3. The cohesive law is then calculated by taking $\sigma(0) = 0$ and:

$$\sigma(\delta_i) = 2\left[S_i - \frac{\delta_i}{\delta_c}\left(S_n - n\sum_{k=i}^{n-1}(S_{k+1} - S_k)ln\frac{k+1}{k}\right)\right] \qquad (4\text{-}6)$$

This practical equation assumes that $R'(\delta_{root})$ is a piecewise linear function connecting the S_i values and then numerically integrates Eq. (4-5) using the n experimental data points.

For example, consider a linear softening law of $\sigma(\delta) = \sigma_c(1 - \delta/\delta_c)$. By Eq. (4-4) the resulting $R(\delta_{root})$ increases linearly from $J_{tip,c}$ up to G_{ss} at δ_c with slope of $\sigma_c/2$. In other words, $S_i = \sigma_c/2$ for i from 1 to $n - 1$ and $S_n = 0$. By Eq. (4-6), the cohesive law is:

$$\sigma(\delta_i) = \sigma_c\left(1 - \frac{\delta_i}{\delta_c} n \ln\left(\frac{n}{n-1}\right)\right) \qquad (4\text{-}7)$$

For a large number of data points ($n \to \infty$), this equation reduces exactly to the linear softening law.

4.2.4 Numerical Modeling

The numerical simulations used the material point method (MPM) and the open-source software NairnMPM (Nairn, 2015). MPM implements explicit cracks by defining a series of massless particles that define the crack path and uses that crack path to partition the analysis into velocity fields above and below the crack plane (Nairn, 2003; Guo & Nairn, 2004). MPM can implement traction laws on the crack surfaces by assigning a traction law to one or more crack particles along the crack (Nairn, 2009). One use of such traction laws is to simulate crack propagation and process zone development in fiber-bridging materials (Matsumoto & Nairn, 2012; Matsumoto & Nairn, 2009; Nairn, 2009).

Simulations that include both crack tip growth and formation of a cohesive zone require a method that can dynamically create cohesive zones. In brief, the simulation starts with an initial crack and no cohesive zone (this approach differs from the common finite element analysis (FEA) method of pre-inserting cohesive elements at the start of the calculations). When the crack tip energy release rate exceeds, $J_{tip,c}$, the crack tip propagates and a cohesive zone is inserted in its wake. As the simulation proceeds, the crack tip continues to propagate at $J_{tip,c}$ and the cohesive zone grows and develops. Eventually, δ_{root} reaches δ_c causing the cohesive zone to start failing and the propagation reaches steady state crack growth. The simulated R curve is determined using Eq. (4-4). MPM can handle this dynamic cohesive zone analysis as explained elsewhere (Matsumoto & Nairn, 2012; Matsumoto & Nairn, 2009; Nairn, 2009).

One challenge in simulating crack propagation is dealing with kinetic energy. In all numerical models of crack propagation, crack growth is simulated by enlarging a crack, which can be by separating nodes in FEA or adding a new crack tip particle in MPM. This change will cause a release of energy. In computational mechanics codes that correctly conserve energy, the energy released by changing crack length will convert mostly to kinetic energy. As simulations proceed, the kinetic energy can dominate the results or cause instabilities. Now, in real materials, the energy released is mostly absorbed by the material

in processes required to create the new crack surfaces. One way to model real absorbed energy is by adding damping to the numerical model, but it is extremely difficult to add realistic damping. A recent paper on crack propagation in MPM calculations has proposed a new form of damping called PIC damping (Nairn, 2015). It selectively damps out kinetic energy in regions of rapid variations in velocity. It appears to work well for crack propagation by damping out kinetic energy without over damping to cause unrealistic results. All simulations here used the PIC damping method proposed in Ref. (Nairn, 2015).

4.3 Results and Discussion

4.3.1 Experimental R(δ) Curves

R curves as a function of crack length, *a*, and converted to be a function crack tip opening displacement, δ, for PVA LVL as a function of number of VPSD cycles are shown in Fig. 4-3. Both $R(a)$ and $R(\delta)$ clearly show degradation as the number of VPSD cycles increased. The generic shapes are similar. Both curves initiate at the same toughness and then increase due to fiber bridging. At long crack length, the curves tend to plateau at a steady state toughness. Note that the curvatures or rate of approaching steady state differ for $R(\delta)$ and $R(a)$. The determination of $\sigma(\delta)$ uses the slope of the *R* curve and requires use of slopes in the $R(\delta)$ curves. Also note that plateau values differ slightly between $R(\delta)$ and $R(a)$. All data were initially recorded as a function of time as the reference parameter for cross plotting. Because the averaging process may include different ranges of *a* or δ, the average *R* values showed some minor differences as well.

The algorithm for finding cohesive law depends on experimental δ_c. In theory, δ_c is the point where $R(\delta)$ becomes flat and equal to G_{ss}, but in heterogeneous materials, including wood based materials, the determination of δ_c can be challenging. We approximated δ_c for PVA LVL as 6 mm and for other materials as 3.5 mm. It is important to note that solid wood does not actually reach G_{ss}, but we assumed it is close to 3.5 mm to have a reference point for determining its bridging traction.

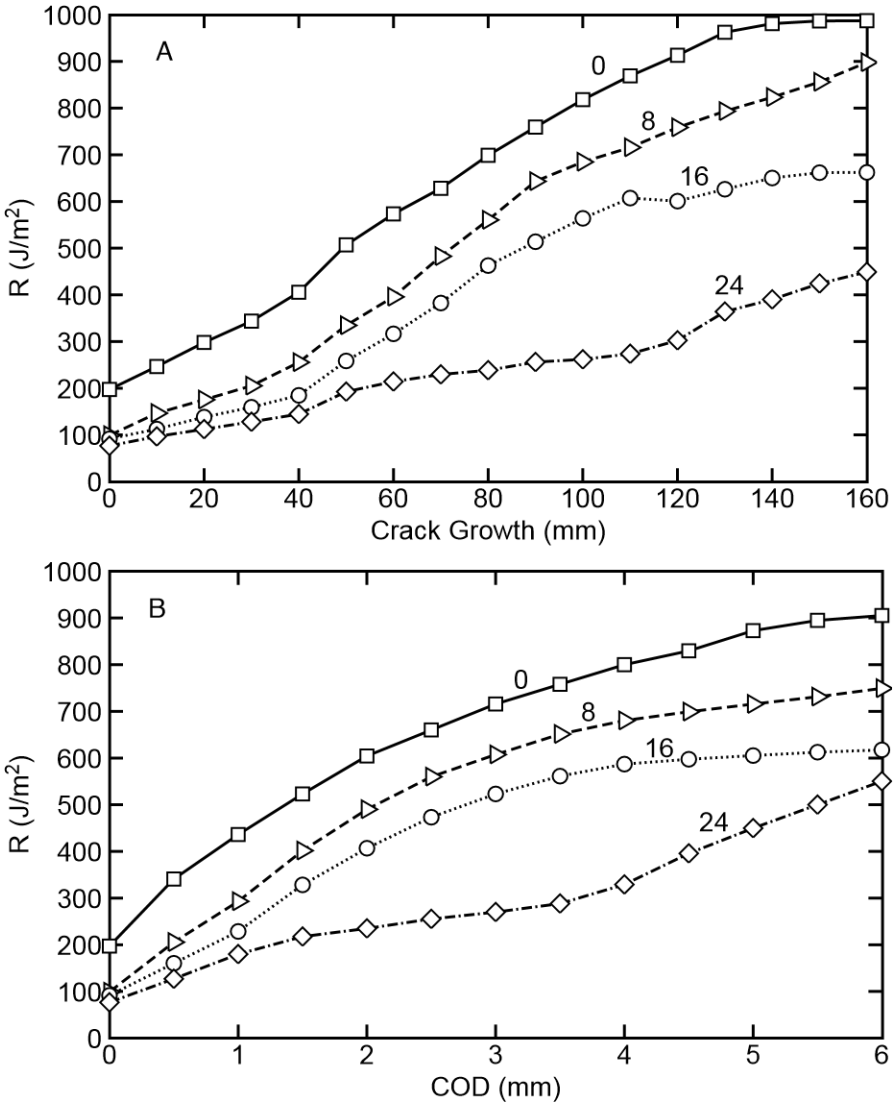

Figure 4-3. R curves of PVA LVL as a function of the number of VPSD cycles: A. R as a function of crack length. B. R as a function of the crack opening displacement, δ.

4.3.2 Experimental σ(δ) Curves

Fiber bridging cohesive laws ($\sigma(\delta)$), determined as explained in Materials and Methods, for PVA LVL as a function of number of VPSD cycles are given in Fig. 4-4a. The bridging stress profiles are characterized by an initial sharp increase up to critical cohesive stress (σ_c) and then monotonic decrease down to zero stress at critical δ_c. While a similar shape

has been reported for bridging ceramics (Gallops, 2011), prior valid cohesive laws for fiber reinforced polymer composites did not report an initial rise (Lindhagen & Berglund, 2000). The cohesive stress for PVA LVL is well correlated with aging and decreased as the number of VPSD cycles increased. The post-peak, or softening region, of the cohesive laws were less affected by aging. Figure 4-5 gives bridging stress profiles for all other adhesives and for solid wood as a function of VSPD cycles. All $\sigma(\delta)$ had similar generic shapes, but unlike $\sigma(\delta)$ for PVA-LVL, the effects of VPSD cycles on other materials were less apparent.

Figure 4-6 compares bridging tractions of solid wood and LVL made with various adhesives for control specimens or for 0 VPSD cycles. Comparing the different LVL specimens, PVA and PRF had the largest and smallest bridging stresses, respectively. Comparing LVL to solid wood, the cohesive stress due to bridging fibers in solid wood (filled black curve) is far below the cohesive stresses for all LVL specimens. This observation implies that fiber bridging is not simply stress carried by wood fibers bridging the crack, but is rather a more complex interaction between wood and adhesive.

The adhesive either reinforces the bridging fibers, making them stronger, or allows a greater number of bridging fibers. Images for fracture surfaces in solid wood and PVA LVL are given in Fig. 4-7. While the fracture surfaces of solid wood were relatively smooth, LVL fracture surfaces exhibited many broken fibers and fiber bundles. These pictures emphasize the role of fiber bridging in enhancing LVL toughness and are consistent with the considerable difference of bridging tractions between solid wood and LVL seen in Fig 4-6.

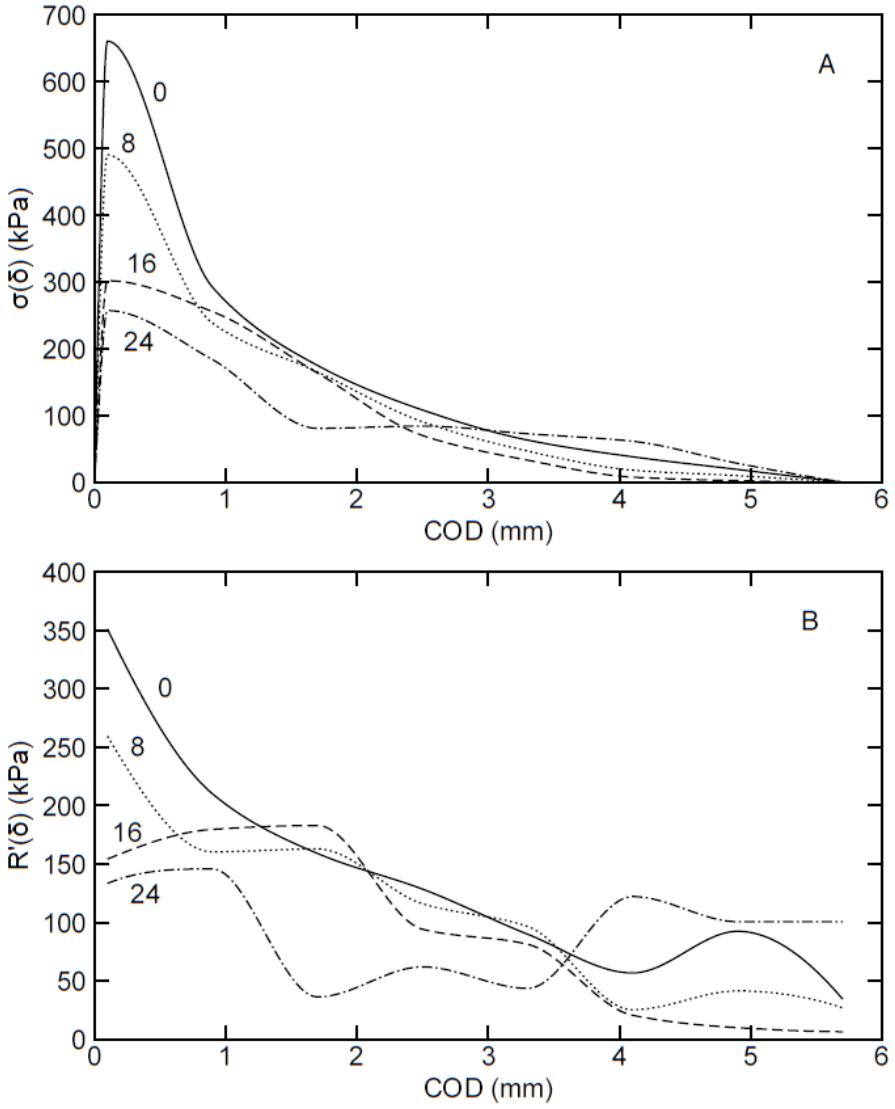

Figure 4-4. σ(δ) curves of PVA LVL as a function of the number of VPSD cycles: A. σ(δ) found using Eq. (5). B. σ(δ) found using R(δ).

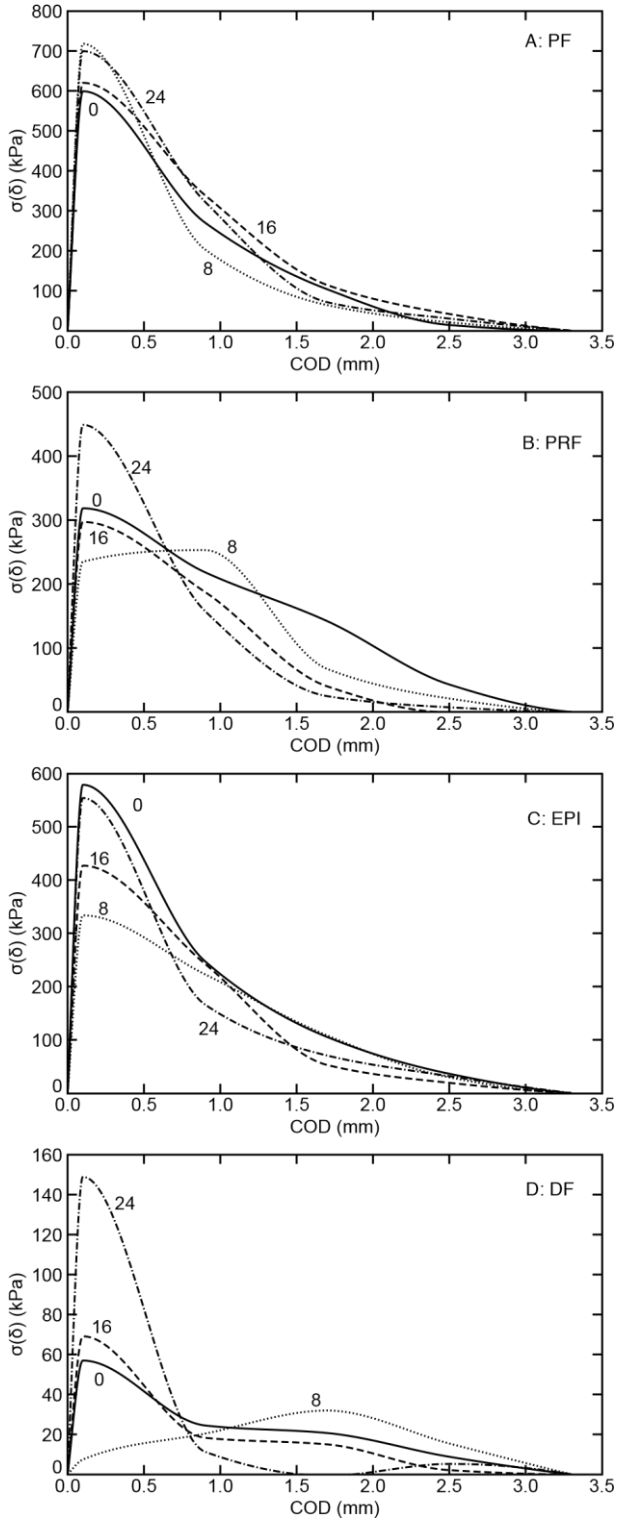

Figure 4-5. σ(δ) curves as a function of the number of VPSD cycles calculated using Eq. (5): A. PF LVL. B. PRF LVL. C. EPI LVL. D. Solid wood Douglas-fir.

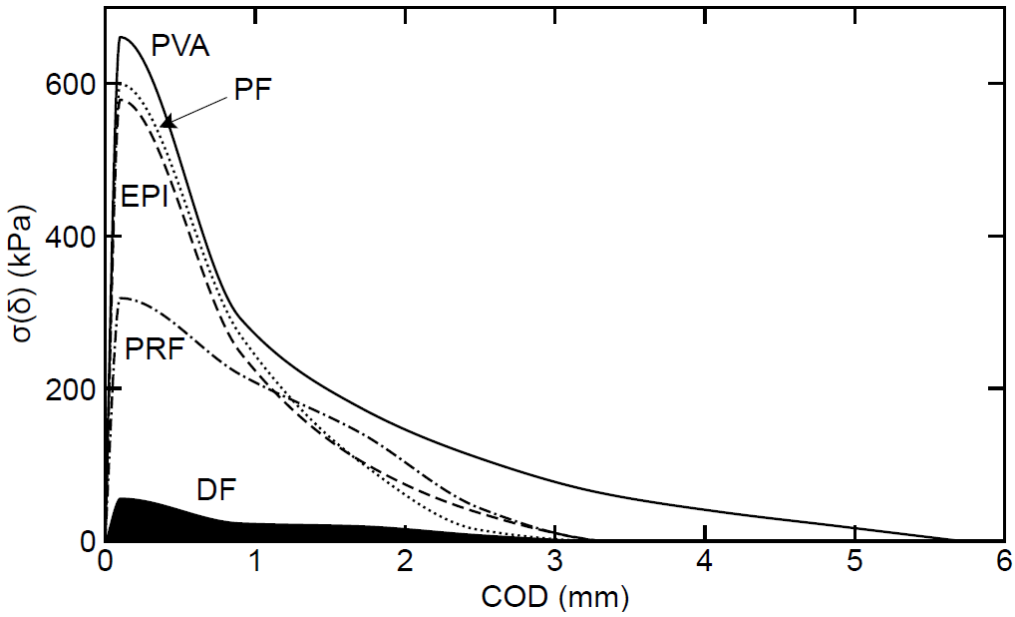

Figure 4-6. σ(δ) curves of all LVL types compared to solid wood Douglas-fir for control specimens (or 0 VPSD cycles).

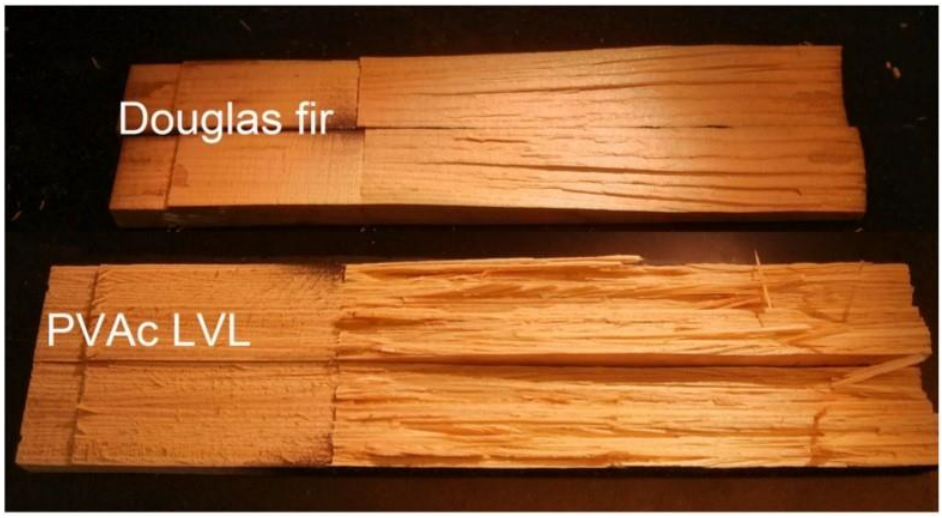

Figure 4-7. Fracture surfaces for DCB specimens of solid Douglas-fir wood (top) and PVA LVL (bottom) [17].

The cohesive laws measured here used a new method inherent in Eq. (4-5). Because most prior work has simply equated $\sigma(\delta)$ to $R'(\delta)$, two questions that arise are — how to evaluate prior methods and how to judge their accuracy? The first step in evaluating prior work is

to assess how they measured R during process zone development. Did they directly track energy or did they use simple fracture equations based on end load (or displacement) and crack length (*e.g.*, beam theory on DCB specimens where the beam theory cannot account for fiber bridging before the bridging law is known (Rice, 1968))? Only direct methods can give actual R curves. The methods used here are acceptable. Another acceptable approach could be to use an experimental compliance calibration method (Hashemi, et al., 1990). Basic linear elastic fracture mechanics equations (*e.g.*, $R = P^2a^2/(BEI)$ for DCB where P is load, a is crack length, B is thickness, E is modulus, and I is moment of inertia) are never correct. For the special case of pure moment loading, such equations do give $J_{ff}(\delta_{root})$, but that is not R during process zone specimen. For more common, end-loaded specimens, the simple equations give neither R nor $J_{ff}(\delta_{root})$. The next evaluation step is to see how the R results were converted to $\sigma(\delta)$. For those who measured the actual R curve, the cohesive law must be determined from Eq. (4-5) (assuming their process zones could be approximated by an elastic damage mechanism). The prevalent use of $\sigma(\delta) = R'(\delta_{root})$ is, at best, inaccurate, and, potentially, a serious error. For those who correctly used beam theory to determine $J_{ff}(\delta_{root})$ (which only applies to pure moment loading), the cohesive law can be derived from simple derivative in Eq. (4-3). For those who measured neither R nor $J_{ff}(\delta_{root})$, no method can extract a valid cohesive law.

Lastly, what is the consequence of using an invalid approach? To test this effect, we determined $\sigma(\delta)$ from our $R(\delta_{root})$ experiments using $R'(\delta)$. These improper results are in Fig. 4b and can be compared to proper results by Eq. (4-5) in Fig. 4a. While the general softening behavior is seen in both methods, the $\sigma(\delta)$ details are different. The proper results show in increase up to the cohesive stress, while it was difficult to detect an increasing regime by numerical differentiation of $R(\delta_{root})$. The peak cohesive stresses by the two methods differ by nearly a factor of 2. The overall softening shapes appear to be more smoothly monotonic in the proper method compared to the improper method. Finally, the areas under the cohesive should be equal to total bridging toughness defined by $G_B = G_{ss} -$

$J_{tip,c}$. Mathematically, integration of both Eq. (4-5) and $R'(\delta)$ leads to G_B. Using the curves in Fig. 4-4, on both proper and improper methods are reasonably close to G_B with average error of 5-10%. In other words, examining the area under a cohesive law is not a good method for judging validity of that law. Sorenson *et al*. (2008) similarly compared a proper method for finding cohesive law (the FBG method described in the introduction) and compared it to an improper method (using $R'(\delta)$ where $R(\delta)$ was found by fracture mechanics equation that gives neither R nor $J_{ff}(\delta_{root})$). Although they claimed both approaches are correct and described the two results as similar, they had differences in cohesive stresses (also a factor of 2). We suggest such differences mean the two methods are different and only the FBG results from their work should be considered as correct.

4.3.3 Representation as Trilinear Traction Law

The cohesive laws in Figs. 4-4 to 4-6 show non-linear softening. Attempts to fit to exponential softening did not work well, but all could be reasonably represented by a trilinear traction law (see Fig. 4-1c). A trilinear traction law, depends on five properties — (δ_1,σ_1) and (δ_2,σ_2) breakpoints and a critical δ_c. The total toughness of the modeled process zone is the area under the traction law curve, which is given by:

$$J_c = \frac{1}{2}(\sigma_1\delta_2 - \sigma_2(\delta_c - \delta_1)) \qquad (4\text{-}8)$$

A potential interpretation of a trilinear law is that it is modeling two physical mechanisms. The first failure mechanism can be identified with the area under the first peak and bounded by the dotted line in Fig. 4-1c. Its toughness is $J_1 = (\sigma_1\delta_2 + \sigma_2\delta_1)/2$ and is likely associated with strong and short bridging fibers close to the crack tip. The second mechanism is the remaining area ($J_2 = \sigma_2\delta_c/2$) and is likely associated with longer and weaker bridging fibers. The reasons for reduction of data to a trilinear traction law were twofold: 1. To reduce to fewer experimental variables that can be examined to give insights about effects of moisture cycling. 2. To provide a convenient form for input of a cohesive law into numerical models (see next section).

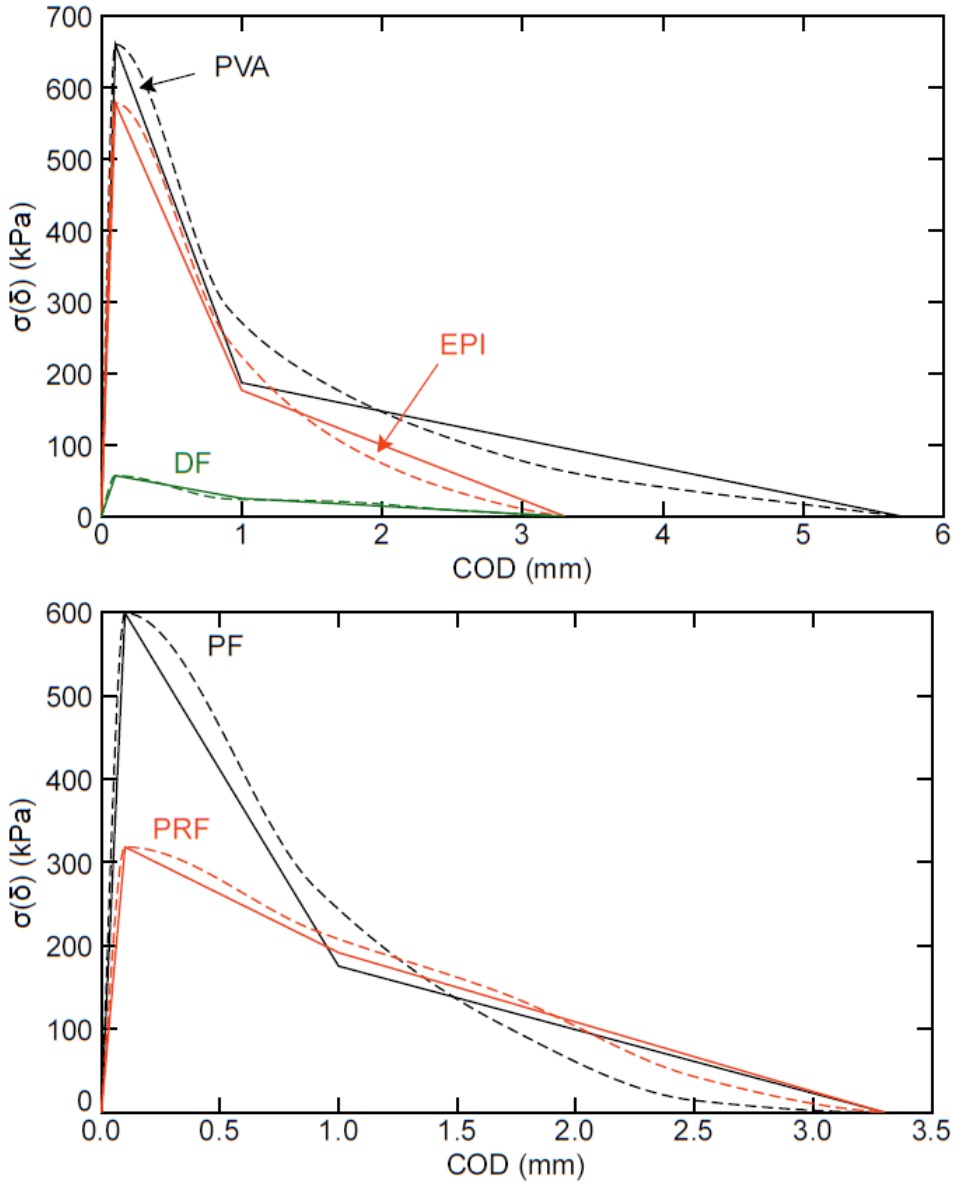

Figure 4-8. Application of trilinear cohesive law to control PVA, PF, EPI, PRF, and DF. The dashed lines are experimental results and solid lines are the trilinear fits.

Trilinear fits for cohesive laws in control specimens are given in Fig. 4-8. It was not possible to accurately determine all five trilinear law properties. We decided to fix $\delta_1 = 0.1$ mm and $\delta_2 = 1.0$ mm, use δ_c from above analysis. Next, a Matlab® script was written to find non-linear best fits to experimental $\sigma(\delta)$ by varying the two cohesive stresses, σ_1 and

σ_2, and the two energies, J_1 and J_2, subject to the constraint that $J_1 + J_2$ matched the measured steady-state toughness. The resulting trilinear parameters for all specimen conditions are in Table 4-1. The last two columns give degradation rate (per cycle) for that property and correlation coefficient for the linear fit. Overall, only a few properties showed degradation and were well correlated. Those properties with correlation coefficient above 0.8 are indicated in bold. For PVA, all properties degraded with cycles. For EPI and PRF, the initial peak is not affected, but the σ_2 and J_2 terms did degrade. Comparing J_2 (or σ_2) degradation rates, PRF degraded faster than EPI. For both PF and DF, the traction laws were uncorrelated with VPSD cycles. These results suggest that PF is the most durable adhesive, followed by EPI, PRF, and PVA, in that order. This ranking is identical to the rankings derived by Mirzaei *et al.* (2016) that were done by observations of *R* curve changes. The fact that PVA was the only material showing correlated degradation of σ_1 and J_1 might be potentially explained by adhesive penetration. PVA penetrated the least of all four adhesives into the wood cells (Mirzaei, et al., 2016). The penetration of other adhesives may have protected the fibers associated with the first peak while they are left open to degradation in PVA composites. Because VPSD cycles are known to affect DF toughness (Mirzaei, et al., 2015), the lack of correlations for DF indicates that moisture affects the initiation toughness much more than the fiber bridging properties.

4.3.4 Fiber Bridging Model

To gain physical insight into the cohesive stress, we attempted to derive an expected cohesive law as a function of the bridging fiber strength, fiber area, and number of bridging fibers. Figure 4-9a shows a fiber bridging zone with fibers bridging from the zone edge (at $x = 0$) to the opposite surface. The location x_b is the point at which the bridged fiber is no longer peeled from the opposite surface or has elongated to the fiber's breaking strain, which ever gives a larger x_b. The force due to bridging fibers at $x = 0$ will be sum of forces from all fibers from x_b to l_b where l_b is current length of the bridging zone. This analysis is restricted to small zones and small openings and is thus aimed at finding cohesive stress

only in the initial phase or up to the peak cohesive stress, σ_c. In this initial phase, it is assumed that the fibers between x_b and l_b have remained intact and have formed at some constant bridging rate (bridged fibers per unit length). Figure 4-9b focuses on a single fiber starting on the top surface and ending on the bottom surface at position x. The fiber strain is approximately:

$$\varepsilon_f = \frac{\sqrt{x^2+{(\delta+\delta(x))^2}/{4}}}{\sqrt{x^2+{(\delta-\delta(x))^2}/{4}}} - 1 \approx \frac{k^2 r}{2(1-r)^2} \qquad (4\text{-}9)$$

where δ and $\delta(x)$ are crack opening displacements at the edge of the zone and at x, and $r = 1 - x/l_b$. For this small displacement condition, it is assumed crack opening displacement is linear ($\delta(x) = k(l_b - x)$) and that its slope (k) is small. Using the small k result of $\sin\alpha = k(1+r)/(2(1-r))$, the total force in the y direction per unit length at $x = 0$ due to all bridging fibers ending at x is:

$$F_y(x) = \frac{E_f A_f N_b k^3 r(r+1)}{4(l_b - x_b)(1-r)^3} \qquad (4\text{-}10)$$

where E_f is fiber modulus, A_f is fiber area, and N_b is total number of bridged fibers at $x = 0$ (which are assumed to have the opposite ends spread out uniformly from $x = x_b$ to l_b). The total force at $x = 0$ is found by integrating $F_y(x)$ from x_b to l_b. Converting to an integral over r and dividing that force by unit area, the cohesive stress is:

$$\sigma(\delta) = \frac{E_f A_f \rho_b}{4 r_b} \int_0^{r_b} \frac{r(r+1)}{(1-r)^3} = \frac{E_f A_f \rho_b k^3}{4} \left(\frac{2r_b - 1}{(1-r_b)^2} - \frac{\ln(1-r_b)}{r_b} \right) \qquad (4\text{-}11)$$

where ρ_b is the bridged fiber density (number of bridged fibers per unit area) and $r_b = 1 - x_b/l_b$.

If x_b is determined by breaking strain of the fiber, it is found by solving for r at which $''\varepsilon_f = ''\varepsilon_{f,b}$:

$$r_b = 1 + \varphi^2 - \varphi\sqrt{2 + \varphi^2} \quad where \quad \varphi = \frac{k}{2\sqrt{\varepsilon_{f,b}}} \qquad (4\text{-}12)$$

Substituting r_b into Eq. (4-11) and expanding as a series in k, and using $k = \delta/l_b$ leads eventually to:

$$\sigma(\delta) = \frac{A_f \rho_b}{2 l_b} \sigma_{f\ b} \delta + O[k^2] \qquad (4\text{-}13)$$

where $\sigma_{f,b} = E_f''_{f,b}$ is the bridging fiber strength. If peeling controls x_b, then solve for r such that the individual fiber force leads to energy release rate for peeling (Kinloch, et al., 1994) that equals the peeling toughness, G_c, for the fiber:

$$G_c = \frac{F_f}{W_f}(1 - \cos(\alpha + \beta)) = \frac{E_f A_f}{4 W_f} \frac{k^4 r}{(1-r)^4} \qquad (4\text{-}14)$$

where W_f is width of the peeling surface. Although solving this 4th order polynomial equation and expanding as a series in k is difficult by hand, it can be done easily in Mathematica® (Wolfram Research, 2012) with the result:

$$\sigma(\delta) = \frac{A_f \rho_b}{2 l_b} \sqrt{\frac{E_f G_c}{r_f} \delta} + O[k^2] \qquad (4\text{-}15)$$

where fibers have been approximated as cylindrical ($A_f = \pi r^2_f$ and $W_f = \pi r_f$). It is tempting to extend this approach beyond the peak stress, but at higher δ, it is likely that some bridging fibers become damaged or broken (causing E_f, N_b, and maybe more terms to no longer be constant), and that opening becomes large (causing k to be too large and δ to be nonlinear). We claim this type of analysis is only appropriate during linear rise up to the maximum cohesive stress.

In principle, given properties of the bridging fibers, we can calculate the bridging density, ρ_b. Although many bridging fiber properties are not known, we can propose a rational range of properties. First, we looked at the amount of crack growth required to reach the peak cohesive stress, which is equal to l_b. The results for all materials in Table 4-1 ranged from

4 to 8 mm. This range is close to the range for individual wood fibers, known as tracheid cells, typically found in softwood Douglas-fir (1.7-7 mm) (Ilvessalo-Pfäffli, 2011), suggesting that bridged fibers leading to peak cohesive stress may be similar to tracheid fibers. The properties for individual tracheid fibers can be estimated as σ_f = 648 MPa , E_f = 40 GPa (Bodig & Jayne, 1982), and r_f = 20 μm (Ilvessalo-Pfäffli, 2011). On the other hand, the bridged fibers may be multiple tracheid fibers bound together (naturally of by the adhesive) and have properties closer to solid wood, such as σ_f = 100 MPa, E_f = 10 GPa (US Forest Products Laboratory, 2010), and r_f = 200 μm (*i.e.*, 10 tracheid fibers in the radius of the bundle). The peel out toughness likely ranges from close to initiation toughness for Douglas-fir (200 J/m^2) to some lower value (*e.g.*, 50 J/m^2). Substituting these values into Eqs. (4-13) and (4-15) with δ = 0.1 mm for all materials gives a range in bridged fiber density from 10 to 120 mm^{-2} for LVL and from 0.3 to 24 mm^{-2} for solid Douglas-fir (all ranges are in Table 4-1). In all calculations, the peeling mechanics determined the cohesive stress, but the differences between peeling and fiber breaking were small.

Table 4-1. Fiber bridging properties for all LVL materials and for solid wood Douglas-fir. The stresses (σ_1 and σ_2) are in kPa, the toughnesses (J_1 and J_2) are in J/m^2; the bridging zone lengths at peak stress (l_b) are in mm, and the bridging densities (ρ_b) are in mm^{-2}.

Matl.	Value	0	8	16	24	Slope	R^2
PVA	σ_1	661	491	302	257	**-17.5**	**0.94**
	J_1	321	238	144	123	**-8.7**	**0.94**
	σ_2	187	154	147	141	**-1.8**	**0.82**
	J_2	533	439	418	403	**-5.1**	**0.82**
	l_b	6.7	5.3	6.4	6.5		
	ρ_b	40-111	24-66	17-49	15-42		
EPI	σ_1	579	334	427	554	0.23	0.00
	J_1	281	158	206	271	0.24	0.00
	σ_2	177	170	144	117	**-2.6**	**0.94**
	J_2	291	281	238	193	**-4.2**	**0.94**
	l_b	8.5	6.1	6.6	8.5		
	ρ_b	44-124	18-51	26-71	42-119		
PRF	σ_1	319	235	297	449	5.7	0.42
	J_1	150	109	143	220	3.1	0.46
	σ_2	192	163	104	81	**-4.9**	**0.97**
	J_2	316	269	172	133	**-8.1**	**0.97**
	l_b	5.6	4.1	6.1	7.4		
	ρ_b	16-45	9-24	16-45	30-84		
PF	σ_1	599	718	620	700	2.5	0.20
	J_1	291	353	299	340	1.2	0.15
	σ_2	176	122	228	190	1.9	0.19
	J_2	290	201	377	314	3.1	0.19
	l_b	4.6	6.6	6.0	6.7		
	ρ_b	25-70	42-119	34-94	42-118		
DF	σ_1	57	7	69	149	4.2	0.55
	J_1	27	2	347	74	2.2	0.55
	σ_2	25	34	166	3	-1.0	0.68
	J_2	42	56	26	5	-1.7	0.68
	l_b	4.4	5.2	5.8	6.3		
	ρ_b	2-6	0.3-1	4-10	8-24		

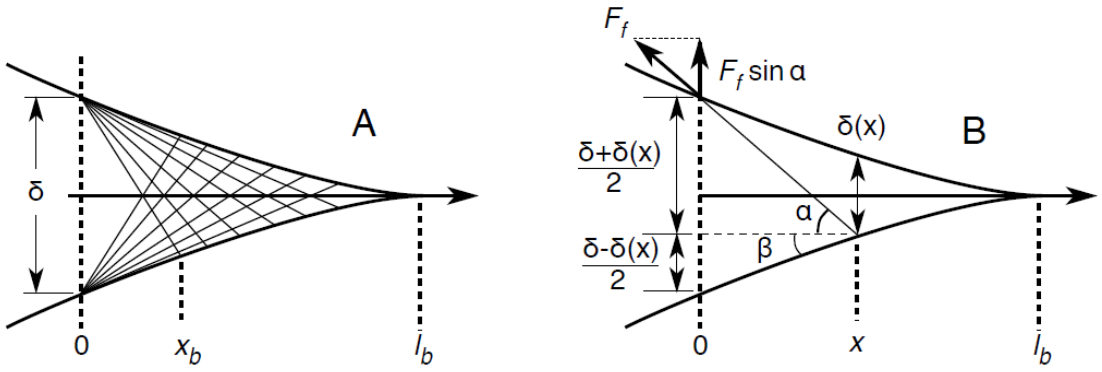

Figure 4-9. A. Fiber bridging zone shows fibers on both surfaces. B. A single bridged fiber from the notch root (at x = 0) to location x on the bottom. δ is the crack opening displacement at the notch root and δ(x) is the opening at x. F_f is the force on the single fiber and α and β indicate two key angles.

4.3.5 Validation — Numerical Modeling

The previous sections presented a new approach to experimental determination of the cohesive law for fiber bridging in composites and reduction of those laws to a form suitable for use in modeling (a trilinear traction law). One use for such laws is to insert them into numerical models to predict fracture properties in the presence of fiber bridging. To validate our experimental curves, we used them in an MPM model for crack growth in which propagation of the crack tip at a crack tip toughness ($J_{tip,c}$) leaves a cohesive zone in its wake. The notch root of the bridging zone debonds when the crack opening displacement reaches the critical value for the bridging law. During process zone development, the crack tip propagates while the notch root remains fixed. Once crack growth reaches steady state, the crack tip and notch root propagate in parallel. The validation goal was to determine if simulated *R* curves as a function of crack length derived using the experimentally determined $\sigma(\delta)$ laws will reproduce the experimentally determined $R(a)$ results.

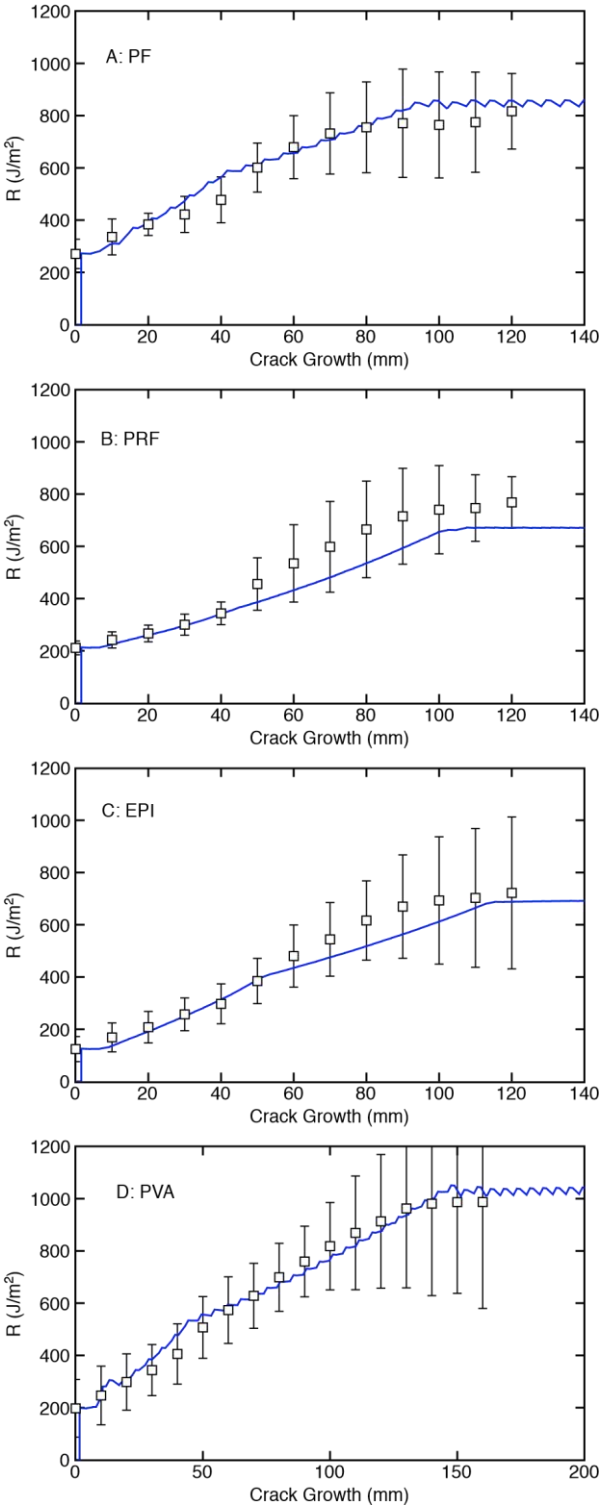

Figure 4-10. Experimental R(a) *curves of all control LVL materials (symbols with error bars) compared to simulated* R *curves using MPM modeling. A. PF LVL. B. EPI LVL. C. PRF LVL. D. PVA LVL.*

The details on the MPM simulation of crack growth are given in the materials and methods section. We input the trilinear cohesive law properties in Table 4-1 for each LVL product, used actual specimen geometry and loading conditions, and numerically propagated the crack tip and bridging zone up to steady state conditions. Comparisons of simulated R curves (solid lines) to experimental results for control specimens of each (with the error bars) are given in Fig. 4-10. The experimental results are from (Mirzaei, et al., 2016). In general, the simulations do a good job of matching experimental results, thus demonstrating self-consistency of experiments, the method to find $\sigma(\delta)$, and the numerical model for R curves. The simulated curves do not match all details of the experiments because the use of trilinear fits, as opposed to complete laws, will numerically smooth over those details.

4.4 Conclusions

We explained why many prior methods that determined cohesive laws from $R'(\delta)$ need to be rethought; in most cases, the specimens that were used are not suitable for simple differentiation of $R(\delta)$. We replaced that prior method with the new method in Eq. (4-5). In brief, the experiments must directly measure energy released to calculate an actual $R(\delta)$ curve and then find cohesive law from Eq. (4-5). The new approach was used to determine cohesive laws for a series of Douglas-fir LVL specimen with different adhesives and after exposure to moisture exposure cycles. Examination of the cohesive laws was used to rank adhesives for their ability to provide durable LVL products and that ranking agreed with a prior ranking determined by other methods (Mirzaei, et al., 2016). Finally, analytical and numeral modeling methods were used to gain insights on the fiber bridging mechanics and to demonstrate an MPM numerical model that can propagate cracks, develop fiber bridging zones, and reach steady state propagation. The MPM numerical modeling results agreed with experimental $R(a)$ curves.

Acknowledgments

Financial support was provided by the National Science Foundation Industry/University Cooperative Research Center for Wood-Based Composites, Award No. IIP-1034975. We thank Momentive ® Specialty Chemicals and Georgia Pacific Chemicals ® for supplying all adhesives and veneer materials.

5 General Conclusions

5.1 Summary

This project explored the expanded use of fracture properties for durability assessment of wood and wood composites. Experimental *R* curves and bridging stress profiles were measured for solid wood and LVL made with the same wood species (Douglas fir) and PVA, PRF, PF and EPI adhesives before and after subjecting DCB specimens to various VPSD aging cycles. Trilinear traction law parameters were used to model experimental *R* curves of LVL using MPM. DIC technique was employed to measure crack propagation and crack opening displacement. Matlab® scripts were created for processing DIC data, statistical analyses and obtaining bridging stress profiles from *R* curves. According to the results of this study, although the G_{init} values of solid wood and LVL are similar, their G_{ss} values considerably vary. The *R* curves of both start at similar toughness but the *R* curve of LVL increases to a higher magnitude than that of the solid wood as a function of crack propagation. That being said, according to the statistical analyses, crack propagation causes the toughness of both to significantly increase. Therefore, monitoring crack propagation is even important for solid wood with much smaller fiber bridging capabilities. Even after subjecting solid wood and LVL to VPSD cycles the G_{init} loss is the same for both materials which suggests that only the toughness of wood drops at the initiation of fracture, not that of the adhesive/composite. The fact that the G_{init} of solid wood and LVL remains very close before and after aging implies that almost no contribution of adhesive to the G_{init}. Therefore, characterizing the durability of adhesives requires emphasis on fracture properties after some amount of crack propagation has occurred. Moreover, it implies that other mechanical properties that rely on the initiation of failure are probably not the best durability indicators.

All *R* curves reported in this dissertation are averages from several replicates. G_{init} and toughness measured close to the end of specimen ligament are highly scattered. Thus, to compare the *R* curves of wood composites, it is better to exclude the two extremes of *R*

curves for sensitivity reasons. The normalized rate of loss due to aging in the *R* curves of each LVL type provided a durability indicator which almost constantly spanned over the substantial amount of crack propagation. Due to the reasons mentioned above regarding the unsuitability of G_{init} to characterize adhesive durability, these results were serviceable after some amount of crack propagation has occurred.

Strength and stiffness tests were also conducted in parallel on the exact same materials, but the results were not helpful to differentiate adhesives with regard to their durability. On the other hand, G_{ss} alone could determine the boundaries, i.e. PVA the least and PF the most durable adhesive. Further differentiation was made possible using degradation rate results which provided full ranking in the order of PF, EPI, PRF and PVA, with PF being the most durable.

A new method was proposed to determine cohesive laws and the unsuitability of simple differentiation of $R(\delta)$ was discussed. The new approach was used to determine cohesive laws for a series of solid wood and LVL specimens with different adhesives before and after subjecting them to various VPSD cycles. Examination of the cohesive laws was used to rank adhesives for their ability to provide durable LVL products and that ranking agreed with a prior ranking determined experimentally. Finally, analytical and numeral modeling methods were used to gain insights on the fiber bridging mechanics and to demonstrate an MPM numerical model that can simulate crack propagation, develop fiber bridging zones, and reach steady state propagation. The MPM numerical modeling results agreed with experimental $R(a)$ curves.

5.2 Practical Implications

While conventional durability assessment criteria of wood composites deal only with pre-peak load regime (stiffness) or initial peak load (strength) of the material, the results of crack propagation fracture experiments revealed that much better durability indicators could be obtained by investigating post-peak load regime. Also, in this study all fracture

tests were conducted in TL direction, in which the crack crosses all bond lines and veneers, in contrary to common tests which attempt to keep failure on the bond line. Since most wood adhesives are formulated to be stronger than wood itself, any crack that is intended to grow on the bond line can potentially deviate into wood. Some configurations have been proposed in the literature to keep crack growth on the bond line (Nicoli, et al., 2012), but those configurations are not regular wood composite products and are not made by industries for product evaluation. This study proposes selecting proper durability indicators which can be achieved by testing regular wood composite products. Degradation occurs due to three factors of wood, adhesive, and the interface. All the manufacturing parameters were kept similar to account for adhesive and the interface. The wood veneers were of same species, same grade and similar moisture content. Thus, everything else was kept constant except the adhesive so that the degradation of wood is similar in all cases and allow to account for degradation caused due to degradation of the adhesive and the interface.

The results show the same trends between the different adhesives when looked to the actual values instead of percentage results. However, for the ease of comparison and to fulfill the objective of ranking the adhesives the results were expressed as percent retained.

Although DIC technique was used here, it is still possible to use a simple imaging technique for continuous crack propagation monitoring according to our preliminary experiments (not shown here) if the objective is comparison/differentiation only. However, scripts created in this study for automated collection of DIC optical data and the subsequent processing significantly reduce the analysis time which is especially helpful for the quality control of composites industry.

Methods proposed in this dissertation for measuring and modeling *R* curves and bridging stress profiles are not limited to wood and its composites, and are advisable for all materials

with significant size of fiber bridging zone. The only assumption is that the bridging process is mostly an elastic damage process.

5.3 Limitations and Assumptions

Crack propagation experiments are more time consuming and elaborate than conventional durability/bond quality assessment methods. However, information-rich crack propagation experiments not only utilize the entire load-deflection regime for durability assessment, but also shed light on the failure mechanisms of cracked/notched engineered wood products which is important in structural design. These experiments have shown in this study to provide more reliable results than conventional modulus/strength tests which justify their use in the Research & Development departments of the composite industry in general, but more specifically the wood composites industry.

Trends of fracture toughness loss at various crack increments due to accelerated aging were measured based on the assumption of linear degradation (Figs 3-4 and 3-5). Linear degradation assumption provided the best fits overall, justified by the squared residual (R^2) values. Although reported degradation trends were considered according to the mentioned assumption, this is still an assumption and the final results based on non-linear degradation may not be consistent with an analysis based on linear degradation rates.

Our moisture cycling experiments were based on an established accelerated aging protocol which still varies from actual outdoor exposure in that water submersion does not normally occur in the latter. Hence, the degradation results provided in this study could be considered conservative. However, to extend the results of this study to design criteria, mechanistic moisture cycling experiments are required.

Measuring fiber bridging profiles and deriving fiber bridging analytical model required few assumptions. Solid wood did not actually reach G_{ss}, but it was estimated to have a reference point for determining its bridging traction. Furthermore, the analytical model was restricted to small zones and small openings and was thus aimed at finding cohesive stress

only in the initial phase or up to the peak cohesive stress. In this initial phase, it was assumed that the fibers between x_b and l_b (bridging length) had remained intact and had formed at some constant bridging rate (Fig 4-9). It was also assumed that crack opening displacement was linear and that its slope (k) was small. Additionally, bridged fibers at x = 0 were assumed to have the opposite ends spread out uniformly from $x = x_b$ to l_b.

5.4 Recommendations for Future Research

There is no consensus in the literature on whether cohesive law is a real material property. In case it is geometry dependent, which traction properties would be affected more by geometry/size? Crack propagation fracture experiments on specimens with different geometries/sizes can help answering these questions.

The fiber bridging analytical model derived in this study is suggested to be coupled with wood fiber pull out experiments to extend/adjust the model applications.

Current approaches are empirical at best. A mechanistic approach will be helpful; correlating accelerated aging tests with actual outdoor exposure experiments is a major step in extending the results of this study, and similar studies relying on accelerated aging methods, beyond classification/comparison to the design criteria.

Verify durability assessment methodology proposed in this study for other adhesives, wood species and composites. To reduce scatter in the R curves, using large enough billets from which all required specimens (per material type) can be cut is suggested.

6 Bibliography

Adamopoulos, S. et al., 2012. Adhesive bonding of beech wood modified with a phenol formaldehyde compound. *Eur. J. Wood Prod*, 70 (6), pp. 897-901.

Anaraki, A. & Fakoors, M., 2010. General mixed mode I/II fracture criterion for wood considering T-stress effects. *Mater. Des.*, Volume 31, p. 4461–4469.

Ardalany, M., Deam, B. & Fragiacomo, M., 2012. Experimental results of fracture energy and fracture toughness of Radiata Pine laminated veneer lumber (LVL) in mode I (opening). *Mater. Struct.* , Volume 45, p. 1189–1205.

Assarar, M. et al., 2011. Influence of water ageing on mechanical properties and damage events of two reinforced composite materials: Flax–fibres and glass–fibres. *Mater. Des.* , Volume 32, p. 788–795.

ASTM D1037, 2012. *Standard Test Methods for Evaluating Properties of Wood-Base Fiber and Particle Panel Materials.* West Conshohocken, PA: ASTM International.

ASTM D2559, 2012. *Standard specification for adhesives for bonded structural wood products for use under exterior exposure conditions.* West Conshohocken, PA: ASTM International.

ASTM E399, 2013. *Standard Test Method for Linear-Elastic Plane-Strain Fracture Toughness Kic of Metallic Materials.* West Conshohocken, PA: ASTM International.

Bao, G. & Suo, Z., 1992. Remarks on crack-bridging concepts. *Appl. Mech. Rev.* , 45(6), p. 355–366.

Bodig, J. & Jayne, B. A., 1982. *Mechanics of Wood and Wood Composites.* New York: Van Nostran-Reinhold Co, Inc..

Bruck, H., McNeill, S., Sutton, M. & Peters, W., 1989. Digital Image Correlation Using Newton-Raphson Method of Partial Differential Correction. *Exp. Mech.* , Volume 28.

Erdil, Y. et al., 2009. Comparison of mechanical properties of solid wood and laminated veneer lumber fabricated from Turkish beech, Scotch pine, and Lombardy poplar. *For. Prod. J.* , Volume 59, p. 55–60.

Follrich, J., Stockel, F. & Konnerth, J., 2010. Macro- and micromechanical characterization of wood adhesive bonds exposed to alternating climate conditions. *Holzforschung* , Volume 64, p. 705–711.

Fruhmann, K., Tschegg, E., Dai, C. & Stanzl-Tschegg, S., 2002. Fracture behaviour of laminated veneer lumber under Mode I and III loading. *Wood Sci. Technol.* , Volume 36, p. 319–334.

Gallops, S., 2011. *Development and Validation of a Fatigue Reliability Method for Bridging Materials (PhD thesis).* Corvallis: Oregon: Oregon State University..

Guo, Y. & Nairn, J. A., 2004. Calculation of j-integral and stress intensity factors using the material point method. *Computer Modeling in Engineering & Sciences* , Volume 6, p. 295–308.

Han, M. & Nairn, J., 2003. Hygrothermal aging of polyimide matrix composite laminates. *Compos. Part A* , Volume 34, p. 979–986.

Hashemi, S., Kinloch, A. J. & Williams, J. G., 1990. The Analysis of Interlaminar Fracture in Uniaxial Fibre-Polymer Composites. *Proc. R. Soc. Lond. A* , Volume 427, pp. 173-199.

Ilvessalo-Pfäffli, M.-S., 2011. *Fiber Atlas: Identification of Papermaking Fibers, 1995th Edition.* Heidelberg, Germany: Springer.

Irwin, G. R., Kies, J. A. & Smith, H. L., 1958. Fracture strengths relative to onset and arrest of crack propagation. *Proc. ASTM* , Volume 58, pp. 640-657.

Kamke, F. A. et al., 2014. Methodology for micromechanical analysis of wood adhesive bonds using X-ray computed tomography and numerical modeling. *Wood and Fiber Science* , 46 (1), pp. 15-28.

Khan, U. et al., 2013. Improved Adhesive Strength and Toughness of Polyvinyl Acetate Glue on Addition of Small Quantities of Graphene. *ACS Appl. Mater. Interfaces* , Volume 5, p. 1423–1428.

Kim, H. W., Grayson, M. A. & Nairn, J. A., 1995. The effect of hygrothermal aging on the microcracking properties of some carbon fiber/polyimide laminates. *Advanced Composites Letters* , Volume 4, pp. 185-188.

Kinloch, A., Lau, C. & Williams, J., 1994. The peeling of flexible laminates. *International Journal of Fracture* , 66 (1), p. 45–70.

Kojima, Y. & Suzuki, S., 2011. Evaluation of wood-based panel durability using bending properties after accelerated aging treatments. *J Wood Sci*, 57(2), p. 126–133.

Lindhagen, J. E. & Berglund, L. A., 2000. Application of bridging-law concepts to short-fibre composites part 1: DCB test procedures for bridging law and fracture energy. *Comp. Sci. & Tech,* Volume 60, p. 871–883.

Liswell, B., 2004. *Exploration of Wood DCB Specimens Using Southern Yellow Pine for Monotonic and Cyclic Loading (Master's thesis).* Blacksburg: Virginia Polytechnic Institute and State University.

MacLean, J. D., 1953. *Effect of steaming on the strength of wood.* Birmingham, AL: American Wood-Preservers' Association.

Manshadi, B. D., Vassilopoulos, A. P. & Botsis, J., 2013. A combined experimental/numerical study of the scaling effects on mode I delamination of GFRP. *Composites Science and Technology* , Volume 83, p. 32 – 39.

Matsumoto, N. & Nairn, J. A., 2009. The fracture toughness of medium density fiberboard (MDF) including the effects of fiber bridging and crackplane interference. *Eng. Fract. Mech.* , Volume 78, p. 2748–2757.

Matsumoto, N. & Nairn, J. A., 2012. Fracture toughness of wood and wood composites during crack propagation. *Wood and Fiber Science* , 44(2), p. 121–133.

Mirzaei, B., Sinha, A. & Nairn, J. A., 2015. Using crack propagation fracture toughness to characterize the durability of wood and wood composites. *Materials & Design* , Volume 87 , p. 586–592.

Mirzaei, B., Sinha, A. & Nairn, J. A., 2016. Assessing the role of adhesives in durability of wood-based composites using fracture mechanics. *Holzforschung*, pp. DOI: 10.1515/hf-2015-0193.

Mohammadi, M. S. & Nairn, J. A., 2014. Crack propagation and fracture toughness of solid balsa used for cores of sandwich composites. *Journal of Sandwich Structures and Materials* , 16(1), p. 22–41.

Nairn, J. A., 2003. Material point method calculations with explicit cracks,. *Computer Modeling in Engineering & Sciences* , Volume 4, p. 649–664.

Nairn, J. A., 2009. Analytical and numerical modeling of R curves for cracks with bridging zones. *Int. J. Fract.* , Volume 155 , p. 167–181.

Nairn, J. A., 2009. Analytical and Numerical Modeling of R Curves for Cracks with Bridging Zones. *International Journal of Fracture*, pp. 167-181.

Nairn, J. A., 2015. Numerical simulation of orthogonal cutting using the material point method. *Engineering Fracture Mechanics* , p. In press .

Nairn, J. A. & Matsumoto, N., 2009. *Fracture Modeling of Crack Propagation in Wood and Wood Composites.* Ottawa, Canada, Proceedings of the 12th International Conference on Fracture.

Nalla, R., Kruzic, J. & Ritchie, R., 2004. On the origin of the toughness of mineralized tissue: microcracking or crack bridging?. *Bone* , Volume 34, p. 790–798.

Nicoli, E., Dillard, D. A., Frazier, C. E. & Zink-Sharp, A., 2012. Characterization of mixed-mode I/II fracture properties of adhesively bonded yellow-poplar by a dual actuator test frame instrument. *Holzforschung*, Volume 66, p. 623–631.

NIST PS1, 2007. *Voluntary Product Standard PS1 Structural Plywood.* Gaithersburg, MD: U.S. Department of Commerce.

Paris, J. L., 2014. *Wood-Adhesive Bondline Analyses with Micro X-ray Computed Tomography (PhD thesis).* Corvallis, OR: Oregon State University.

Pizzi, A. & Mittal, K. A., 2003. *Handbook of Adhesive Technology*. New York: Marcel Dekker, Inc.

Raftery, G. M., Harte, A. M. & Rodd, P. D., 2009. Bond quality at the FRP–wood interface using wood-laminating adhesives. *International Journal of Adhesion & Adhesives,* Volume 29, p. 101– 110.

Rice, J. R., 1968. A path independent integral and the approximate analysis of strain concentration by notches and cracks. *J. Applied Mech.* , p. 379–386.

Shokrieh, M., Heidari-Rarani, M. & Ayatollahi, M., 2012. Delamination R-curve as a material property of unidirectional glass/epoxy composites. *Mater. Des.* , Volume 34, p. 211–218.

Sinha, A., Gupta, R. & Nairn, J. A., 2011. Thermal degradation of bending properties of structural wood and wood-based composites. *Holzforschung* , 65 (2), pp. 221-229.

Sinha, A., Nairn, J. A. & Gupta, R., 2012. The effect of elevated temperature exposure on the fracture toughness of solid wood and structural wood composites. *Wood Sci Technol,* Volume 46, p. 1127–1149.

Sinha, A., Nairn, J. A. & Gupta, R., 2012. The effect of elevated temperature exposure on the fracture toughness of solid wood and structural wood composites. *Wood Science & Technology* , Volume 44, p. 1127–1149.

Smith, I., Landis, E. & Gong, M., 2003. *Fracture and Fatigue in Wood.* Chichester: Wiley.

Smith, I. & S. Vasic, 2003. Fracture behaviour of softwood. *Mech. Mater.* , Volume 35, p. 803–815.

Sorensen, L., Botsis, J., Gmur, T. & Humbert, L., 2008. Bridging tractions in mode I delamination: Measurements and simulations. *Composites Sciences and Technology,* Volume 68, p. 2350–2358.

Stanzl-Tchegg, S. & Navi, P., 2009. Fracture behaviour of wood and its composites. A review COST Action E35 2004–2008: Wood machining – micromechanics and fracture. *Holzforschung* , Volume 68 .

Stoeckel, F., Konnerth, J. & Gindl-Altmutter, W., 2013. Mechanical properties of adhesives for bonding wood—A review. *International Journal of Adhesion & Adhesives,* Volume 45, p. 32–41.

Stutz, S., Cugnoni, J. & Botsis, J., 2011. Crack – fiber sensor interaction and characterization of the bridging tractions in mode i delamination. *Engineering Fracture Mechanics* , 78(6), p. 890 – 900.

Stutz, S., Cugnoni, J. & Botsis, J., 2011. Studies of mode I delamination in monotonic and fatigue loading using FBG wavelength multiplexing and numerical analysis. *Composites Science and Technology* , 71(4), p. 443 – 449.

Sulaiman, O. et al., 2009. Evaluation on the suitability of some adhesives for laminated veneer lumber from oil palm trunks. *Mater. Des.* , Volume 30 , p. 3572–3580.

Sutton, M. A. et al., 1983. Determination of displacement using improved digital image correlation method. *Image and Vision Computing* , 1(3), p. 133–139.

Suzuki, M. & Schniewind, A. P., 1987. Relationship between fracture toughness and acoustic emission during cleavage failure in adhesive joints. *Wood Science and Technology* , 21 (2), pp. 121-130.

US Forest Products Laboratory, 2010. *Wood handbook: wood as an engineering material.* Madison, WI: United States Government Printing.

Vasic, S. & Stanzl-Tschegg, S., 2007. Experimental and numerical investigation of wood fracture mechanisms at different humidity levels. *Holzforschung* , 61 (4), p. 367–374.

Wang, B. J. & Dai, C., 2005. Hot-pressing stress graded aspen veneer for laminated veneer lumber (LVL). *Holzforschung*, 59(1), pp. 10-17.

Wilson, E., Mohammadi, M. S. & Nairn, J. A., 2013. Crack propagation fracture toughness of several wood species. *Advances in Civil Engineering Materials* , 2(1), p. 316–327.

Wolfram Research, 2012. *Mathematica 9.0.* Champaign, IL: Wolfram Research.

7 Appendix

(Matlab® Scripts)

7.1 Script 1

```
%Gathering crack propagation data from DIC output
%Inputs: directory_name (input files path)
directory_name = 'D:\FolderPath';
files = dir(directory_name);
fileIndex = find(~[files.isdir]);
minimum=[];
for fidN = 1:length(fileIndex)
   try
      %Creating file path
      filename = strcat(directory_name,'\',files(fileIndex(fidN)).name);
      if( size(strfind(filename, '.csv'),1)>0)
         %Reading the data in the file
         data= csvread(filename,1,0);
         %X: Horizental crack tip position
         X = 1;
         %Y= Vertical strain
         Y = 17;
         %Gathering crack positions whose strain is closest to 1%
         [~,idx] = min(abs(data(:,Y) - 0.01));
         Answer=data(idx,X);
         L=length(filename);
         %Finding file index from  file number (file name
```

```
            %format: filename-xxxx-0.csv)
            fileInd=filename(L-9:L-6);
            j=str2num(fileInd);
            %Ignoring first files due to noise in crack data
            if(j>30)
                minimum(j+1,:) = [j,Answer];
            end
        end
    catch ('File not found.');
    end;
end
%Keeping all numbers in the vector which are larger than any previous number
keep = false(size(minimum, 1), 1);
largest = -Inf;
for i = 1:size(minimum, 1)
    if minimum(i,2) > largest
        largest = minimum(i,2);
        keep(i) = true;
    end
end
newdata = minimum(keep,:)
```

7.2 Script 2

```
%Error analysis script (Used in manuscript 2 Figures 4 & 5)
%Input: filename(data file path)
filename = 'D:\FilePath\FileName.xlsx';
%matrix of data
A = xlsread(filename);
%n=number of rows of A
n=size(A,1);
%B keeps the position of Nan value
B=isnan(A);
B=1-B;
treatment=-8;
% ZeroTreatment, EightTreatment, SixteenTreatment and TwentyfourTreatment
% are toughness data as a function of crack growth at respective treatment
ZeroTreatment=[];
EightTreatment=[];
SixteenTreatment=[];
TwentyfourTreatment=[];
%Separating toughness data (A) of different treatments
for(i=1:n)
%Toughness data of different treatments are separated by a row which
%contains treatment cycle number
   if(sum(B(i,:))==1)
      treatment=treatment+8;
      if(treatment==0)
         rows=0;
```

```
    for(r=1:n)
        rows=rows+1;
        if(isnan(A(i+r,1))==1)
            break;
        end
    end
    ZeroTreatment=A(i+1:i+rows-1,:);ZeroTreatment=ZeroTreatment';
    ZeroTreatment(any(isnan(ZeroTreatment),2),:)=[];
end
if(treatment==8)
    rows=0;
    for(r=1:n)
        rows=rows+1;
        if(isnan(A(i+r,1))==1)
            break;
        end
    end
    EightTreatment=A(i+1:i+rows-1,:);EightTreatment=EightTreatment';
    EightTreatment(any(isnan(EightTreatment),2),:)=[];
end
if(treatment==16)
    rows=0;
    for(r=1:n)
        rows=rows+1;
        if(isnan(A(i+r,1))==1)
            break;
        end
```

```
            end
            SixteenTreatment=A(i+1:i+rows-1,:);SixteenTreatment=SixteenTreatment';
            SixteenTreatment(any(isnan(SixteenTreatment),2),:)=[];
        end
        if(treatment==24)

TwentyfourTreatment=A(i+1:size(A,1),:);TwentyfourTreatment=TwentyfourTreatment';
            TwentyfourTreatment(any(isnan(TwentyfourTreatment),2),:)=[];
        end
    end
end
% CrackSize is the number of crack growth increments (crack growth from 0
% to 120 mm with 10 mm increments)
CrackSize=size(ZeroTreatment,2);
%StoreSample keeps all posible slopes
StoreSample =
zeros(size(ZeroTreatment,1)*size(SixteenTreatment,1)*size(EightTreatment,1)*size(Twe
ntyfourTreatment,1),CrackSize)
for(l=1:CrackSize)
    count=0;
    for(k =1:size(ZeroTreatment,1))
        for(j =1:size(EightTreatment,1))
            for(i =1:size(SixteenTreatment,1))
                for(m = 1:size(TwentyfourTreatment,1))
                    count=count+1;
                     a=ZeroTreatment(k,l);
                     b=EightTreatment(j,l);
```

```
                c=SixteenTreatment(i,l);
                d=TwentyfourTreatment(m,l);
                %Finding a linear fit for sampled data from each
                %treatment(Y=aX+b , p(1)=a and p(2)=b)
                p= polyfit([0 8 16 24],[a b c d],1);
                %normalizing fit slope by fit intercept
                StoreSample(count,l)=p(1)/p(2);
            end
        end
    end
end
M=[];
%M keeps crack size (first column) and nomalized slopes (second column)
for(t=1:CrackSize)
  temp=(t-1)*10*ones(size(StoreSample,1),1);
  temp2=[temp StoreSample(:,t)];
  M=[M;temp2];
end
%Printing average and standard deviation of normalized slopes per crack
%size
for (k=1:CrackSize)
   disp(strcat('crack size',num2str((k-1)*10),'-----mean =',
num2str(mean(StoreSample(:,k))),'-----std  =',num2str(std(StoreSample(:,k)))))
end
```

7.3 Script 3

```
%Used in manuscript 2
%Finding test statistic (t) and degree of freedom (df) using real sample size (n)
%Statistical method: two-sample unpooled t-test, unequal variances (Welch's t-test)
%Input: directory_name (data file path), Real sample size
%Input file format : material name(first column), crack size (second column), normalized
slope(third column)
%Each  input file contains data of one crack size/material


%Real sample size
      PFn=20;
      PVAn=31;
      PRFn=29;
      EPIn=23;
directory_name = 'D:\FilePath';
files = dir(directory_name);
fileIndex = find(~[files.isdir]);
minimum=[];
for fidN = 1:length(fileIndex)
   try
      %Creating file path
      filename = strcat(directory_name,'\',files(fileIndex(fidN)).name);
      if( size(strfind(filename, '.xl'),1)>0)
      %B keeps the first column of data
      %C keeps the second and third columns of data
```

```
[B C]= xlsread(filename);
%#Combinations of results for finding all possible linear fits
N=size(B,1)
%material keeps the material name
material=unique(C(:,1));
MaterialType=size(material,1);
%Seperating data by material type
for(k=1:MaterialType)
   temp=[];
   for(i=1:N)
      vv=strfind(material(k,1), char(C(i,1)));
      v=vv{1};
      if(size(v,1) >0)
         temp=[temp;B(i,2)];
      end
   end
   %Saving the data of each  material in  a new sheet
   xlswrite(filename,temp,k+1);
end
%test statistic (t) and degree of freedom (df)
t=[];df=[];
for(k=1:MaterialType)
  for(j=k+1:MaterialType)
      A1=xlsread(filename,k+1);
      A2=xlsread(filename,j+1);
      %Extracting data for two-sample test
      vv=strfind(material(k,1),'PF');
```

```
 v=vv{1};
if(size(v,1) >0)
   n1=PFn;
end
vv=strfind(material(k,1),'PVA');
 v=vv{1};
if(size(v,1) >0)
   n1=PVAn;
end
vv=strfind(material(k,1),'PRF');
 v=vv{1};
if(size(v,1) >0)
   n1=PRFn;
end
vv=strfind(material(k,1),'EPI');
 v=vv{1};
if(size(v,1) >0)
   n1=EPIn;
end
vv=strfind(material(j,1),'PF');
 v=vv{1};
if(size(v,1) >0)
   n2=PFn;
end
vv=strfind(material(j,1),'PVA');
 v=vv{1};
if(size(v,1) >0)
```

```
            n2=PVAn;
        end
        vv=strfind(material(j,1),'PRF');
         v=vv{1};
        if(size(v,1) >0)
            n2=PRFn;
        end
        vv=strfind(material(j,1),'EPI');
         v=vv{1};
        if(size(v,1) >0)
            n2=EPIn;
        end
        t(k,j)=(mean(A1)-mean(A2))/sqrt(std(A1)^2/n1+std(A2)^2/n2);t(j,k)=t(k,j);
        df(k,j)=(std(A1)^2/n1+std(A2)^2/n2)^2/((std(A1)^2/n1)^2/(n1-
1)+(std(A2)^2/n2)^2/(n2-1));df(j,k)=df(k,j);
      end
    end
    %Saving t to sheet 7
    xlswrite(filename,material,7,'A2');
    xlswrite(filename,material',7,'B1');
    xlswrite(filename,t,7,'B2');
    %Saving df to sheet 8
     xlswrite(filename,material,8,'A2');
    xlswrite(filename,material',8,'B1');
     xlswrite(filename,df,8,'B2');
    end
  catch ('File not found.');
```

```
    end;
end
```

7.4 Script 4

```
%Obtaining bridging stress profile from experimental R curve following the
%algorithm described in manuscript 3
%filename: input file path
%directory: output folder path
%Input file format: Excel file, each tab contains data for one type of
%material, first column is delta followed by columns of toughness data for
%respective treatments with headers indicating the number of cyclic treatment
clear all
filename = 'D:\InputFilePath.xlsx';
directory='D:\OutputFolderPath\';
%Windowsize is the window size for differentiating/smoothing of R
%Window progresses one delta at each step
WindowSize=2;
%Junmp is inversely correlated with the overlap of windows
Jump=8;
%Sheets keeps sheet names of the input file
[status,sheets] = xlsfinfo(filename)
sn=length(sheets);
%Computing sigma for each material
for(sh=1:sn)
```

```
%Removing the header
 A = xlsread(filename,sh);
 if(sum(isnan(A(1:size(A,2))))>0)
    A=A(2:size(A,1),:);
 end
 %n=number of delta entries
 n=size(A,1);
 n=n-WindowSize/2;
 % Treatment keeps number of treatments
 Treatment=size(A,2);
 %Final keeps all original sigma values for saving into output file
 Final=[];
 %Final keeps all interpolated sigma values for saving into output file
 Final2=[];
 %Final keeps all interpolated R' values for saving into output file
 Final3=[];
 %BridgingToughness is the area under briging stress plot
 BridgingToughness=[];
 %interval is the difference of two consecutive delta
 interval=A(2,1)-A(1,1);
 for(j=2:Treatment)
    %slop keeps the slopes of linear fits for each window
    slop=[];
    %sigma keeps the sigma values
    sigma=[];
    %delta2 keeps the average delta for each window
    delta2=[];
```

```
%slop keeps the slopes of linear fits for windows chosen by Jump
slop2=[];
 %delta2 keeps the average delta for windows whose slopes are
 %kept in slop2
delta3=[];
%delta keeps the original delta entries
delta=[];delta=A(:,1);
for(i=WindowSize/2+1:n)
   delta2(i-WindowSize/2)= delta(i);
   %x keeps delta values for each window
   x=delta(i-WindowSize/2:i+WindowSize/2);
   %x keeps delta values for each window
   y=A(i-WindowSize/2:i+WindowSize/2,j);
   P = polyfit(x,y,1);
   slop(i-WindowSize/2)=P(1);
end
%N keeps the number of slopes after applying Jump
N=floor(length(slop)/Jump);
%Jump defines the number of disregarded windows between maintained windows
for(k=1:N+1)
    if(Jump*(k-1)+1<length(slop))
        slop2(k)=slop(Jump*(k-1)+1);
        delta3(k)=delta2(Jump*(k-1)+1);
    else
        slop2(k)=slop(length(slop));
        delta3(k)=delta2(length(slop));
    end
```

```
end
delta2=[];delta2=delta3;
slop=[];slop=slop2;
nn = numel(delta2); % number of original entries
if(j==2)
   %xiR keeps interpolated delta values for R'
   xiR = interp1( 1:nn, delta2, linspace(1, nn, 30*nn) );
   %xi  keeps interpolated delta values for sigma
   xi = interp1( 1:nn+1, [0 delta2], linspace(1, nn+1, 30*(nn+1)) );
end
%yiR keeps R' values obtained by PCHIP
yiR=pchip(delta2,slop,xiR);
%Plotting interpolated R' vs delta
f2= figure;
plot(xiR,yiR,'color','red');
xlabel('\delta');
ylabel('R\prime(\delta)');
%Saving the plot
name=strcat(directory,sheets{sh},int2str(j-1),'_slop','.png')
saveas(gcf, name);
close(f2);
 %Computing sigma
for(i=1:length(slop))
   sumRLog=0;
   for(k=i:length(slop)-1)
      sumRLog=sumRLog+(slop(k+1)-slop(k))*log((k+1)/k);
   end
```

```
        sigma(i)=2*(slop(i)-delta2(i)/delta2(length(slop))*(slop(length(slop))-
length(slop)*sumRLog));
    end
     %yi keeps sigma values obtained by PCHIP
    yi=pchip([0 delta2],[0 sigma],xi);
     %Plotting interpolated sigma vs delta
    f3=figure
    plot(xi,yi,'color','red');
    xlabel('\delta(mm)');
    ylabel('\sigma(\delta) (kPa)');
    %Saving the plot
    name=strcat(directory,sheets{sh},int2str(j-1),'_final','.png')
    saveas(gcf, name);
    close(f3)
    if(j==2)
        Final=[0;delta2'];
        Final2=xi';
        Final3=xiR';
    end
    Final=[Final [0;sigma']];temp=0;
    Final2=[Final2 yi'];
    Final3=[Final3 yiR'];
    sigma=[0 sigma];
    delta2=[0 delta2];
    for(k=2:length(sigma))
        temp=temp+(sigma(k)+sigma(k-1))*(delta2(k)-delta2(k-1))/2;
    end
```

```
        BridgingToughness= [BridgingToughness;temp];
    end
    BridgingToughness=[0;BridgingToughness];
    Final=[Final;BridgingToughness'];
    %Saving results into excel file
    xlswrite(strcat(directory,sheets{sh},'result.xlsx'),Final)
    xlswrite(strcat(directory,sheets{sh},'Interpolate.xlsx'),Final2)
    xlswrite(strcat(directory,sheets{sh},'InterpolateR.xlsx'),Final3)
end
```

7.5 Script 5

```
%Used in manuscript 3 to find Trilinear fits for experimental sigma vs
%delta plots
%filename : input file address
%directory: output folder address
clear all
filename = 'D:\InputFilePath.xlsx';
directory='D:\OutputFolderPath\';
%X keeps the second break point which is fixed for all data
X=1;
%sheet keeps the data containing sheet number
sheet=1;
%percent determines the match% area of Trilinear fit and experimental curve
percent=0.9
%Flag determines the area to which Trilinear fit matches (PCHIP or original)
```

```
%If Flag is true then the area of the orginal sigma values are considered
%as reference for matching with the area under Triliear
%fit, otherwise the area PCHIP is considered as a reference
Flag=true;
[status,sheets] = xlsfinfo(filename)
sn=length(sheet);

%Reading the data from input file
A = xlsread(filename,sheet);
%Removing the header
if(sum(isnan(A(1,:)))>0)
   A=A(2:size(A,1),:);
end
%Delta keeps delta values
delta=A(:,1);
%Final keeps the Trilinear fit data for saving into output file
Final=[];
%treatment keeps number of treatments
treatment=size(A,2);
%Finding the best Trilinear fit
for(i=2:treatment+1)
   %y keeps sigma values
   y=A(:,i);
   %areaMain keeps the area under sigma curve
   areaMain=0;
   for(k=2:size(y,1))
      areaMain=areaMain+(y(k,1)+y(k-1,1))*(delta(k,1)-delta(k-1,1))/2;
```

```
end
n = numel(delta); % number of original points
%deltaNew keeps break point delta values
deltaNew=[];
%xi interpolates delta to improve integration
xi = interp1( 1:n, delta, linspace(1, n, 30*n) );
%yi keeps sigma values for xi by fitting Piecewise Cubic Hermite
%Interpolating Polynomial (PCHIP) to orginal data
yi=pchip(delta,y,xi);
%area keeps the area under PCHIP curve
area=0;
for(k=2:length(xi))
   area=area+(yi(k)+yi(k-1))*(xi(k)-xi(k-1))/2;
end
%maxY keeps the first break point sigma
maxY=y(2,1);
ind=2;
%area2 keeps the total area under Trilinear fit
area2=delta(ind,1)*maxY/2;
area2=area2+ (X-delta(ind,1))*maxY/2;
AreasDiff=area-areaMain
if(Flag==false)
   %opt is the optimal sigma for second break point such that the
   %area under Trilinear fit matches to the refrence area according to
   %percent
   opt=(area*percent-area2)*2/((X-delta(ind,1))+ (delta(size(delta,1),1)-X));
else
```

```
    opt=(areaMain*percent-area2)*2/((X-delta(ind,1))+ (delta(size(delta,1),1)-X));
end
 a = [delta(ind,1);maxY;0] - [0;0;0];
 b = [X;opt;0] - [0;0;0];
 d = norm(cross(a,b)) / norm(a);
  %triArea1 is the area of first triangle
  triArea1=d*norm(a)/2;
  %triArea2 is the area of second triangle
  triArea2=opt*delta(size(delta,1),1)/2;
yNew=[0 y(ind,1) opt 0 ]';
deltaNew=[0 delta(ind,1) X delta(size(delta,1),1)]';
if(i==2)
    Final=[Final [deltaNew;0;0]];
end
Final=[Final [yNew;triArea1;triArea2]];
%Plotting Trilinear fit
f=figure;
plot(xi,yi,'color','red');
xlabel('\delta(mm)');
ylabel('\sigma(\delta) (kPa)');
hold on
plot(deltaNew,yNew,'color','blue');
plot([0 X],[0 opt],'color','blue');
%plot(delta,y,'color','black');
hold off;
%Saving figures
name=strcat(directory,sheets{sheet},int2str((i-2)*8),'_final','.png');
```

```
    saveas(gcf, name);
    close(f)
end
xlswrite(strcat(directory,sheets{sheet},'result.xlsx'),Final)
```

Published with MATLAB® R2012b